Variations of the chemical characteristics and source regions of aerosols at the Cape Point GAW station

Thesis presented for the degree of Master of Science

In the Department of Oceanography

University of Cape Town

By: Kurt Spence

Student number: SPNKUR001

Supervisor: Dr Katye Altieri

Co-supervisor: Casper Labuschagne (SAWS)

Table of Contents

Plagiarism declaration

Declaration

I know that plagiarism is wrong. Plagiarism is to use another's work and pretend that it is one's own.

I have used the Harvard convention for citation and referencing. Each contribution to, and quotation in this essay/report/project from the work(s) of other people has been attributed, and has been cited and referenced.

This essay/report/project is my own work.

I have not allowed, and will not allow, anyone to copy my work with the intention of passing it off as his or her own work.

Signed by candidate

Signature _____ Date 12/01/2022

Note that agreement to this statement did not exonerate you from the University's plagiarism rules (http://www.uct.ac.za/uct/policies/plagiarism_students.pdf)

Abstract

Nitrogen is an essential component for life. The natural nitrogen cycle has been greatly disturbed by the production of fertilizer and use of fossil fuels, such that it has doubled the amount of reactive nitrogen (Nr) produced globally. Excessive additions of Nr to the environment can have negative effects, including eutrophication, loss of biodiversity, enhanced greenhouse gas emissions, acidification, increased tropospheric ozone, and damage to human health. Excess ammonia (NH_3) and nitrogen oxide (NO_x) emissions lead to increased aerosol loading via secondary aerosol formation processes. Increased aerosol loading has impacts on the climate and on human health. Furthermore, the aerosols formed from Nr from continental sources can get deposited to the open ocean, which is usually nitrogen limited. Knowing the concentrations of different aerosol species from a pollution free environment, such as the remote open ocean, can give insights into the natural preindustrial conditions and be used as a baseline for looking into the impacts of anthropogenic activities. This thesis focuses on establishing the Cape Point Global Atmosphere Watch (GAW) station as a site for collecting aerosol samples from pristine marine air masses. The use of a tower site allows for high temporal resolution sampling across multiple seasons and years, which is logistically difficult when relying on ship-based sampling of pristine marine environments. Results are presented from the chemical composition analysis of aerosols sampled at the Cape Point GAW station, including comparisons of two different aerosol sampling systems (tall-tower PM_{10} and ground-based size-segregated). Furthermore, the installation and testing of a sector-controlled sampling system designed to reduce continental influence on samples is evaluated. Air mass back trajectories and radon (^{222}Rn) concentrations were used to classify the air masses of each aerosol sample as either marine, modified marine, or continental. We found that continental samples had elevated concentrations of NH_4^+, NO_3^-, and non-sea-salt SO_4^{2-}, whereas the marine samples had elevated concentrations of Cl^-, and Na^+, as expected. A comparison of the tall-tower PM_{10} and ground-based size-segregated sampling systems showed that the ground-based sampler measured higher concentrations of coarse mode aerosols. This is attributed to the settling of large aerosols within the long sampling intake tube from the tower sampling system. The sector-controlled sampling system based on wind speed and direction was able to remove some of the influence of continental air masses, however some continental influence could not be avoided as the continental air masses circulated over the ocean before being sampled from the marine sector. This system could be improved by having additional cut-off limits defined for sampling, such as particle number, black carbon, or carbon monoxide (CO) concentrations.

1. Introduction and literature review

1.1 Introduction

Aerosols can have large impacts on climate through direct and indirect effects. Aerosols have a direct impact on the radiative forcing of the atmosphere as they scatter and absorb incoming solar and infrared radiation (Figure 1.1). They also act as cloud condensation nuclei (CCN) and have an indirect effect on radiative forcing by influencing cloud droplet size distribution, cloud albedo, and lifetime (Penner et al., 2001; Cavalli, 2004). Aerosols in remote regions have little to no influence from anthropogenic activities, and in a study that aimed to identify clean regions of the atmosphere, most of the pristine regions that Hamilton et al., 2014 found were in the southern hemisphere and over the ocean. Pristine areas can be used as a proxy for preindustrial times and provide information on the natural aerosol levels (Hamilton et al., 2014). These areas can be used to monitor the extent to which anthropogenic activities have altered the natural systems and be used to predict how further changes will impact ecosystems in different climate projections.

Natural and anthropogenic reactive nitrogen (Nr) aerosols get deposited to the ocean surface and can influence the biogeochemistry of the surface ocean. If the original source of the Nr aerosols being deposited onto the surface ocean is from terrestrial origin, it represents a source of new Nr to the system and can be expected to rise in the future (Duce et al., 2008). If the original source of Nr aerosols is from the ocean, then the Nr is cycling between the ocean and the atmosphere and would not be expected to rise in the future.

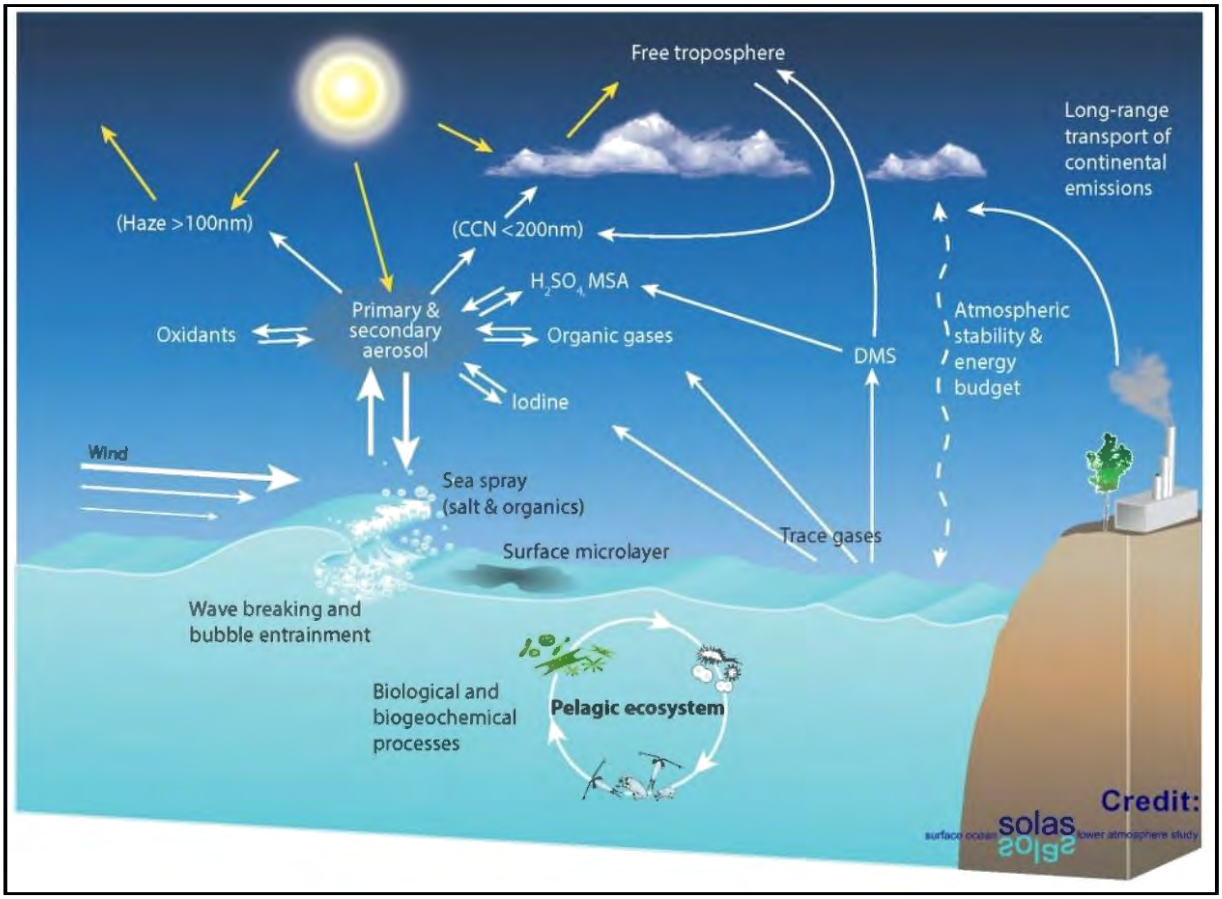

Figure 1.1: Primary and secondary aerosol formation processes over the open ocean, and subsequent atmospheric processing and radiative impacts (Brévière & SOLAS Scientific Steering Committee (eds.), 2016).

1.1.1 Aims and objectives

The primary objective of this thesis was to establish the Cape Point GAW station as a reliable field site to collect and study clean marine aerosols that originate in the remote atmosphere of the Southern Ocean. This thesis focuses on the inorganic aerosol composition, and in particular nitrogen-containing aerosols due to their biogeochemical and climate relevance, as well as potential for complex mixed sources and chemistry in polluted coastal regions. In order to address this objective, the aims of the thesis were to:

1) Compare existing tall-tower and newly installed ground-level aerosol collection systems at the GAW station.
2) Install and test a sector-controller for excluding pollution episodes from aerosol collection at the GAW station.
3) Characterize aerosol chemical composition as a function of aerosol size, atmospheric source region, and season.

1.1.2 Thesis overview

Aerosol sizes, composition and concentrations vary depending on the source, with coastal aerosols having features of both terrestrial and marine sources, which are quite distinct. In this thesis, the Cape Point Global Atmosphere Watch (GAW) Station is used to study aerosols in air masses passing over both the pristine Southern Ocean and anthropogenic pollution from the city of Cape Town. During the sampling campaign two different sampling systems, tall-tower, and ground-level, were compared and a system to exclude sampling from continental air masses was installed and tested.

The rest of Chapter 1 is a review of the relevant literature on the perturbations of the global nitrogen cycle, the unique features of coastal aerosols, and a description of tower sampling as a research tool in marine atmospheric chemistry. In the methods section (Chapter 2), the study site is described first, followed by the procedure for sample collection, sample extraction and concentration determination. Specific details are given for the two sampling systems and different methods for concentration determination. The process for air mass back trajectory determination is explained, followed by the usefulness of different auxiliary data provided by the GAW station. The final section of the methods describes the sector-controller that shuts off the sampling system when the wind direction is from the land. In the results section (Chapter 3), the general atmospheric conditions are described for the time period of the sampling campaign. The aerosol concentrations from the two different sampling systems are presented, focusing on seasonal changes as well as sector-controlled and non-sector-controlled data. The results section also presents the data based on air mass history. In the discussion and conclusion section (Chapter 4), the two sampling systems are compared with the tall-tower system seemingly under sampling the coarse mode fraction of the aerosols. The effectiveness of the sector-controlled sampling system is then presented, with it being evident that some continental air masses circulate over the ocean before being sampled. The chemical composition of the aerosols are then characterized with air mass history showing a clear relationship between the concentrations of aerosol species and their source regions.

1.2 Anthropogenic impacts on the global nitrogen cycle

Nitrogen is an essential element for life. It is the most abundant major essential element, but it is generally the least readily available. This is because over 99% of nitrogen exists as N_2, a very stable triple bonded molecule, which is unusable by over 99% of living organisms (Galloway et al., 2003). The breaking of this triple bond has significant energy requirements and converts N_2, unreactive nitrogen, to reactive nitrogen (Nr) species, this only happens in high-temperature environments or by specialized nitrogen fixing microorganisms (Duce et al., 2008). Nr species are nitrogen compounds that are biologically, photochemically or radiatively active, and include nitrate (NO_3^-), nitrite (NO_2^-), nitrous oxide (N_2O), ammonium (NH_4^+), ammonia (NH_3) and organic nitrogen species (e.g., amino acids, alkylnitrates) (Karl & Michaels, 2001; Galloway et al., 2003; Voss & Hietanen, 2013). There is a natural balance between the creation of Nr, through lightning and biological nitrogen fixation (BNF), and the removal of Nr, through the conversion of Nr to N_2 via the microbial processes of denitrification and anammox. This balance prevents the accumulation of Nr over long-term time-scales, which causes Nr to often be the limiting factor for primary production (Galloway et al., 2003; Gruber & Galloway, 2008). Due to the generally low concentration of Nr, natural processes have adapted to use Nr efficiently and there is a symbiotic relationship between animals, plants, and soil life allowing for increased biodiversity (Galloway et al., 2014).

The nitrogen cycle is the systematic transformation between different forms of nitrogen as it moves through different environments and is processed by different organisms (Karl & Michaels, 2001). Nitrogen can transform between organic and inorganic forms as well as reduced and oxidized forms as it is affected by different processes. The nitrogen cycle is interconnected between the different Earth systems and there are constant fluxes between them, for example nitrogen species can exchange between the atmosphere and the surface ocean through either gas fluxes, dry deposition, or wet deposition. The nitrogen cycle is also interconnected to the phosphorus and carbon cycle, via the creation of organic matter and its remineralization (Karl & Michaels, 2001).

The biologically limiting nature of Nr also influenced the growth of the human population. Humans needed Nr to fertilize the crops they were growing to feed the population. At first renewable sources were used, such as manure and the promotion of BNF through the cultivation of legumes. Then turning to non-renewable sources such as the naturally built up reserves of guano and saltpetre (Galloway et al., 2014). The human population continued to grow and the global demand for food was higher than the natural and cultivation-induced BNF (C-BNF) supply. This led to the creation of artificial processes, such as the Haber-Bosch process, to create Nr. The Haber-Bosch

process produces NH_3 by reacting atmospheric N_2 with hydrogen in the presence of iron in a high temperature environment (Erisman et al., 2008). During this period there was also a rise in the use of fossil fuels to power the industrial revolution. The increased use of the Haber-Bosch process and increased use of fossil fuels, both of which produce Nr and CO_2, has caused a dramatic increase in the production of Nr (Galloway et al., 2003). From 1850 to present there has been a rapid increase in human population, along with increased Nr creation per-capita as lifestyles shifted to use more energy and consume more animal products (Galloway, 1998). Approximately half of the human population is currently fed with crops grown using nitrogen fertilizers created with the Haber-Bosch process (Erisman et al., 2008). Consequently, the total anthropogenic production of Nr has increased more than 10 fold from 15 Tg N $year^{-1}$ in 1860 to 165 Tg N $year^{-1}$ in 2000 (Galloway et al., 2003; Gruber & Galloway, 2008). The additional anthropogenic Nr that is added to the environment has doubled the cycling of nitrogen on the planet (Fowler et al., 2013).

The natural nitrogen cycle has been greatly perturbed by the additional Nr added to the environment, which can offset the balance of N_2 fixation and denitrification and lead to the accumulation of Nr in ecosystems, with implications for biogeochemical cycling (e.g., changes in nutrient limitation) and climate (e.g., N_2O emissions). If an ecosystem is removed from Nr limitation, primary productivity can increase, which will use additional carbon, phosphorus, and other nutrients. This will affect both the carbon and phosphorus cycles, including the exchange of CO_2 between the surface ocean and the atmosphere, impacting climate (Karl & Michaels, 2001). The additional Nr added to the earth system has substantial consequences for the health of both the environment and humans (Galloway et al., 2014), some of which include, eutrophication of ecosystems, global acidification (lithosphere, atmosphere, and hydrosphere), production of aerosols, production of tropospheric ozone (through reactions between NO_x and volatile organic compounds) and loss of stratospheric ozone (through a reaction between chlorine and bromide, which is catalysed by nitric oxide (NO, produced through the decomposition of N_2O)) (Wolfe & Patz, 2002; Galloway et al., 2003). These can have direct impacts on human health as well as indirect impacts through alterations of global climate. Nr is rapidly spreading throughout the environment due to efficient atmospheric and hydrological transport processes and its ability to easily transform into various Nr species. This leads to an effect known as the nitrogen cascade, whereby one molecule of a Nr species can have numerous effects on multiple systems as it passes through them and is altered by them (Galloway, 1998). For example, a molecule of NO, released from fossil fuel combustion into the atmosphere, can produce photochemical smog, and increase ozone concentrations. That molecule can then be oxidized to nitric acid and increase precipitation acidity and then be deposited terrestrially, which can cause acidification and eutrophication in the

ecosystem. It could then be discharged into the hydrological system and increase water acidity and cause eutrophication. The Nr molecule could then be converted to N_2O and emitted to the atmosphere, increasing greenhouse gas concentrations and decreasing stratospheric ozone (Galloway et al., 2003; Gruber & Galloway, 2008). After the Nr is released into the environment the initial source becomes irrelevant as the Nr can rapidly convert to different species and cascade through ecosystems, with the only stopping point being when the Nr is converted back to N_2 via denitrification (Galloway et al., 2003).

The majority of anthropogenically created Nr that reaches the oceans is deposited into coastal areas through riverine input (Jickells et al., 2017). In moderation, additional Nr can increase algal growth and increase the production of harvestable fish (Nixon, 1988; Richardson & Jørgensen, 1996). In excess, additional Nr can cause eutrophication and an increase in hypoxia/anoxia (Galloway et al., 2003; Voss & Hietanen, 2013). The vast majority of the Nr added to coastal systems gets converted to N_2 through microbial denitrification, with a fraction being converted to N_2O and NO (Seitzinger & Kroeze, 1998). Very little of the Nr added to the coastal area is transported across the continental shelf to the open ocean, so the majority of anthropogenically created Nr that reaches the open ocean is through atmospheric deposition.

In the oceans Nr is generally a limiting factor on productivity and it has an uneven distribution in surface waters. The surface concentrations of Nr are generally low in mid latitude waters and high in the high latitudes, along the equator, and near the coast (Figure 1.2) (Sigman & Hain, 2012). The variations in concentrations are a result of the supply and demand of Nr, with either insufficient supply of Nr (mid latitudes), a strong supply of Nr (upwelling along the equator and western continental boundaries, terrestrial outflows along the coast), or other limiting factors reducing demand for Nr (iron and light limitations in the high latitudes) (Sigman & Hain, 2012; Fowler et al., 2013). The open ocean receives a smaller portion of anthropogenic created Nr than the coastal areas, but it can be significant due to the very low concentrations found in the open ocean surface (Galloway, 1998; Galloway et al., 2003). Almost all the Nr added to the open ocean though atmospheric deposition will be assimilated into organic matter. The majority of this will be decomposed in deep water, but some can be emitted to the atmosphere, either after it has been denitrified or in a reactive form such as NH_3 (Galloway et al., 1995).

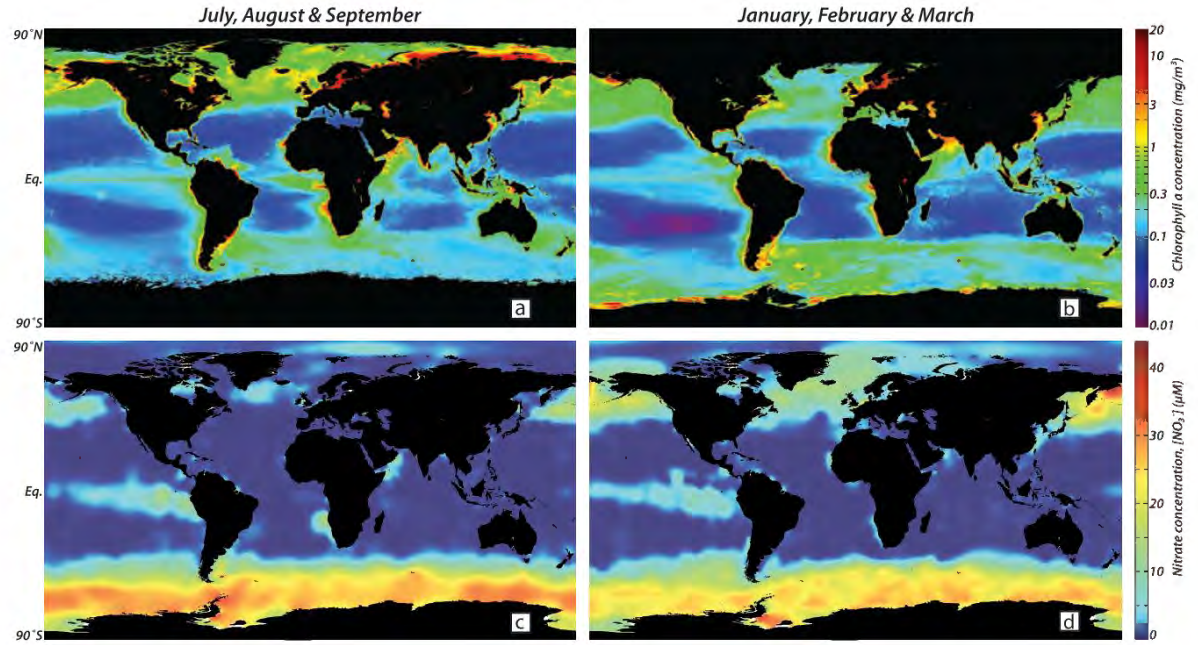

Figure 1.2: Composite maps of the satellite-derived chlorophyll (panels a and b) and ship-sampled nitrate (dominant form of Nr, panels c and d) for the global oceans. Left panels show northern hemisphere summer and right shows southern hemisphere summer (Sigman & Hain, 2012).

1.2.1 Ammonium in the marine atmosphere

NH_3 is the dominant alkaline gas in the atmosphere, and it readily reacts to neutralize sulfate, nitrate and other acidic gases (Wentworth et al., 2016). This forms NH_4^+ aerosols such as ammonium nitrate (NH_4NO_3), ammonium bisulfate ($(NH_4)HSO_4$) and ammonium sulfate ($(NH_4)_2SO_4$). NH_3 is emitted to the atmosphere through both natural and anthropogenic activities, with emissions from anthropogenic activities having risen dramatically over the past century (and they are predicted to continue to rise) (Duce et al., 2008). Although most anthropogenic emissions are terrestrial, the atmosphere is efficient at transporting gases and aerosols, so these can easily reach the open ocean. Natural terrestrial emissions of NH_3 can also be transported to the open ocean, although they represent a much smaller fraction of the total. The oceans can also be a source of NH_3 to the atmosphere due to outgassing. The strength of this source depends on several factors including the concentration gradient between the atmosphere and the surface ocean, sea surface temperature, pH and salinity, which influence the outgassing rate of NH_3 from the ocean (Paulot et al., 2015; Altieri, Fawcett & Hastings, 2021). The concentration of NH_4^+ in the surface ocean is dependent on several processes that can either increase the concentration, such as N_2 fixation, ammonification and grazing of phytoplankton by zooplankton (through excretion, egestion, and messy feeding (Steinberg & Saba, 2008)), or decrease the concentration, such as nitrification and assimilation into organic matter (Karl & Michaels, 2001). After the conversion from NH_3 to NH_4^+ in the atmosphere, the aerosol is usually deposited through wet and/or dry deposition.

The net flux of NH_3 has changed from an ocean-to-land flux in preindustrial times to a land-to-ocean flux due to anthropogenic influences (Galloway et al., 2008). The flux between the atmosphere and the ocean varies greatly, with the high latitude oceans having a negative NH_3 flux and a positive NH_3 flux in the low latitude oceans due to the temperature dependence of the flux (Johnson & Bell, 2008). The emissions, deposition, and the air-sea flux of NH_3 all have large uncertainties, but nitrogen isotopes of NH_4^+ have been used to identify if the aerosol is of terrestrial or oceanic origin, which can help constrain some uncertainties (Jickells et al., 2003; Johnson & Bell, 2008). However, Altieri et al., (2014) did not find a clear correlation between the isotopic ratios of NH_4^+ in rainwater, in the island of Bermuda, with the origin of the air mass (terrestrial or marine) and they conclude that the ocean is an important source for atmospheric NH_4^+ throughout the year. There is a large range in the estimates of anthropogenic NH_4^+ deposition to the open ocean (50-87.5%, Galloway et al., 1995; Duce et al., 2008), this shows the high level of uncertainties and the need to better understand the natural oceanic source to predict how human caused perturbations will influence the system.

1.2.2 Nitrate in the marine atmosphere

Atmospheric nitrate (NO_3^-) is produced from the oxidation of nitrogen oxides (NO_x = NO + NO_2) and has impacts on air quality and the climate, through the contribution to atmospheric particulate matter and the radiative heat budget (Park & Kim, 2005; Boucher et al., 2013). Nitrate in the atmosphere is acidic, usually found in the form of nitric acid (HNO_3), which is readily neutralized by NH_3 gas to form fine mode aerosol NH_4NO_3. As the air mass moves away from its sources the concentrations of HNO_3 and NH_3 drop, then the NH_4NO_3 can dissociate (Allen, Harrison & Erisman, 1989). If this occurs near the coast, then the HNO_3 can react with sea salt aerosols to form coarse mode $NaNO_3$ (Pakkanen, 1996). The combustion of fossil fuels is the primary emission source of NO_x, and anthropogenic activities have dramatically increased its emission and the subsequent NO_3^- deposition has also increased (Galloway et al., 2003). Natural NO_x emission sources include biomass burning (Finlayson-Pitts & Pitts, 2000), lightning (Schumann & Huntrieser, 2007), and soil processes (Davidson & Kingerlee, 1997). The emissions of alkyl nitrates from the surface ocean have also been proposed as a source of NO_x to the marine atmosphere in remote regions (Kamezaki et al., 2019). The South Atlantic and Southern Ocean will primarily contain NO_3^- aerosols produced through natural sources of NO_x, and the aerosols from these regions can be used as proxy for the preindustrial atmosphere, which can be used to understand anthropogenic perturbations to the system (Hamilton et al., 2014).

1.3 Aerosol impacts on climate, visibility, and health

Aerosols can have large impacts on climate through direct and indirect effects. The aerosols over the ocean can have a large impact on climate effects because they can form clouds which are effective reflecting layers above the dark ocean (Charlson, Lovelockt & Warren, 1987; O'Dowd et al., 2014). The emissions of certain aerosols can lead to increased concentrations of ozone and enhance the greenhouse potential of the atmosphere (Galloway et al., 2003).

Aerosols in polluted areas have high concentrations and can influence visibility and health. High concentrations of aerosols will decrease atmospheric visibility, contributing to regional haze (Galloway et al., 2003). Increases in aerosol concentrations will also increase the concentrations of fine particulate matter in the atmosphere (Park & Kim, 2005). Increases in ozone concentrations and fine particulate matter have serious impacts on human health (Pope et al., 1995). Particulate air pollution has been linked with serious respiratory infection and illness, and cardiopulmonary and lung cancer (Pope et al., 1995; Follett & Hatfield, 2001).

1.4 Aerosols impacting a coastal region

Coastal areas can be influenced by both polluted air masses coming from cities as well as pristine air masses coming from open ocean. This allows a unique sampling region where important features of multiple sources can be observed. Coastal aerosol sampling allows for unique observations as it can give insight into the natural production, concentrations, and composition of marine aerosols. It can also provide insight into the impact of continental and anthropogenic aerosol sources that are moving off the land and over the ocean, which may be deposited to the marine environment. Coastal sampling can provide improved temporal sampling of marine air masses as it is accessible year round, which can support ship borne measurements that have lower sampling frequency. This sampling may be subject to coastal influences, such as enhanced aerosol production due to higher biological activity depending on the region. Rinaldi et al., (2009) compared simultaneous coastal and open ocean sampling of the same region and found that both had similar mass size distributions of the main aerosol chemical components and very similar relative chemical composition. The only local coastal influence that Rinaldi et al., (2009) found was elevated nucleation mode concentrations at the coastal site compared to the open ocean. This points to a coastal source of new particles that is not representative of the open ocean, however due to the negligible contribution of this size class to the total mass of aerosols, this does not influence the aerosol chemical composition (Rinaldi et al., 2009).

Regional climate and air quality models struggle to simulate coastal areas due to the mixing of emission types (e.g., dust, urban pollutants, and ocean emissions) (Paton-Walsh et al., 2018) and

complex meteorology (e.g., land-sea breezes) (Freeman et al., 2017), and model evaluation is limited due to a lack of observational data sets and difficulty in retrieving satellite images in cloudy coastal areas (Seinfeld et al., 2016). Urban regions are typically associated with high aerosol concentrations and poor air quality due to anthropogenic emissions of aerosols and their precursor gases (Monks et al., 2009). Marine regions are known to have emissions of sea spray, halogens, NH_3, and reduced sulfur species, and are the largest source of natural aerosols globally (Saltzman, 2009). The air quality and climate impacts of aerosols in coastal cities are difficult to predict due to the complex mixing of these anthropogenic and ocean emissions (Paton-walsh et al., 2017).

1.4.1 Anthropogenic and marine sulfur sources

Sulfate aerosols are one of the most abundant particles within the marine atmosphere and are a considerable source of cloud condensation nuclei. The precursor to sulfate (SO_4^{2-}) aerosols formed in the atmosphere is sulfur dioxide (SO_2) (Saltzman, 2009). SO_2 is emitted from anthropogenic activities, such as fossil fuel combustion, coal power plants, domestic burning and industry, as well as natural sources, such as volcanoes and oceanic emissions of dimethyl sulfide (DMS). DMS is produced through biological activity in the oceans surface and is emitted to the atmosphere. Once DMS is in the atmosphere it is oxidized, usually by OH, and can produce a variety of products such as SO_2, dimethyl sulfoxide, dimethyl sulfone, and methanesulfonic acid (Saltzman, 2009). SO_2 gas undergoes oxidation in the atmosphere by OH, with O_2 and H_2O, to form SO_4^{2-}. Sulfate contributes to the acidity of marine aerosols but is neutralized by NH_3, to form $(NH_4)_2SO_4$ or $(NH_4)HSO_4$ aerosols, if NH_3 is present. Sulfate aerosols that form from gaseous precursors are termed non-sea-salt sulfate, whereas sulfate aerosols that form directly from sea water, due to sea spray or bubble bursting, are termed sea-salt sulfate (Figure 1.1). Sea-salt sulfate is usually found in the coarse mode, whereas non-sea-salt sulfate is usually in the fine mode (Saltzman, 2009).

1.4.2 Other inorganic aerosol ions

Aerosols are comprised of a variety of other inorganic ions, such as sodium, chloride, potassium, calcium, and magnesium. Depending on the source of the aerosol, whether it is polluted, continental or marine, the composition of the aerosol will vary. Analysing the aerosol for its inorganic ion composition can give insights into the source and even specific processes that formed the aerosols, such as indicators of biomass burning.

Sea spray aerosols primarily consist of unaltered bulk seawater (Saltzman, 2009). In terms of inorganic ions, this is dominated by sodium and chloride. The concentrations of sodium in aerosols have been used as a tracer of sea-salt aerosols. The ratio of sodium to other ions in sea water has

been used to remove the sea-salt portion of that ion in the aerosol to determine the concentration of the ion coming from other sources (Pio et al., 2007). Sodium chloride aerosols can react with nitrate or sulfate and displace the chloride as HCl gas, this results in a deficit of chloride relative to other ions from sea water (Saltzman, 2009). Chloride can also be emitted through natural and anthropogenic activities such as biomass burning, dust storms, volcanic eruptions, coal combustion and industrial emissions, although the vast majority is through sea-salt aerosols (Luo et al., 2019). Chloride in the atmosphere can react with other species to form aerosols, such as ammonium chloride (Vignati, 1999).

Potassium is naturally found in both minerals on land and in seawater, it is also a major electrolyte in the cytoplasm of plant matter (Pio et al., 2008). Therefore potassium aerosols have a large range of emission sources, such as dust, sea spray and the combustion of plant matter from natural and anthropogenic activities (wood fires, waste incineration and agricultural burning) (Andreae, 1983). The ratios of potassium to calcium, iron, sodium, and silicon have been used to remove the aerosol potassium concentrations emitted from soil dust and sea water, leaving excess potassium which is attributed to biomass burning. This allows potassium to be used as an indicator of biomass burning when determining the sources of aerosol samples (Pachon et al., 2013).

Calcium is naturally found on land and in seawater, it is also an essential element for the growth of plants (Thor, 2019). Calcium has a higher boiling point than potassium (Ca 1484 ˚C, K 759 ˚C) and won't evaporate as easily during biomass burning, but rather accumulates in ash and smoke (Popovicheva et al., 2014; Mlonka-Mędrala et al., 2020). Calcium also has several anthropogenic sources, such as construction of buildings, vehicle exhaust emissions and cement factories. Calcium can react with acidic aerosols such as SO_4^{2-} and NO_3^- forming coarse mode salts, which can enhance aerosol deposition (Henning et al., 2003).

Magnesium is present in both the land and oceans, and is a critical part in living cells (Li et al., 2001). It can be introduced into aerosol form through dust, sea spray and has been found in smoke from biomass burning (Li et al., 2003; Safai et al., 2010; Popovicheva et al., 2014). Magnesium aerosols have fewer anthropogenic sources in the forms of coal combustion and metal production (Popescu & Ionel, 2010; Klouda, Brdka & Othal, 2012).

1.5 AEROCE and other tower sites

Coastal sites have been established worldwide for monitoring the marine atmosphere. Different programs have been focused on different aspects, with the Atmospheric/Ocean Chemistry Experiment (AEROCE) being one of the largest programs. AEROCE was established as a coordinated multi-institutional research program on atmospheric and ocean chemistry in the

North Atlantic. AEROCE used atmospheric sampling stations in Barbados (West Indies), Bermuda, Mace Head (Ireland), and Tenerife (Canary Islands) (Levy, 1988). AEROCE investigated the climatology of background tropospheric ozone and the oxidising capacity of the atmosphere. It monitored aerosol chemical and physical properties (specifically for nitrogen and sulfur species from combustion, and trace metal and mineral aerosols) and their sources and sinks. AEROCE explored the role of aerosols in influencing climate as well as the chemical air/sea exchange (Levy, 1988; Savoie, 2001). The North Atlantic Ocean was chosen as the study region as, at the time, it was the oceanic region most likely affected from the atmospheric transport from continents. The Bermuda site was extremely important for this as it receives quite clean marine air from the central North Atlantic Ocean as well as natural and polluted continental air from North America, Africa, and Europe (Savoie, 2001).

The data generated through the AEROCE program has provided insights into its main focus as well as other research areas. The program recorded the large-scale spatial and temporal variability (daily, seasonally, interannually) of precipitation, aerosols, and gases of interest over the North Atlantic Ocean, this data set has been used for analysing large-scale transport models (Penner et al., 2001; Prospero, 2001). The data has also been used to ground truth and calibrate satellite sensors and is used as part of the NASA Global Aerosol Climatology Project (Prospero, 2001). AEROCE setup a network of several ozonesonde sites that has given the ozone distributions of the North Atlantic Ocean over multiple years, this provides insight into the variability and importance of different sources over the region (Oltmans et al., 1996). This has allowed the characterization of the meteorological mechanisms and seasonal meteorological conditions that explain the observed vertical and horizontal distributions and transport of ozone and other pollutants over the North American east coast and the North Atlantic Ocean (Moody et al., 1995; Prados et al., 1999). The dust data generated from AEROCE, and other sites from around the world, were used alongside satellite data to provide information on the global sources of dust and the processes that influence dust mobilization, which has been used to setup and validate models (Ginoux et al., 2001). The dust deposition data generated by AEROCE served as a foundation for the hypothesis that African dust has greatly affected the nitrogen cycle by providing iron to nitrogen fixing organisms in the North Atlantic Ocean (Michaels 1996). Deep-sea sediment traps found the dust deposition in the Sargasso Sea (near Bermuda) to be consistent with the atmospheric dust loadings that were measured at Bermuda, with differing seasonal variations due to surface water biological activity, and annual variations in the sediment traps due to variations in efficiency of atmospheric transport of dust from the source as opposed to the variations in the strength of the source (Jickells et al., 1998). Dust has been found to be the major light scattering aerosol over a

large area of the North Atlantic Ocean, which can have a large influence on radiative processes (Maring et al., 2000). The radiative forcing of dust has been extrapolated over large areas using combined ground-based and satellite measurements (Díaz et al., 2001). Dust transported from Africa to the United States will increase the loading of particles of $PM_{2.5}$, and could have implications on air-quality and exceed the Environmental Protection Agency $PM_{2.5}$ ambient air quality standard (Prospero, 1999).

Mace Head (Ireland) was a site in the AEROCE program that has also become a Global Atmosphere Watch station. Aerosol measurements were first taken at this site in 1958 and it has since grown to be one of the most crucial sites for marine atmospheric research in the northern hemisphere ("History of Mace Head", n.d.). Mace Head has been extensively used for numerous national and international research projects. The research station has grown with laboratories and a 20 m sampling tower being constructed. The sampling equipment and methods have also improved over time. For example, sampling criteria to sample clean marine air masses have improved, first by being sector-controlled and then having cut offs for total particle number concentration and black carbon concentration (O'Dowd et al., 2014).

Mace Head has been used as a research station for several decades and it has served as a staging ground for numerous research projects. The continuous long-term measurements made at Mace Head have explained seasonal cycles in aerosol properties as well as some medium-term trends. Some of the focused research projects main findings summarized by O'Connor, Jennings & O'Dowd, (2008) include: The background marine aerosols have a significant seasonal cycle with sea salt dominant in winter and the summer submicron size being dominated by biogenic organic aerosols. Nss-sulfate is present year round, with a maximum in summer, but generally does not dominate the submicron aerosol mass (Yoon et al., 2007). The organic aerosol has a water soluble component, attributed to secondary aerosol creation processes, and a water insoluble component, attributed to organic enhancement in the primary emitted sea-spray aerosol (Ceburnis et al., 2008). Detected regular coastal nucleation bursts with iodine oxide identified as the main candidate for particle nucleation and growth at nm scales, with condensation of organic vapours and sulfuric acid contributing to further growth (O'dowd et al., 2002; Vaattovaara et al., 2006). Sea-spray fluxes occur at all times and have a strong contribution to the aerosol optical depth (AOD) which range from 0.05 at low wind speeds and ~0.4 at high wind speeds (18 m/s). The upper end of this range is comparable to those found in polluted air (Mulcahy et al., 2008). Anthropogenic produced sulfate can be transported over long ranges and accounted for 85-90% of the nss-sulfate from the marine sector between 1988-1991 (Savoie, 2002). Long range transport

of aerosols were also detected due to emissions of forest fires in Canada that influenced the CO and black carbon (BC) measurements at Mace Head (Forster et al., 2001).

2. Methods

The goal of the sampling campaign was to measure the major ion concentrations of aerosols collected at Cape Point. Two different sampling systems were used to collect aerosol samples. Contextual data and HYSPLIT air mass back trajectories were used to classify the aerosol samples by the regions that the air masses were influenced by. A sector-controller was installed to reduce the continental influenced air masses from being sampled. The sections below go into further detail to explain the region, sampling systems, chemical analysis, sample classification, and the operation of the sector-controller.

2.1 Study site

The World Meteorological Organisation established the Global Atmosphere Watch programme in 1989 by consolidating two existing atmospheric observing networks, the Global Ozone Observing System and the Background Air Pollution Monitoring Network, which have existed since the 1950's and 1960's. The GAW programme obtains data from 31 global stations and over 400 regional stations, with additional satellite data providing near global coverage ("GAW stations network and other measurements | World Metereological Organization", n.d.). The main focal areas for GAW are the long-term observation of aerosols, atmospheric deposition, greenhouse gases, ozone, specific reactive gases, and UV radiation. Many of these focal areas have social and economic impacts on climate, weather, water supply, water quality, agricultural production, and human and ecosystem health. GAW studies provide insight into earth system interactions and how atmospheric chemistry responds to natural and anthropogenic changes. The data from monitoring programmes, such as GAW, are vital in the implementation of policies, the creation of international agreements, and the assessment of the effectiveness of these schemes ("Background and History | World Metereological Organization", n.d.).

The Cape Point GAW station, which is the only global GAW station in southern Africa, was founded in 1977 and is situated in a nature reserve 60 km south of the city of Cape Town at the southern tip of the Cape Peninsula in South Africa (Figure 2.1) (Brunke et al., 2004). The station was built on top of a cliff, 230 m above sea level, with a 30 m high tower used for air intake and mounting meteorological equipment. In 1995 a new station was built adjoining the old station ("Global Atmosphere Watch Station Information System (GAWSIS)", n.d.). The Cape Peninsula experiences a Mediterranean-type climate with moderate temperatures, dry and windy summers, and high

rainfall during winter. The dominant wind direction at Cape Point alternates between southwest, south, and southeast, therefore the station receives predominantly marine air masses from the South Atlantic and Southern Ocean (Figure 2.1) ("Global Atmosphere Watch Station Information System (GAWSIS)", n.d.; Brunke et al., 2004) .

The Cape Point GAW station measures a large variety of meteorological variables that provide data for several projects and organisations. Weather predictions make use of measurements of wind speed and direction, temperature, atmospheric pressure, and relative humidity ("Global Atmosphere Watch Station Information System (GAWSIS)", n.d.). Measurements of longwave and shortwave radiation are used to study temporal variations of incoming radiation, as well as the chemical and physical processes that may alter incoming radiation. The physical and chemical properties of aerosols (i.e., chemical composition, optical properties, and number concentration) have implications for the absorption and scattering of radiation, cloud condensation nuclei, and human and ecosystem health (Calvo et al., 2013; Erisman et al., 2013). The physical and chemical properties of aerosols measured at Cape Point include fine organic carbonaceous material, aerosol absorption optical depth, light coefficients of absorption, backscattering and scattering, multiwavelength optical depth, and number concentration. In addition, measurements of trace gases, such as ozone, methane, carbon dioxide, nitrous oxide, nitrogen dioxide, sulfur dioxide, and volatile organic compounds, are important for the study of chemical processes occurring in the atmosphere, including the absorption of incoming UV radiation, greenhouse effects, and the formation of secondary atmospheric compounds ("Global Atmosphere Watch Station Information System (GAWSIS)", n.d.). Radionuclide concentrations are used to identify the length of time that an air mass has been exposed to a certain natural source ("Global Atmosphere Watch Station Information System (GAWSIS)", n.d.). The Cape Point GAW station provides data that offers valuable insight into many different processes with far-reaching implications. This makes the Cape Point GAW station an ideal site for extended field campaigns as there is a wealth and long history of contextual atmospheric and climatic data.

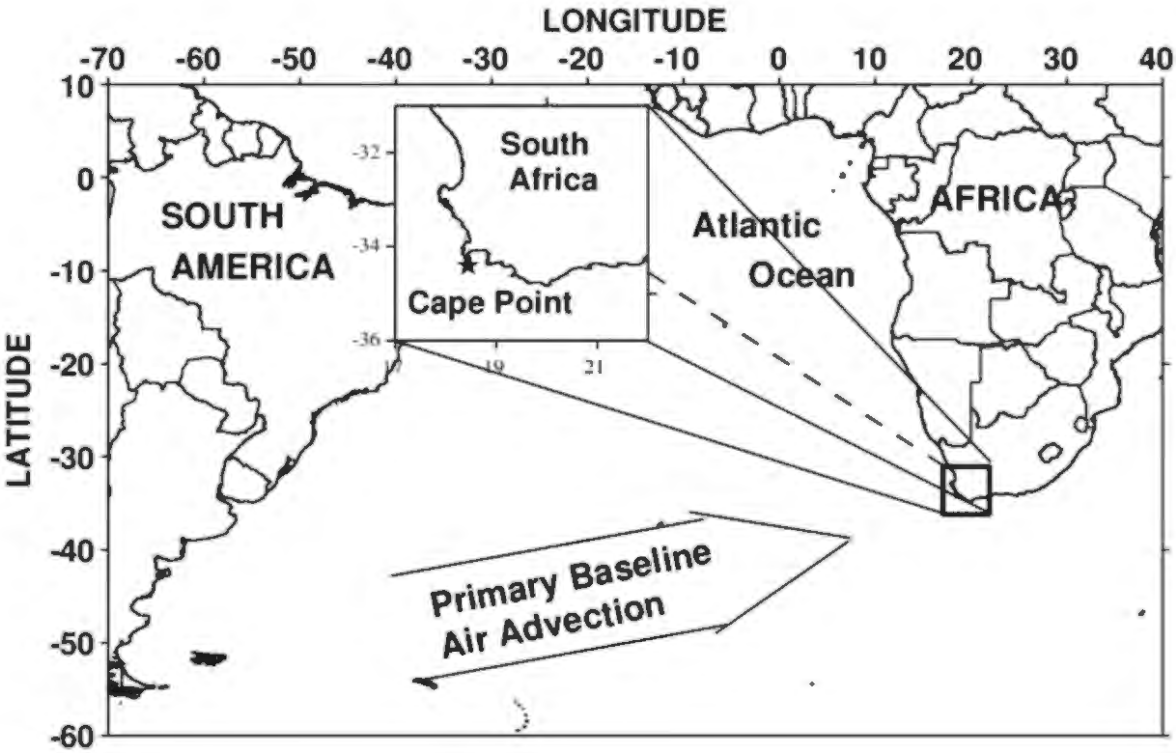

Figure 2.1: Location of Cape Point GAW station and dominant wind direction (Brunke et al., 2004)

2.2 Aerosol collection

2.2.1 Tall-tower PM_{10}

At the Cape Point GAW station, air is sampled from the top of the 30 m tower. The sampling setup was custom built by NOAA (National Oceanic and Atmospheric Administration). The sampling line has a high-volume turbulent flow (~275 CFM (Cubic Feet per Minute)), through a 250 mm pipe down the tower, produced by an Ametek Windjammer blower fan at the base of the pipe. From this high-volume flow, a carbon-vane pump draws 5 CFM through a 5-way splitter (each line drawing 1 CFM). One of these lines passes through a cyclonic size cut for 10 µm and is sampled for aerosols in the coarse mode (PM_{10}, particles ≤ 10 µm). The filters for collecting the aerosol samples are located inside the laboratory at the base of the tower and are in front of any flow devices, such that aerosols are not perturbed by pumps or the Gallus volumetric gas counter before being sampled. All the tubing from the base of the 250 mm intake tube is 1 inch stainless steel and non-conductive tubing. The samples were collected onto TE-G653-47 47 mm diameter glass fibre filters (GFF; from Tisch Environmental) that were pre-combusted at 450 ˚C for 4 hours. The clean GFFs were stored in muffled foil in zip lock bags until they were ready to be deployed. All steps in placing, removing, and analysing filters were done with gloves to minimize contamination. Combusted foil was used as a clean working surface and the forceps and filter

holders were wiped with Kimwipes and ethanol. The filters were stored at -20˚C at the Cape Point laboratory until they were transported to the University of Cape Town (UCT) Marine Biogeochemistry Laboratory (MBL) and stored at -20˚C prior to analysis (detailed below in Section 2.3.1). The sampling campaign for this study ranged from 19 June 2017 to 24 August 2018 (Table 2.1). The samples were collected twice a week from 19 June 2017 to 05 July 2018, with the exception of an intensive sampling period from 13 May 2018 to 17 May 2018 where samples were collected daily (i.e., every 24 hours). The sector-controller (Section 2.6) was installed on 05 July 2018, after which samples were collected weekly.

Table 2.1: Dates, durations, and different sampling conditions of the campaign

Dates	Tall-tower PM_{10}	Ground-based HVAS	Sector-controller	Intensive campaign	PM_{10} Field blanks	HVAS Field blanks
19/06/2017 - 19/04/2018	X				21/09/2017	
19/04/2018 - 13/05/2018	X	X				
13/05/2018 - 17/05/2018	X	X		X		15/05/2018
17/05/2018 - 05/07/2018	X	X			21/06/2018	21/06/2018
05/07/2018 - 24/08/2018	X	X	X		24/08/2018	24/08/2018
24/08/2018 - 30/08/2018		X		X		
30/08/2018 - 05/11/2018		X	X			
05/11/2018 - 10/11/2018		X		X		

2.2.2 Ground-based, size-segregated cascade impactor

A mass flow controlled high volume air sampler (HVAS) (Tisch Environmental TE-5170X) was installed at the base of the sampling tower at the Cape Point GAW station. Samples were collected from 19 April 2018 to 10 November 2018, note that these dates are different than for tall-tower PM_{10} (Table 2.1). The samples were collected a) twice a week before the sector-controller was installed, b) once a week under the sector-control, and c) intermittently during intensive sampling periods, where the sampling frequency was altered and sector-control was turned off, from 13 May 2018 to 17 May 2018, 24 August 2018 to 30 August 2018, and 05 November 2018 to 10 November 2018. The HVAS used a five-stage cascade impactor (Tisch Environmental TE-235) to hold the sampling filters. Filters used were TE-230-GF (Tisch Environmental) glass fibre slotted collection substrates for stages 1-5 and TE-G653 (Tisch Environmental) 8” x 10” glass fibre filters for the back-up filter. These filters were combusted at 450 ˚C for 4 hours before use. The cascade impactor segregates the aerosols into different size fractions according to the following cut off sizes at a flow rate of 40 CFM, from stage 1 to stage 5: > 7.2 µm > 3.0 µm > 1.5 µm > 0.95 µm > 0.49 µm, with the back-up filter sampling everything < 0.49 µm (“HiVol Cascade Impactors - Tisch

Environmental", n.d.). Stages 1-4 were summed to the coarse mode fraction (defined as > 1 µm) and stage 5 and back-up filter were summed to get the fine mode fraction (defined as < 1 µm). The HVAS has a chart recorder that records the flow rate and an elapsed time indicator that counts how long the HVAS was operational. The clean GFFs were stored in muffled foil in zip lock bags until they were ready to be deployed. All steps in placing, removing, and analysing filters were done with gloves to minimize contamination. Combusted foil was used as a clean working surface and the forceps and cascade impactor were wiped with Kimwipes and ethanol. The filters were stored at -20˚C at the Cape Point laboratory until they were transported to the University of Cape Town (UCT) Marine Biogeochemistry Laboratory (MBL) and stored at -20˚C prior to analysis (detailed below in Section 2.3.1).

The HVAS was calibrated after installation with a HVAS calibrator (Tisch Environmental TE-5028). The calibration data were used to accurately calculate the volume of air sampled, along with the recorder chart, temperature, and pressure data for each sample. The volume of air sampled is required to calculate the concentration of the aerosols. To calibrate the HVAS, a new recorder chart was placed in the recorder, the calibrator was mounted to the intake of the HVAS and connected to a water manometer. The calibrator was slightly opened or closed and the response on the recorder chart and the manometer was recorded. This was repeated at least five times. The date, the time, the location, the ambient air temperature, and ambient barometric pressure were also recorded. The readings, the temperature and the pressure data were added to the calibration worksheet (Tisch Environmental). The standard flow rate and the corrected chart response for each measurement of the calibration are used in a linear regression to calculate the slope, intercept, and correlation coefficient. A correlation coefficient of at least 0.990 is required for a good calibration ("(30) Calibration and Operation of a High Volume Mass Flow Controlled Ambient Particulate Sampler - YouTube", n.d.). Two calibrations were performed, on 11 June 2018 and 09 September 2018, (Appendix Figure A1 and A2) they had correlation coefficients of 0.9992 and 0.9996, their slopes were 54.5966 and 54.5154, and their intercepts were 6.0495 and 6.1477. This leads to a difference of 0.6% between the calculated flow rates and shows that the calibration did not vary much over time.

2.2.3 Field blanks

Field blanks were taken using the procedure described above to place and remove GFFs, but without turning the vacuum pumps or the HVAS on. The field blanks were treated the same as samples. Field blanks were taken to determine possible sources of contamination from the transport and handling at the GAW station as well as possible contamination during the analysis. Field blanks for the tower sampling system (PM_{10}) were taken on 21 September 2017, 21 June

2018, and 24 August 2018. Field blanks for the HVAS were taken on 15 May 2018, 21 June 2018, and 24 August 2018. Field blanks were quantified for all major ions (Na^+, NH_4^+, K^+, Mg^{2+}, Ca^{2+}, Cl^-, NO_3^- and SO_4^{2-}). The average concentrations for the field blanks are in Table 2.2 (PM_{10} and HVAS, average concentrations for HVAS field blanks for each stage in Appendix Table A1). All sample results (Section 3) were corrected using their respective field blank values (i.e., PM_{10} samples were corrected using PM_{10} field blanks; further detail on field blank correction in Section 2.3.4). The NH_4^+, NO_3^-, and SO_4^{2-} concentrations were of particular interest for this study due to their natural and anthropogenic sources and were therefore the main focus for the concentration range of the standard curve prepared. The concentrations of K^+, Mg^{2+}, and Ca^{2+} were of similar orders of magnitude to NH_4^+, NO_3^-, and SO_4^{2-} and were therefore covered in the standard curve used. It should be noted that the blanks as well as the samples had much higher concentrations of Na^+ and Cl^- than the other ions. Therefore Na^+ and Cl^- were outside of the range of the standard curve and the concentrations are known with less accuracy. This may impact the accuracy of the non-sea-salt sulfate (nss-SO_4^{2-}) concentration as it uses the Na^+ concentration to calculate nss-SO_4^{2-} (Section 2.3.4, equation 3). The samples were not run on a higher standard curve, with a focus on Na^+ and Cl^-, due to limited surface area of the tall-tower PM_{10} samples and time limitations.

Table 2.2: Average concentration of major ions (nmol/filter) in the tall-tower PM_{10} and ground-based HVAS field blanks (standard deviation in parenthesis).

	Na^+	NH_4^+	K^+	Mg^{2+}	Ca^{2+}	Cl^-	NO_3^-	SO_4^{2-}
Tall-tower PM_{10}								
PM_{10}	1759.0 (213.0)	40.5 (22.0)	135.1 (35.9)	10.9 (5.6)	41.3 (24.5)	880.2 (328.8)	216.5 (86.7)	27.7 (8.2)
Ground-based HVAS								
Coarse mode	44363.5 (5879.1)	599.0 (81.4)	2782.6 (449.1)	181.3 (38.4)	950.4 (174.8)	14834.5 (3978.9)	1268.3 (396.8)	246.7 (90.0)
Fine mode	50888.6 (5959.5)	490.3 (65.1)	2806.9 (341.1)	172.4 (26.2)	802.0 (192.6)	20236.9 (4282.8)	1038.0 (528.9)	138.2 (149.3)

2.3 Aerosol chemical composition analysis

2.3.1 Aerosol extraction

When extracting the filters, all sample handling was done inside a laminar flow cabinet (Air Science). All surfaces and items were wiped with Kimwipes and ethanol before encountering any samples. Care was taken when handling the sample filters to only touch the edges of the filters as the edges do not contain any sample and are not extracted. For tall-tower PM_{10} and the cascade impactor back-up filter, the circle cutter was used to remove a 1.38 cm diameter circle of the filter

for analysis. For the slotted filters (cascade impactor stages 1-5), ceramic scissors were used to cut a section of the filter. This section was accurately measured using a set of Vernier calipers. The sampled section of the filter was then placed in an acid washed centrifuge tube. A carefully measured aliquot of Milli-Q water was added to the centrifuge tubes. The centrifuge tubes were then placed in an ultrasonic bath (Bransonic, M1800-E) and sonicated for one hour. After sonication, the centrifuge tubes were placed in a refrigerator at 4˚C for at least 12 hours. The samples were then filtered through a 0.2 µm filter into an acid washed HDPE bottle. The extracts were then analysed using a colorimetric method or Ion Chromatography (Sections 2.3.2 and 2.3.3).

2.3.2 Ammonium colorimetric method

The colorimetric method for measuring NH_4^+ concentrations was used alongside Ion Chromatography as the coastal aerosols have a high salt content, and the Na^+ peak in the ion chromatogram can obscure the NH_4^+ peak. Standards and the extracts from the samples and field blanks were analysed for NH_4^+ concentrations using the Holmes fluorometric method (Holmes et al., 1999). Gloves were worn during all steps of collection and analysis to minimize contamination.

Standard solutions of known concentrations were prepared every day that samples were analysed. The standards were made up from a primary ammonium chloride (NH_4Cl) standard of 100 µM, that was made up from a mother stock of 10 mM. The standards made had concentrations that were chosen to cover the expected sample concentration range (0-40 µM). Standards and sample extracts were poured into 'aged' HDPE bottles (i.e., bottles stored with the orthophthaldialdehyde (OPA) working reagent to remove any NH_4^+ present) after first rinsing with the standard or sample.

OPA working reagent was added to the sample extracts and standards using a dispensette, in a ratio of 1:5 v/v (OPA:Sample). Samples were stored in the dark for 2-4 hours to react, allowing them to reach maximum fluorescence. The relative fluorescence units (RFU) were measured using a Trilogy Fluorometer with a UV module. The cuvette for the fluorometer was rinsed multiple times with Milli-Q water and once with the sample before filling the cuvette with the sample and taking two readings, with care being taken to ensure it stayed clean and dry. This was repeated with the same sample for a second set of readings, before starting with the next sample. Milli-Q water was measured at random intervals throughout the analysis process to ensure that the cuvette did not get scratched or dirtied and the instrument did not drift. Approximately 10% of the sample filters were extracted in duplicate. Standard curves were used to calculate the NH_4^+ concentrations of the samples, by plotting the RFU of the standards against the concentrations of the standards. Due to the large difference in concentrations between samples two standard

curves were used. A straight line for the lower concentration range (0-10 µM) and third order polynomial for the higher concentration range (10-40 µM). The RFU of the samples were then used to determine their concentration. The standard curves had at least 5 points and an R^2 value of at least 0.9 to be acceptable. Some of the samples had higher concentrations than expected and were not covered by the concentration range of the standard curve. These samples were run again with a modified standard curve.

2.3.3 Ion chromatography

Aerosol extract samples were analysed using two Dionex Aquion Ion Chromatography systems (IC) (Thermo Scientific), one for the analysis of anions and one for the analysis of cations. The anion IC contains a guard column (AG22 RFIC 4x50 mm), and an analytical column (AS22 RFIC 4x250 mm). The baseline signal is enhanced by suppressing eluent conductivity signal with the ADRS 600 4 mm RFIC ERS suppressor. A solution of 4.5 mM sodium carbonate and 1.4 mM sodium bicarbonate were used as an eluent with a flow rate of 1.2 mL/min. The anion IC was calibrated using a seven ion standard containing fluoride, bromide, chloride, nitrite, nitrate, sulfate and phosphate (Dionex Seven Anion Standard II). The standards were made up by diluting the stock seven ion standard in dilutions of 1/5000, 1/1000, 1/500, 1/100, 1/50 and a Milli-Q water blank. The cation IC contains a guard column (CG12A-5µm RFIC 3x30 mm), and an analytical column (CS12A-5µm RFIC 3x150 mm). The baseline signal is enhanced by suppressing eluent conductivity signal with the CDRS 600 4 mm RFIC ERS suppressor. A 20 mM methansulfonic acid solution is used as an eluent with a flow rate of 0.5 mL/min. The cation IC was calibrated using a six ion standard containing lithium, sodium, ammonium, potassium, magnesium, and calcium (Dionex Six Cation-II Standard). The standards were made up by diluting the stock six ion standard in dilutions of 1/10000, 1/5000, 1/1000, 1/500, 1/100 and a Milli-Q water blank. 1500 µL of samples and standards were injected into the IC's with a Dionex AS-DV autosampler from Thermo Scientific. The autosampler vials were rinsed three times with Milli-Q water, then rinsed with sample/standard before being filled with the sample/standard and capped. The standards were made up on the day that samples were analysed. The ICs and the autosampler are controlled by a dedicated computer with Chromeleon software (v 7.2.10) that can identify the sample peaks, plot the standard curves, and calculate the concentrations of the different ions in the samples. Average R^2 values for each ion are as follows: Na^+ 0.9995, K^+ 0.9999, Mg^{2+} 0.9999, Ca^{2+} 0.9999, Cl^- 0.9978, $N0_3^-$ 0.9987, and SO_4^{2-} 0.9993.

2.3.4 Aerosol concentration calculations

The concentration of the aerosol extract solution was determined through either colorimetric methods or through Ion Chromatography. This concentration was multiplied by the volume of

Milli-Q that was used to extract the sample, to calculate the number of moles of analyte in the solution. The number of moles in the solution came from the filter cut and possible sources of contamination, such as the Milli-Q water and the sample solution container. The area of the filter extracted was used to calculate the number of moles per square centimetre, which was extrapolated to the size of the sampling area on the filter. This was used as the total number of moles on the filter (equation 1). The total number of moles on the field blank filter was subtracted from the total number of moles on the sample filter. This gave the total number of moles of each ion per aerosol sample excluding the filter itself or any contamination that may be present that was not from the atmospheric aerosol. The total number of moles of the sample divided by the volume of air that had passed through the filters were used to calculate the atmospheric concentration of the aerosols (equation 2; nmol/m^3). Ions that had negative concentrations after having the field blank concentration subtracted from them were set to zero. Concentrations that are zero represent values that are below the method detection limit.

Equation 1:

$$Filter\ moles\ (nmoles) = \frac{Solution\ concentration\ \left(\frac{nmoles}{L}\right) * Solution\ volume\ (L) * Filter\ total\ area\ (cm^2)}{Filter\ extract\ area\ (cm^2)}$$

Equation 2:

$$Aerosol\ Concentration\ \left(\frac{nmol}{m^3}\right) = \frac{Sample\ filter\ moles\ (nmol) - Field\ blank\ filter\ moles\ (nmol)}{Volume\ air\ sampled\ (m^3)}$$

Non-sea-salt sulfate (nss-SO_4^{2-}) was calculated (equation 3) by converting the molar concentrations of Na^+ and SO_4^{2-} to their weight by multiplying them by their atomic mass (22.989769 g/mol and 96.06 g/mol respectively). The [Na^+] is then multiplied by the mass ratio of SO_4^{2-}/Na^+ in sea water (0.2516 (Millero, 2013)) to determine the amount of SO_4^{2-} coming from seawater. The seawater SO_4^{2-} is subtracted from the total SO_4^{2-} to give the nss-SO_4^{2-}, this is then divided by the atomic mass to convert it back to the molar concentration.

Equation 3:

$$\mathrm{nss} - \mathrm{SO_4^{2-}}\left(\frac{nmol}{m^3}\right) = \frac{\left([SO_4^{2-}]\left(\frac{nmol}{m^3}\right) * 96.06\left(\frac{g}{mol}\right)\right) - \left([Na^+]\left(\frac{nmol}{m^3}\right) * 22.989769\left(\frac{g}{mol}\right) * 0.2516\right)}{96.06\left(\frac{g}{mol}\right)}$$

2.4 HYSPLIT air mass back trajectory

Air mass back trajectories were computed for each aerosol sample using NOAA's Hybrid Single-Particle Lagrangian Integrated Trajectory (HYSPLIT v4) with NCEP Global Data Assimilation System (GDAS) output. HYSPLIT uses a simple particle dispersion simulation and meteorological data to compute air parcel trajectories. Back trajectories were run for each hour when the filter was deployed. When the sampling was sector-controlled (discussed below in Section 2.6), the air mass back trajectories were calculated every hour that the pumps were running for at least 45 min of the hour. The PySPLIT (Cross, 2015) package in Python was used to generate and plot the HYSPLIT air mass back trajectories. NH_4^+ aerosols have a lifetime in the atmosphere of 3.2 to 4.2 days (Xu & Penner, 2012)(Adams, Seinfeld & Koch, 1999). NO_3^- aerosols have a lifetime in the atmosphere of about 3.9 days (Xu & Penner, 2012). Given the lifetime of the atmospheric aerosols of interest (i.e., NO_3^- and NH_4^+), 5 days was considered a sufficient length of time for the air mass back trajectories. Scarchilli, Frezzotti & Ruti, 2011 also used 5 day HYSPLIT air mass back trajectories and found that the uncertainties, from both the resolution of the meteorological dataset and the numerical truncations in the calculation algorithm, resulted in a total error of 15-30 % of the total travel distance of the airmass. Therefore, longer air mass back trajectories have greater total errors. The HYSPLIT air mass back trajectories identify the regions that the air masses passed over before reaching the sampling location.

2.5 Auxiliary data from the GAW station

2.5.1 Radon (^{222}Rn)

Radon is a radioactive gas produced through the radioactive decay of radium. Radium is found in many rocks and when it decays to ^{222}Rn it is released to the atmosphere. ^{222}Rn is the most stable isotope of radon and it has a half-life of 3.8 days (Brunke et al., 2004). ^{222}Rn in air can be used as a signature of land contact of said air mass. In marine air ^{222}Rn decays to very low concentrations (1 – 2 orders of magnitude less) due to its relatively short half-life (Brunke et al., 2004). This makes the ^{222}Rn concentration an ideal tool to separate out marine and terrestrial signals. The Australian Nuclear Science and Technology Organisation (ANSTO) designed and built a 1500 L dual flow loop two filter radon detector that was installed at the Cape Point GAW station in 2011. It has monthly calibration checks and every 3 months sample flow is shut off to evaluate the instrumental background reading. The detector records data as 30-minute average readings. The ^{222}Rn concentration is measured continuously at the Cape Point GAW station as part of a long-term analysis of trace gases found in the air originating from remote environments (Brunke et al., 2004). These data were made available by the South African Weather Service (SAWS) for this project.

2.5.2 Temperature, barometric pressure, and relative humidity

The Cape Point GAW station routinely measures temperature, barometric pressure, and relative humidity as part of their weather service activities. The relative humidity and temperature are measured with a Vaisala 110, and barometric pressure is measured with a Vaisala PTB101, and both record 5-minute average readings. These data were made available for use for this project. Temperature and barometric pressure were used when the ground-based HVAS was calibrated, and average values were used for each sample period to accurately determine the ground-based HVAS flow rate.

2.6 Sector-controller

A sector sampling system (Campbell Scientific Africa) was installed at the Cape Point GAW station on 05 July 2018. The 03002 wind sentry anemometer and vane, manufactured by R.M Young, was mounted to an existing pole. The wind sentry has a range of 0 – 50 m/s ± 0.5 m/s wind speed and 360˚ mechanical and 352˚ electrical (8˚ open) azimuth with ± 5˚ accuracy. The signal wires from the wind sentry were wired into a CR300 data logger located in the SAWS laboratory. The data logger was connected to two relay switches, which were wired to feed power to the two different sampling systems, i.e., the ground-based HVAS and the tall-tower PM_{10}. The data logger was programmed such that it would only switch the relays and power the pumps when the wind was within a specified angle range, above 135° and less than 290° (Figure 2.2). The angle was originally set to above 130°, but this was adjusted on the 09 September 2018 after HYSPLIT air mass back trajectories showed continental air masses coming from the Cape Agulhas region still being sampled. It was programmed such that the specified conditions would need to be met for a minimum of 5 minutes before the relays would feed power to the pumps to switch on. This prevents the pumps from turning on when a gust of wind comes from the specified direction, but the major air mass still is mainly of a non-targeted source. The ability to specify the wind direction and speed to be sampled allows for targeted sampling of pure marine or continental air masses. Although a specific area will be targeted it is not necessarily truly a pure signal as air masses can circulate over land and water before being sampled from the specified sector. The air mass histories for each sample were also confirmed by using HYSPLIT air mass back trajectories and radon data.

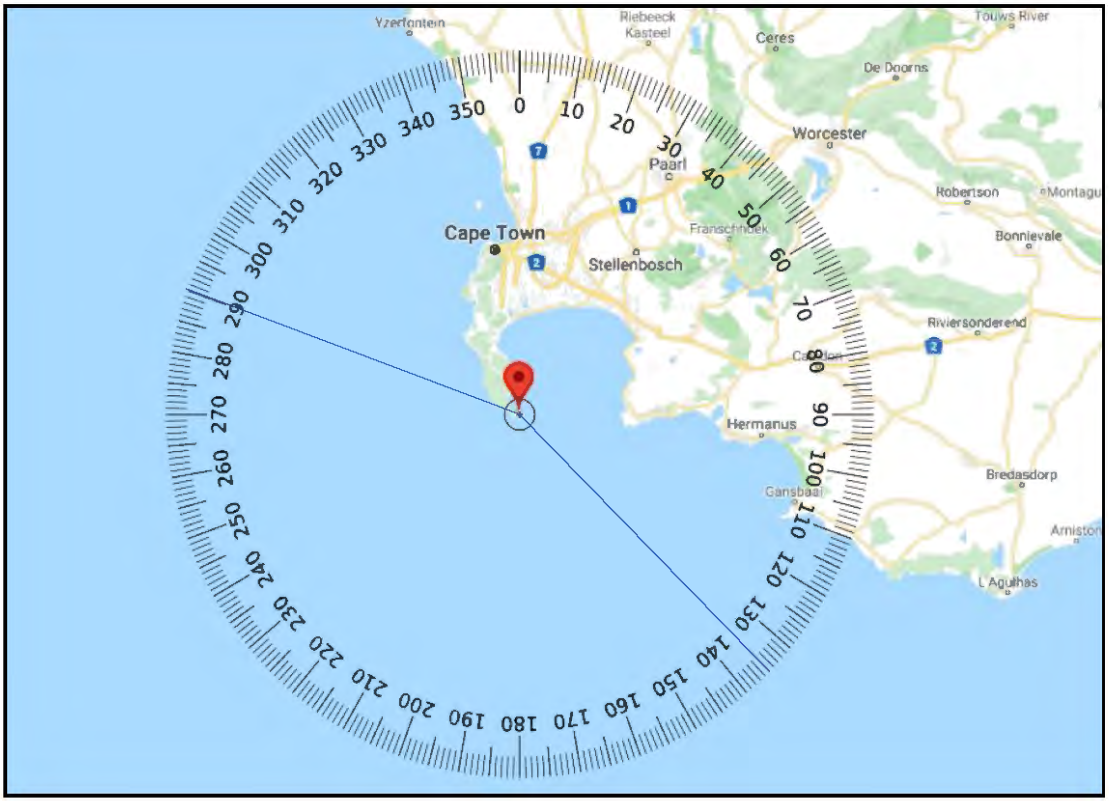

Figure 2.2: Marine sampling sector at Cape Point

3. Results

3.1 Atmospheric conditions

Atmospheric temperature and rainfall data are recorded at the Cape Point GAW station by SAWS, and have been averaged hourly for atmospheric temperature and summed to daily values for rainfall. The daily average minimum and maximum atmospheric temperatures from 2017 to 2019 (Figure 3.1A) and daily rain amounts (Figure 3.1B) are presented to provide context on the typical seasonality at Cape Point. The aerosol sampling period only covered a fraction of this time and is highlighted in the figures in grey. Seasonal variability is more pronounced than interannual variability, with the average daily maximum varying from 22.6˚C in the summer to 16.3˚C in the winter (Figure 3.1A). The difference between the daily maximum and minimum is 6.11˚C on average and is fairly consistent throughout the seasons. During the aerosol sampling periods there was a maximum temperature of 34.8˚C, a minimum temperature of 4.2˚C and an average temperature of 15.0˚C. The wind speed had a maximum of 27.2 m/s, minimum of 1.1 m/s and an average of 7.3 m/s (Appendix Figure A3). Wind direction has a distinct seasonality at Cape Point (Figure 3.2), as has been established in previous work (Brunke et al., 2004), with a dominant east/southeast wind the majority of the year and a shift to west/northwest winds during winter.

There is more interannual variability in rainfall than in temperature and wind speed, although in general rainfall is more consistent and intense in winter (Figure 3.1B).

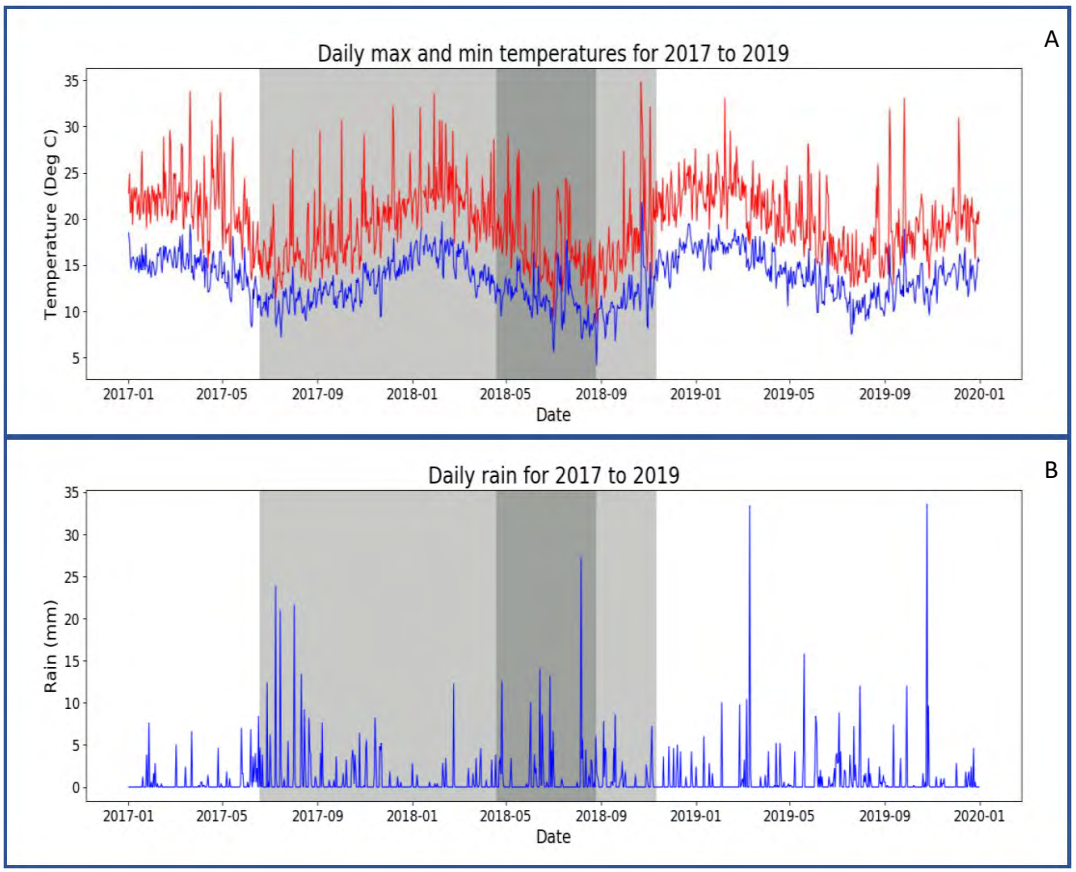

Figure 3.1: A) Daily max (red) and min (blue) temperatures, B) Daily rainfall at Cape Point from 2017 to 2019. The aerosol sampling period is highlighted in grey, the first grey block indicates tall-tower PM_{10} and then the second indicates ground-based HVAS, with the sampling overlap in darker grey.

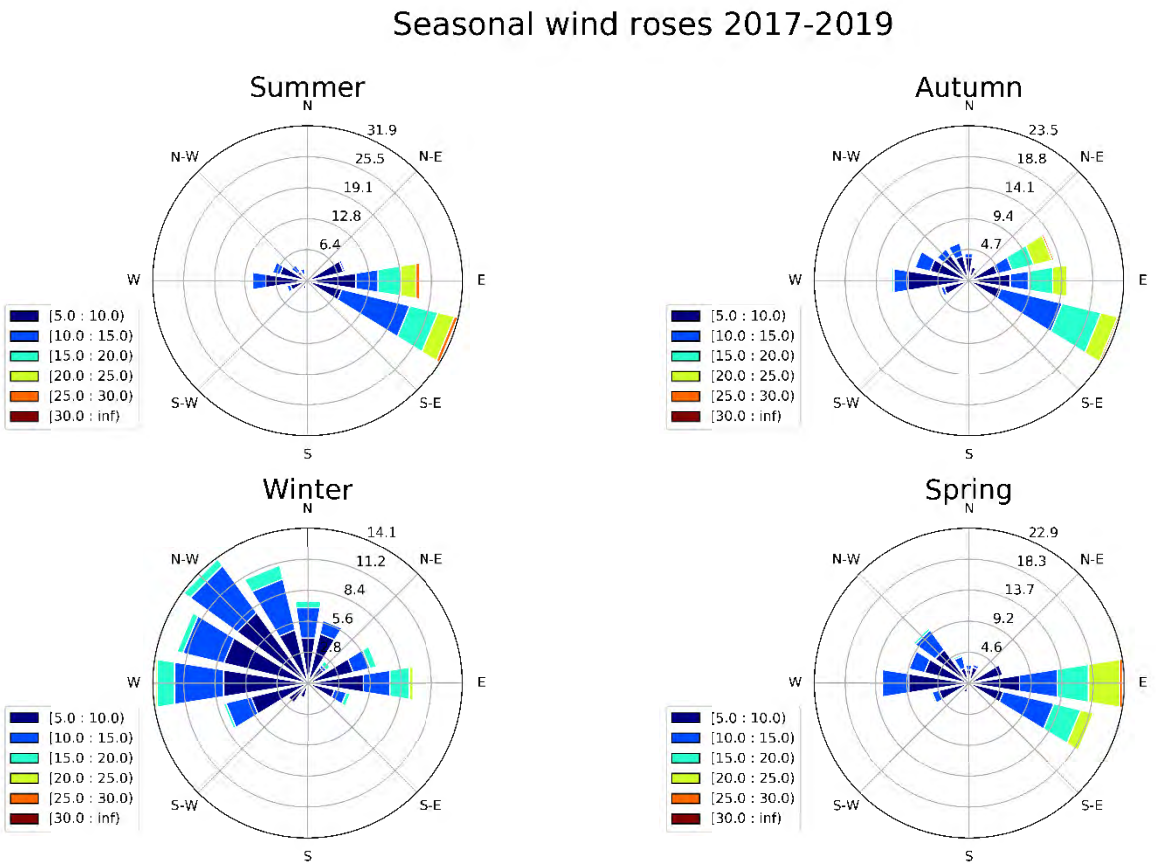

Figure 3.2: Seasonal wind roses for 2017-2019, for wind speeds greater than 5m/s.

3.2 Aerosol major ion concentrations

3.2.1 Tall-tower PM_{10}

A total of 80 samples were collected, with 73 samples collected with no air mass sector restrictions (non-sector-controlled; 19 June 2017 to 05 July 2018) across all seasons, and 7 samples collected using the sector-controller (09 July 2018 to 24 August 2018) during winter. Major ion concentrations were determined for all bulk aerosol tall-tower PM_{10} samples (Figure 3.3). Figure 3.3 below show seasonal boxplots for each of the major ions, with sector and non-sector-controlled samples shown separately. All boxplots presented are defined as follows. A box extending from the first quartile (Q1) to the third quartile (Q3) with a line at the median value. The boxes have whiskers that extend to the maximum and minimum values that are not outliers. Outliers are defined as values that are greater than 1.5 times the interquartile range (IQR, Q3-Q1) added to Q3, or less than 1.5 times the interquartile range subtracted from Q1 (outliers > (Q3 + 1.5*IQR) & outliers < (Q1 – 1.5*IQR)).

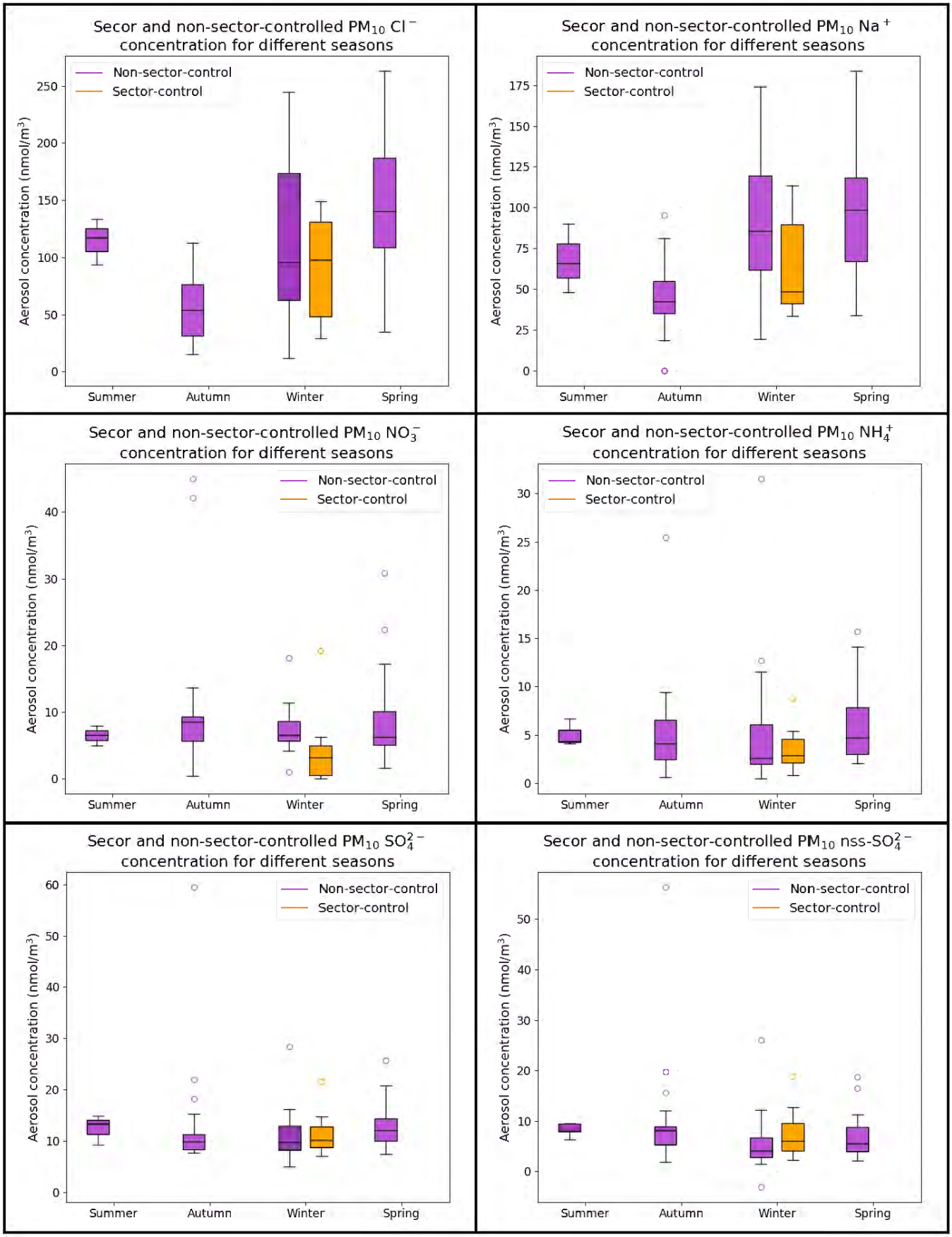

Figure 3.3: Box and whisker plots of seasonal tall-tower PM_{10} aerosol concentrations specifying sector and non-sector-controlled samples.

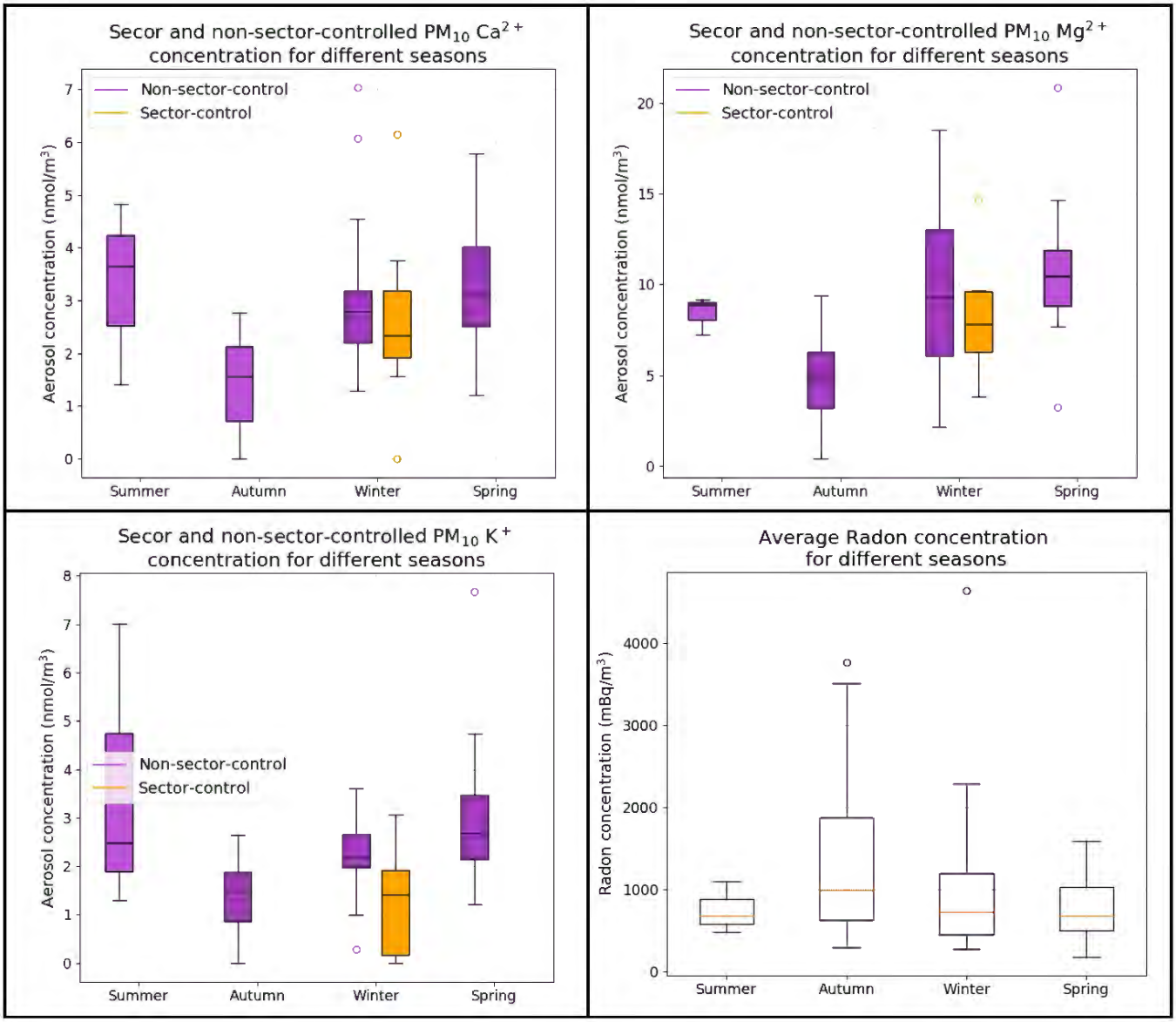

Figure 3.3 (continued): Box and whisker plots of seasonal tall-tower PM_{10} aerosol concentrations specifying sector and non-sector-controlled samples.

3.2.1.1 Non-sector-controlled

For the non-sector-controlled samples (n=73, 19 June 2017 to 05 July 2018), Na^+ ranged from 0.0 – 183.9 nmol/m^3, with an average of 76.6 nmol/m^3. The Na^+ concentrations have the highest average in spring and lowest in autumn. NH_4^+ ranged from 0.5 – 31.6 nmol/m^3, with an average of 5.1 nmol/m^3 and have the highest average concentrations in spring and lowest in summer. K^+ ranged from 0.0 – 7.7 nmol/m^3, with an average of 2.2 nmol/m^3 and have the highest average concentrations in summer and lowest in autumn. Mg^{2+} ranged from 0.4 – 20.9 nmol/m^3, with an average of 8.2 nmol/m^3 and have the highest average concentrations in spring and lowest in autumn. Ca^{2+} ranged from 0.0 – 7.0 nmol/m^3, with an average of 2.6 nmol/m^3 and have the highest average concentrations in spring and lowest in autumn. Cl^- ranged from 11.9 – 263.1 nmol/m^3,

with an average of 102.1 nmol/m^3 and have the highest average concentrations in spring and lowest in autumn. NO_3^- ranged from 0.3 – 45.0 nmol/m^3, with an average of 8.7 nmol/m^3 and have the highest average concentrations in autumn and lowest in summer. SO_4^{2-} ranged from 5.0 – 59.5 nmol/m^3, with an average of 12.1 nmol/m^3 and have the highest average concentrations in spring and lowest in winter. Nss-SO_4^{2-} ranged from -3.1 – 56.4 nmol/m^3, with an average of 7.5 nmol/m^3 and have the highest average concentration in autumn and lowest in winter (Figure 3.3).

3.2.1.2 Sector-controlled

For the sector-controlled samples (n=7, 09 July 2018 to 24 August 2018), Na^+ ranged from 33.6 – 113.5 nmol/m^3, with an average of 65.2 nmol/m^3. NH_4^+ ranged from 0.8 – 8.7 nmol/m^3, with an average of 3.7 nmol/m^3. K^+ ranged from 0.0 – 3.1 nmol/m^3, with an average of 1.2 nmol/m^3. Mg^{2+} ranged from 3.8 – 14.7 nmol/m^3, with an average of 8.3 nmol/m^3. Ca^{2+} ranged from 0.0 – 6.2 nmol/m^3, with an average of 2.7 nmol/m^3. Cl^- ranged from 29.1 – 148.9 nmol/m^3, with an average of 90.5 nmol/m^3. NO_3^- ranged from 0.0 – 19.2 nmol/m^3, with an average of 4.8 nmol/m^3. SO_4^{2-} ranged from 7.0 – 21.6 nmol/m^3, with an average of 11.7 nmol/m^3. Nss-SO_4^{2-} ranged from 2.3 – 18.8 nmol/m^3, with an average of 7.8 nmol/m^3 (Figure 3.3).

3.2.2 Ground-based high volume air sampler

A total of 33 samples were collected with 20 samples collected with no air mass sector restrictions across all seasons except summer, and 13 samples collected using the sector-controller during winter and spring. Major ion concentrations were determined for all aerosol samples (Appendix Figure A4 presents ion concentrations for individual impactor stages). Figure 3.4 below show seasonal boxplots for each of the major ions.

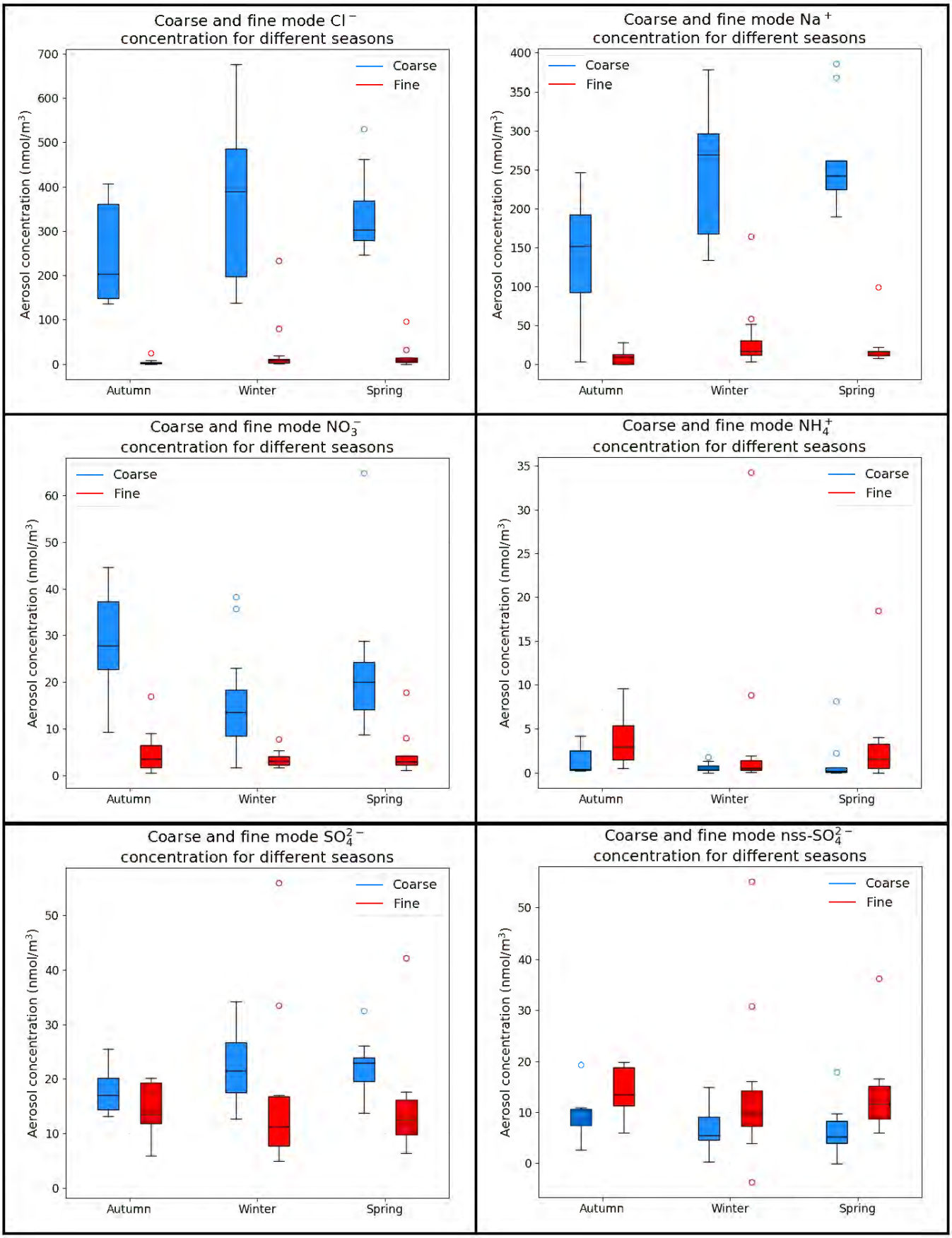

Figure 3.4: Box and whisker plots of ground-based HVAS seasonal aerosol concentrations.

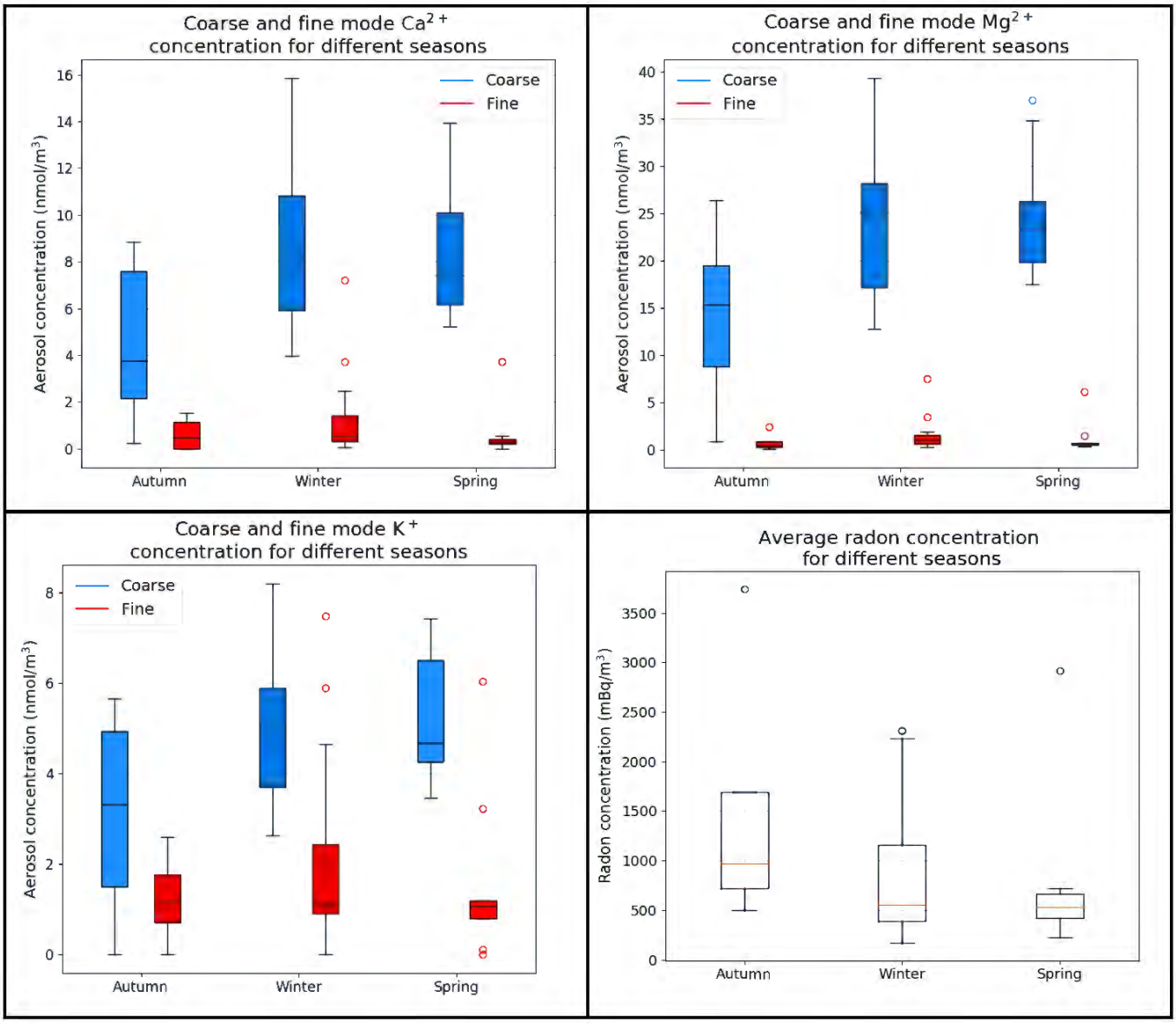

Figure 3.4 (continued): Box and whisker plots of ground-based HVAS seasonal aerosol concentrations.

3.2.2.1 Non-sector-controlled

For the non-sector-controlled ground-based HVAS samples (n=20, 16 April 2018 to 05 July 2018, 24 August 2018 to 30 August 2018, and 05 November 2018 to 10 November 2018), the total Na^+ ranged from 3.2 - 457.3 nmol/m^3, with an average of 231.2 nmol/m^3. The Na^+ concentrations are much higher in the coarse mode than in the fine mode. Total NH_4^+ ranged from 0.1 – 34.5 nmol/m^3, with an average of 5.1 nmol/m^3 and have higher average concentrations in fine mode than in the coarse mode. Total K^+ ranged from 0.4 – 9.2 nmol/m^3, with an average of 5.7 nmol/m^3 and have higher average concentrations in the coarse mode than in the fine mode. Total Mg^{2+} ranged from 1.1 – 41.2 nmol/m^3, with an average of 22.1 nmol/m^3 and have higher average concentrations in the coarse mode than the fine mode. Total Ca^{2+} ranged from 0.7 – 23.1 nmol/m^3, with an average of 7.9 nmol/m^3 and have higher average concentrations in the coarse mode than in the fine mode. Total Cl^- ranged from 141.2 – 687.6 nmol/m^3, with an average of 354.3 nmol/m^3 and have much higher average concentrations in the coarse mode than in the fine mode. Total NO_3^- ranged from 8.9 – 61.5 nmol/m^3, with an average of 24.0 nmol/m^3 and have higher average concentrations in the coarse mode than in the fine mode. Total SO_4^{2-} ranged from 22.4 – 68.6 nmol/m^3, with an average of 34.1 nmol/m^3 and have higher average concentrations in the coarse mode than in the fine mode. Total Nss-SO_4^{2-} ranged from -0.1 – 59.7 nmol/m^3, with an average of 20.4 nmol/m^3 and have higher average concentrations in the fine mode than in the coarse mode (Figure 3.5).

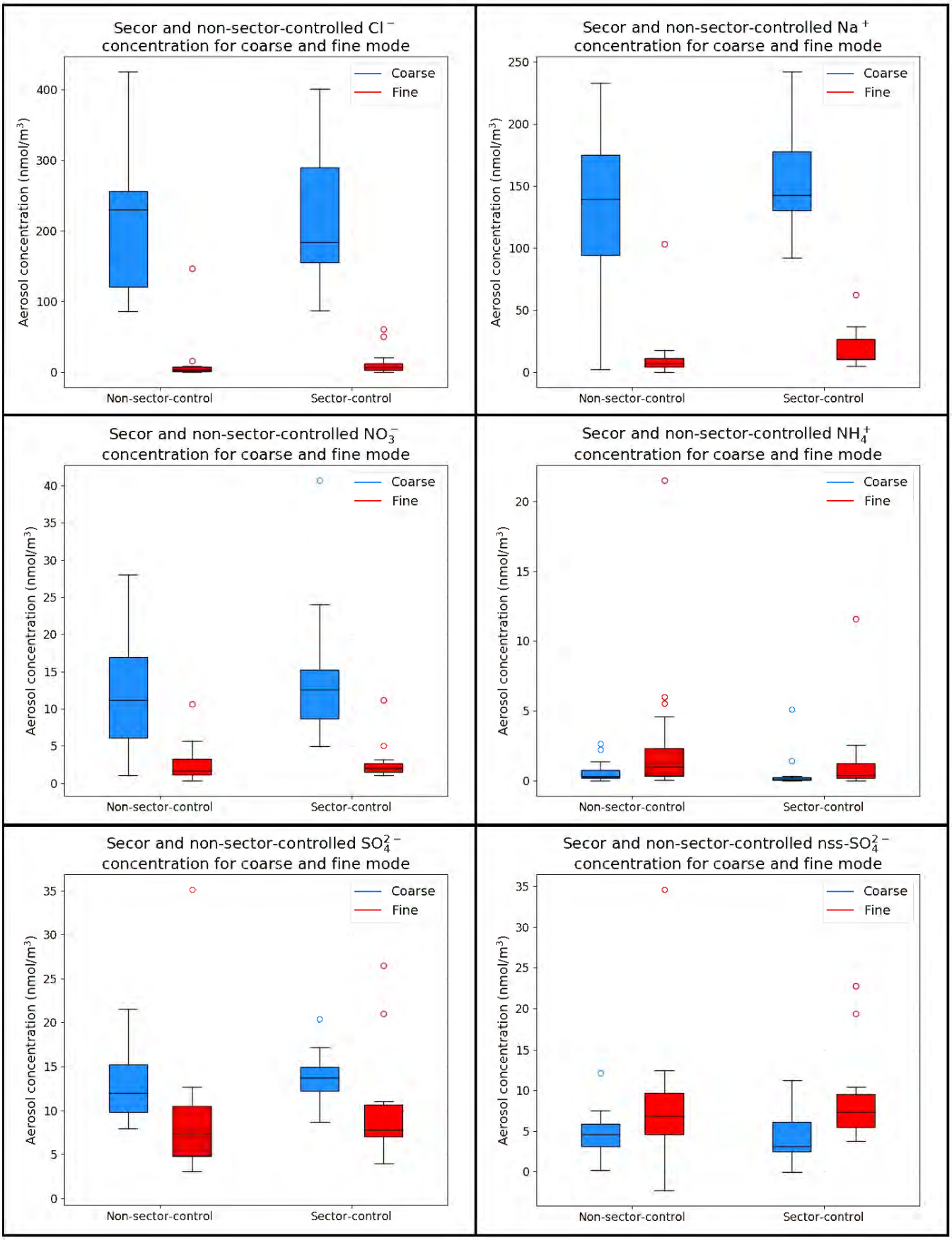

Figure 3.5: Ground-based HVAS sector and non-sector-controlled major ion concentrations.

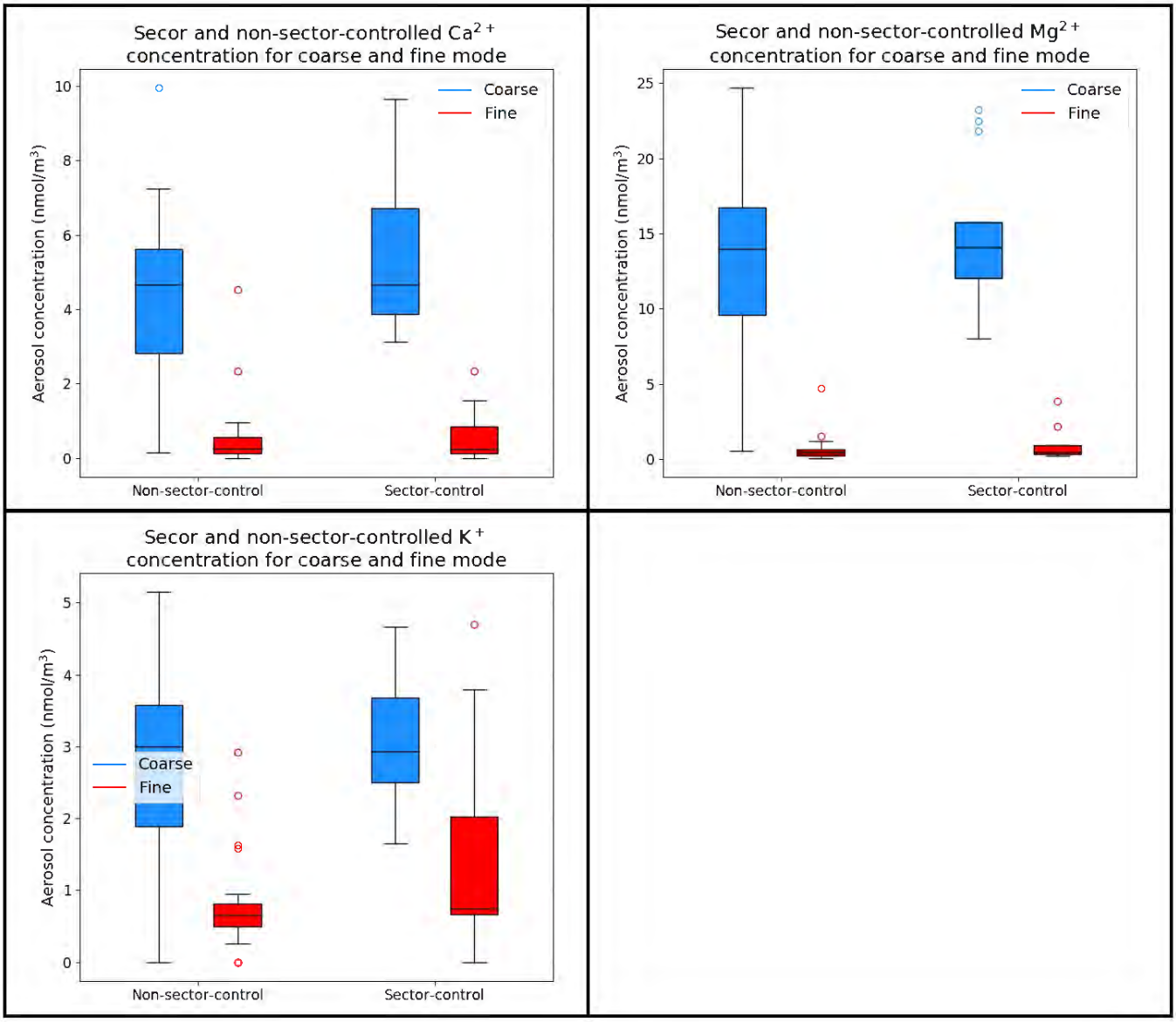

Figure 3.5 (continued): Ground-based HVAS sector and non-sector-controlled major ion concentrations.

3.2.2.2 Sector-controlled

For the sector-controlled ground-based HVAS samples (n=13, 09 July 2018 to 24 August 2018, and 30 August 2018 to 05 November 2018), the total Na^+ ranged from 164.4 – 398.9 nmol/m^3, with an average of 282.3 nmol/m^3. The Na^+ concentrations are much higher in the coarse mode than in the fine mode. Total NH_4^+ ranged from 0.1 – 26.6 nmol/m^3, with an average of 3.4 nmol/m^3 and have higher average concentrations in fine mode than in the coarse mode. Total K^+ ranged from 3.6 – 13.2 nmol/m^3, with an average of 7.3 nmol/m^3 and have higher average concentrations in the coarse mode than in the fine mode. Total Mg^{2+} ranged from 13.2 – 38.5 nmol/m^3, with an average of 24.9 nmol/m^3 and have higher average concentrations in the coarse mode than the fine mode. Total Ca^{2+} ranged from 5.4 – 17.8 nmol/m^3, with an average of 9.5 nmol/m^3 and have

higher average concentrations in the coarse mode than in the fine mode. Total Cl^- ranged from 139.6 – 648.3 nmol/m^3, with an average of 355.0 nmol/m^3 and have higher average concentrations in the coarse mode than in the fine mode. Total NO_3^- ranged from 9.5 – 82.7 nmol/m^3, with an average of 26.7 nmol/m^3 and have higher average concentrations in the coarse mode than in the fine mode. Total SO_4^{2-} ranged from 20.2 – 74.7 nmol/m^3, with an average of 38.5 nmol/m^3 and have higher average concentrations in the coarse mode than in the fine mode. Total Nss-SO_4^{2-} ranged from 8.3 – 54.1 nmol/m^3, with an average of 21.5 nmol/m^3 and have higher average concentrations in the fine mode than in the coarse mode (Figure 3.5).

3.3 Air mass history

The air masses that reach Cape Point can have influences from both marine and continental sources, this can be affected by wind direction which varies seasonally. The radon concentrations measured at Cape Point provide insight into the regions that influenced the air masses. The seasonality in radon concentration is due to the changes in wind direction (Figure 3.6). Most of the seasons have a strong east/southeast component, except for winter which has a more variable wind direction coming from the northwest (Figure 3.2). During the sampling period the radon had a maximum concentration of 9344 mBq/m^3, a minimum concentration of 92 mBq/m^3 and an average concentration of 999 mBq/m^3.

Samples have been classified by their air mass back trajectories into one of three groups, either marine, modified marine, or continental using HYSPLIT air mass back trajectories. The radon concentrations are then used to confirm the air mass classifications. Samples with HYSPLIT air mass back trajectories that do not encounter land before reaching the sampling site for at least 120 hours have been classified as marine samples (Figure 3.7A and 3.8A). Marine samples classified using HYSPLIT have an average radon concentration of 264 mBq/m^3. Samples that have air mass back trajectories that are predominantly over the ocean, with some continental influence, have been classified as modified marine samples (Figure 3.7B and 3.8B). Modified marine samples have an average radon concentration of 763 mBq/m^3. Samples with a large continental influence have been classified as continental samples (Figure 3.7C and 3.8C). It should be noted that due to the location and wind patterns of the sampling area the continental samples are not samples from a pure continental source, but rather a marine sample with a large continental influence. Continental samples have an average radon concentration of 1859 mBq/m^3. Tables 3.9 and 3.10 present the numbers of samples and seasonal variations for the classified air masses. Figures 3.9 – 3.10 present the concentrations for the different ions from the classified air masses. These data are discussed in more detail in Section 4.3.

Table 3.9: Seasonal count of sample classification for all tall-tower PM_{10} samples.

Season	Total	Marine	Modified Marine	Continental
Summer	3	--	2	1
Autumn	24	1	15	8
Winter	34	5	19	10
Spring	19	2	9	8

Table 3.10: Seasonal count of sample classification for all ground-based HVAS samples.

Season	Total	Marine	Modified Marine	Continental
Summer	0	--	--	--
Autumn	8	0	4	4
Winter	16	5	6	5
Spring	9	1	7	1

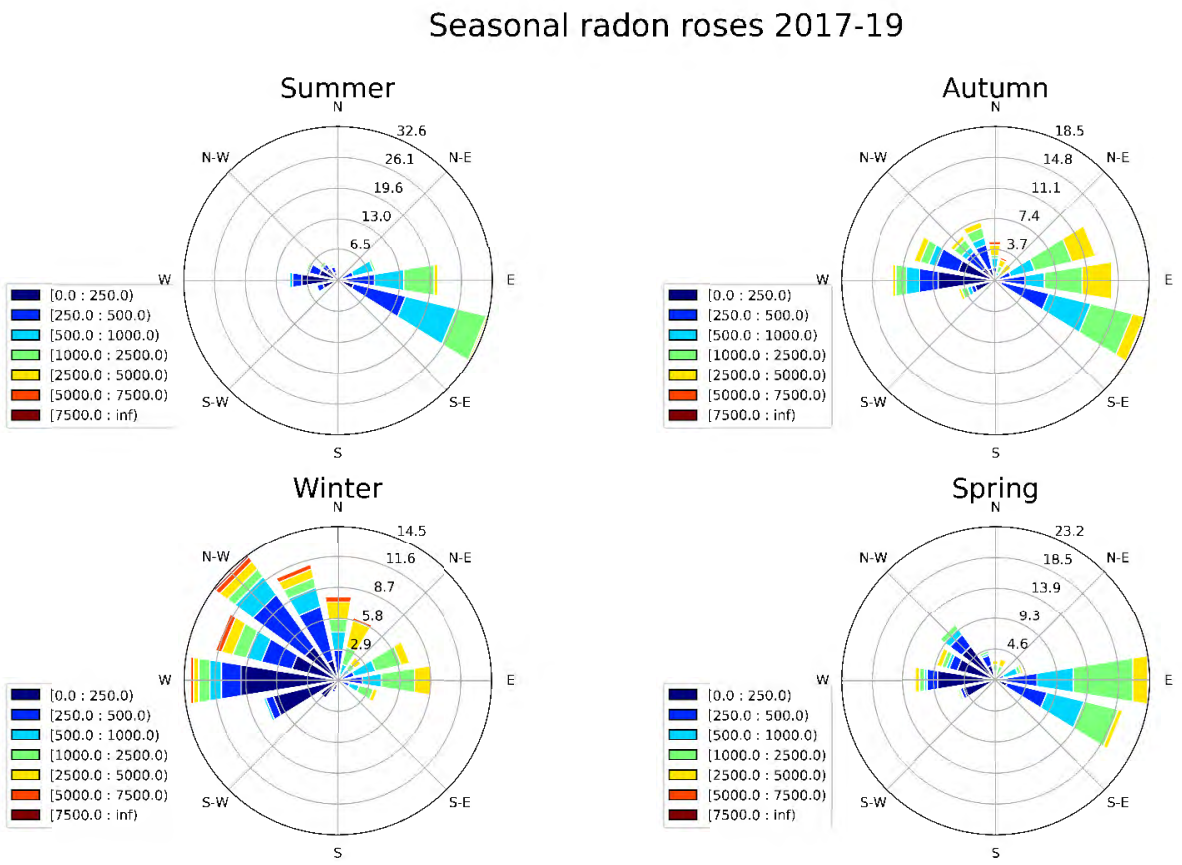

Figure 3.6: Seasonal radon roses from 2017 to 2019 (mBq/m^3). Note that irregular bin intervals were used to cover the dataset more appropriately.

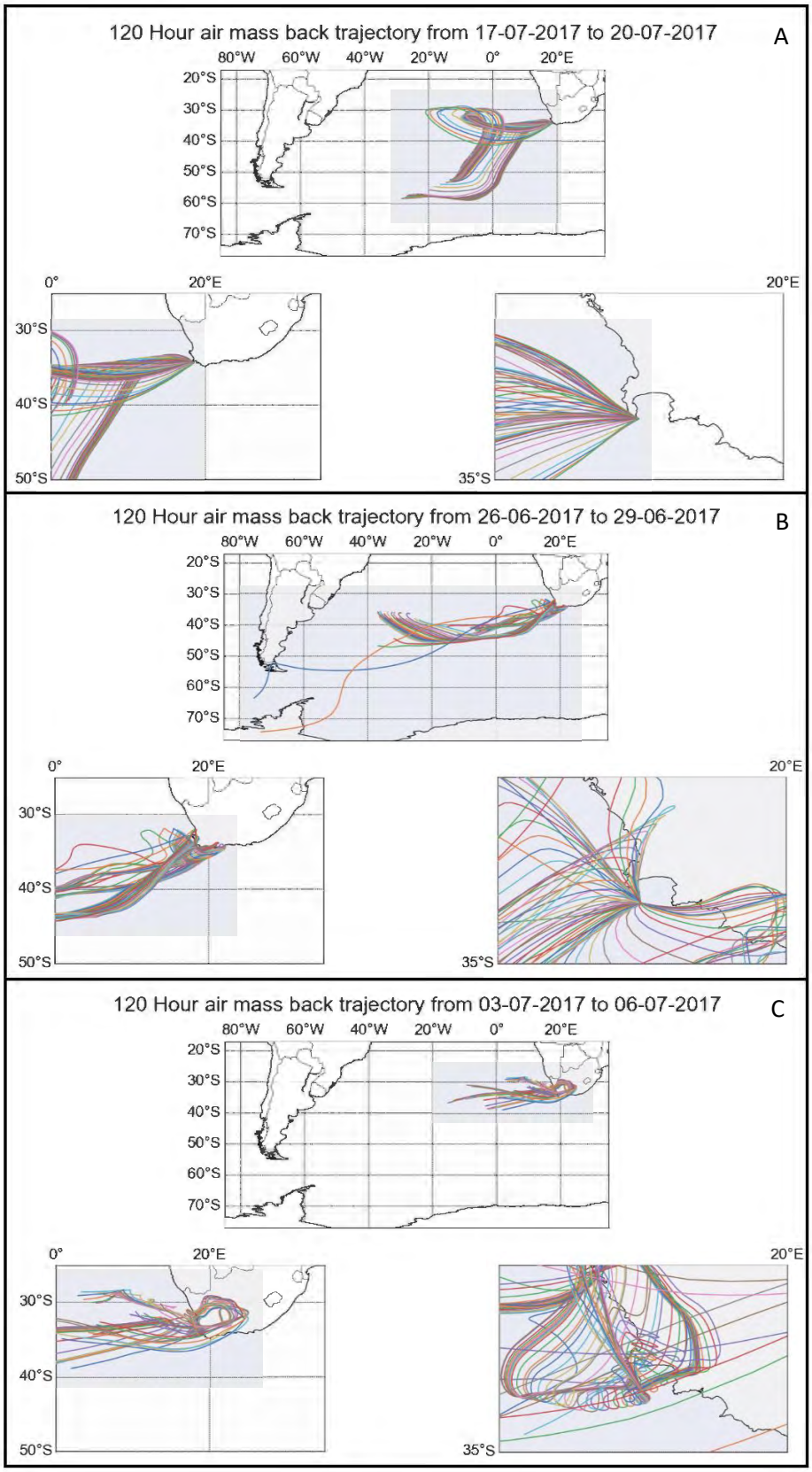

Figure 3.7: Examples of a) marine, b) modified marine and c) continental air mass back trajectories, calculated with HYSPLIT for 120 hours. Note the bottom two images in each panel are zoomed in portions of the main image.

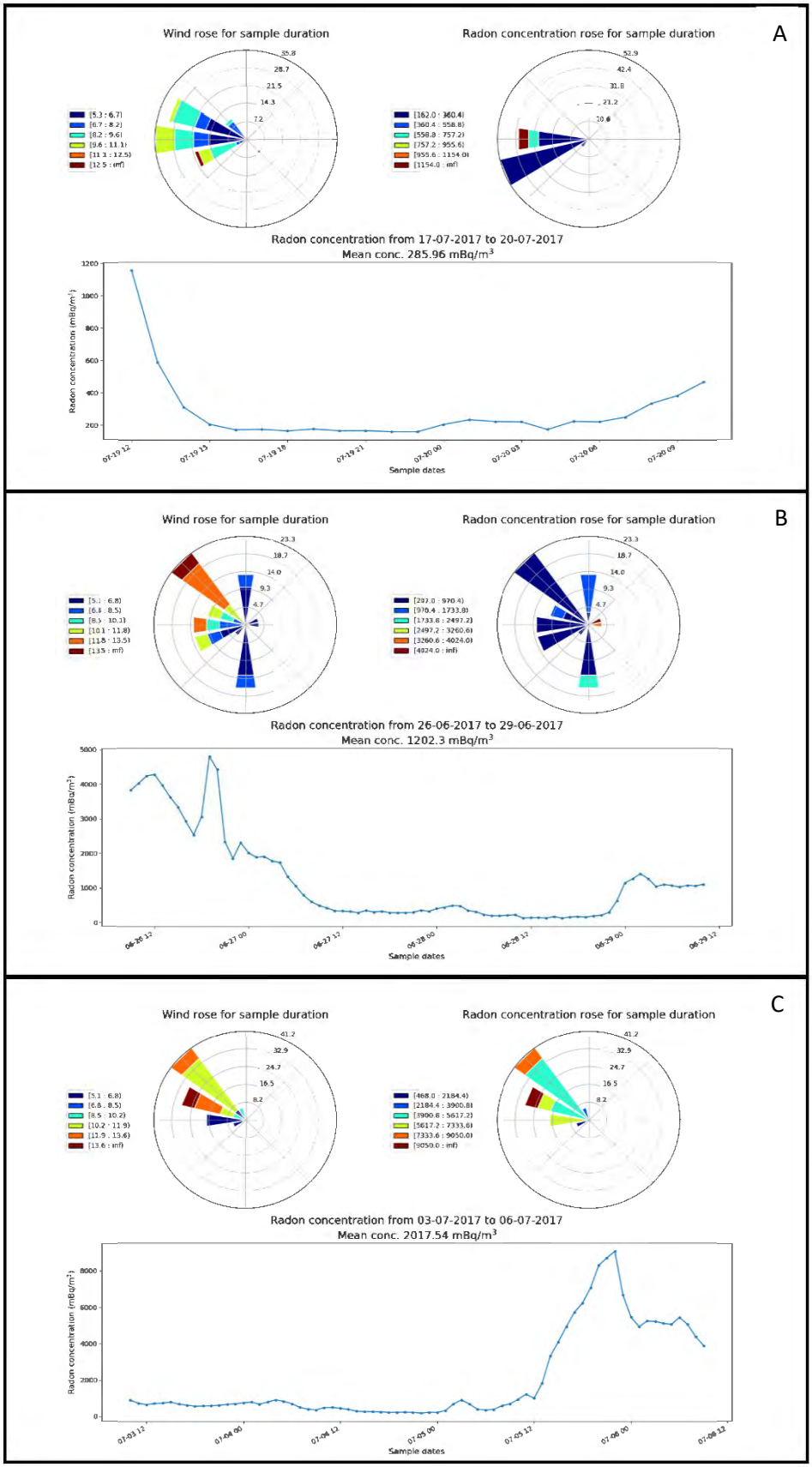

Figure 3.8: Radon plots for the a) marine, b) modified marine, and c) continental air mass examples. Note change in y-axis scale.

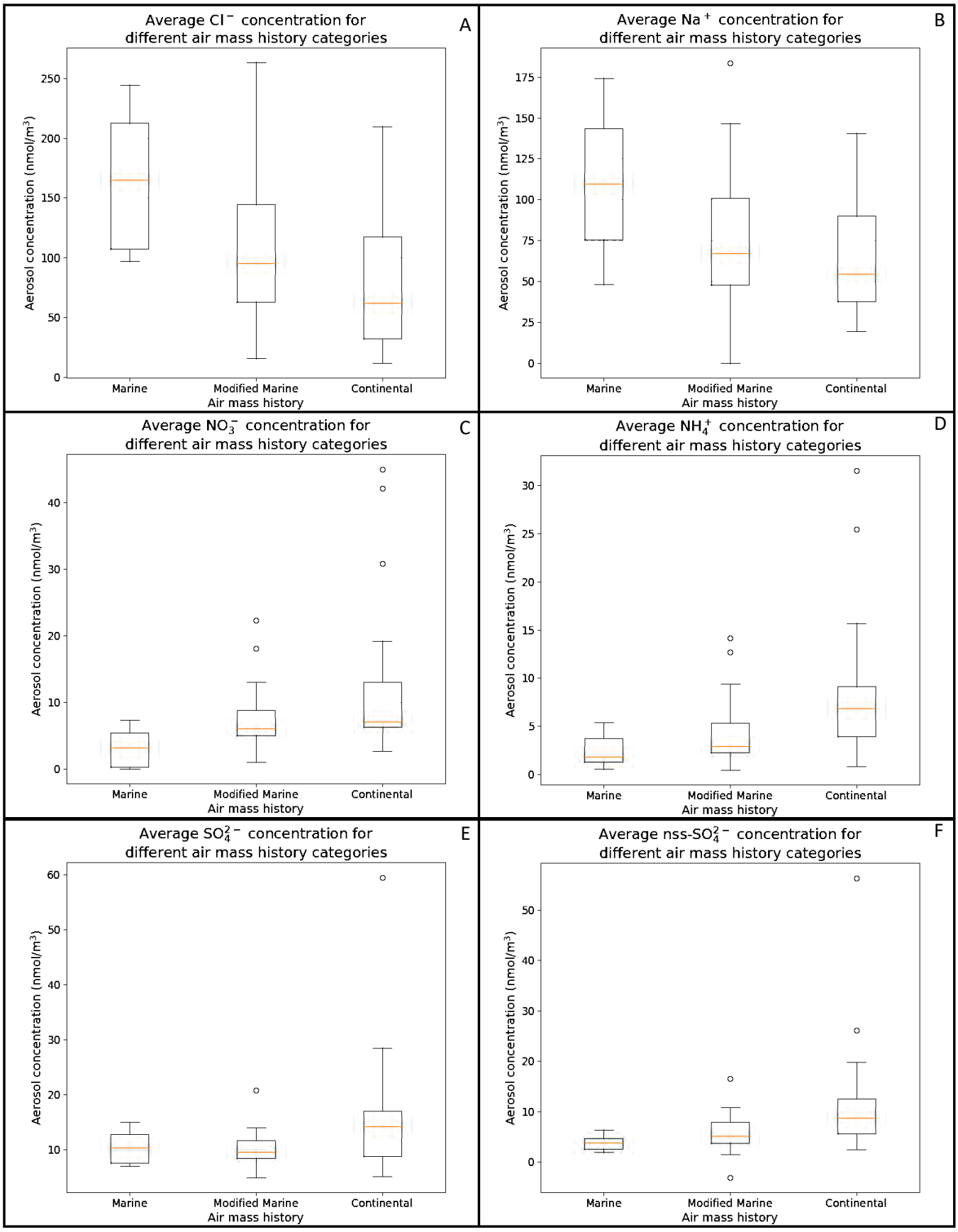

Figure 3.9: Box and whisker plots of tall-tower PM_{10} aerosol concentrations for classified samples.

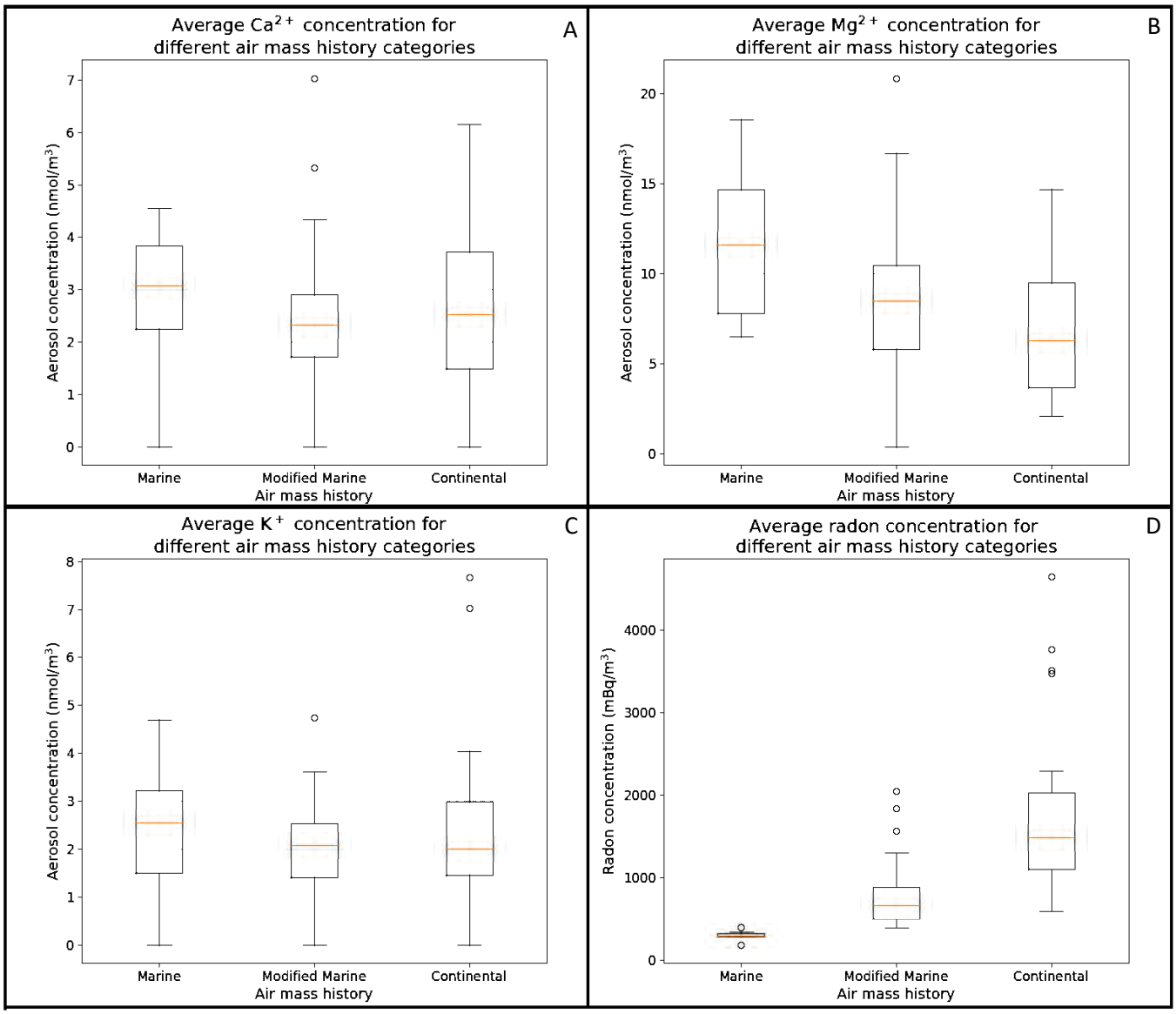

Figure 3.9 (continued): Tall-tower PM_{10} aerosol concentration ranges for classified samples.

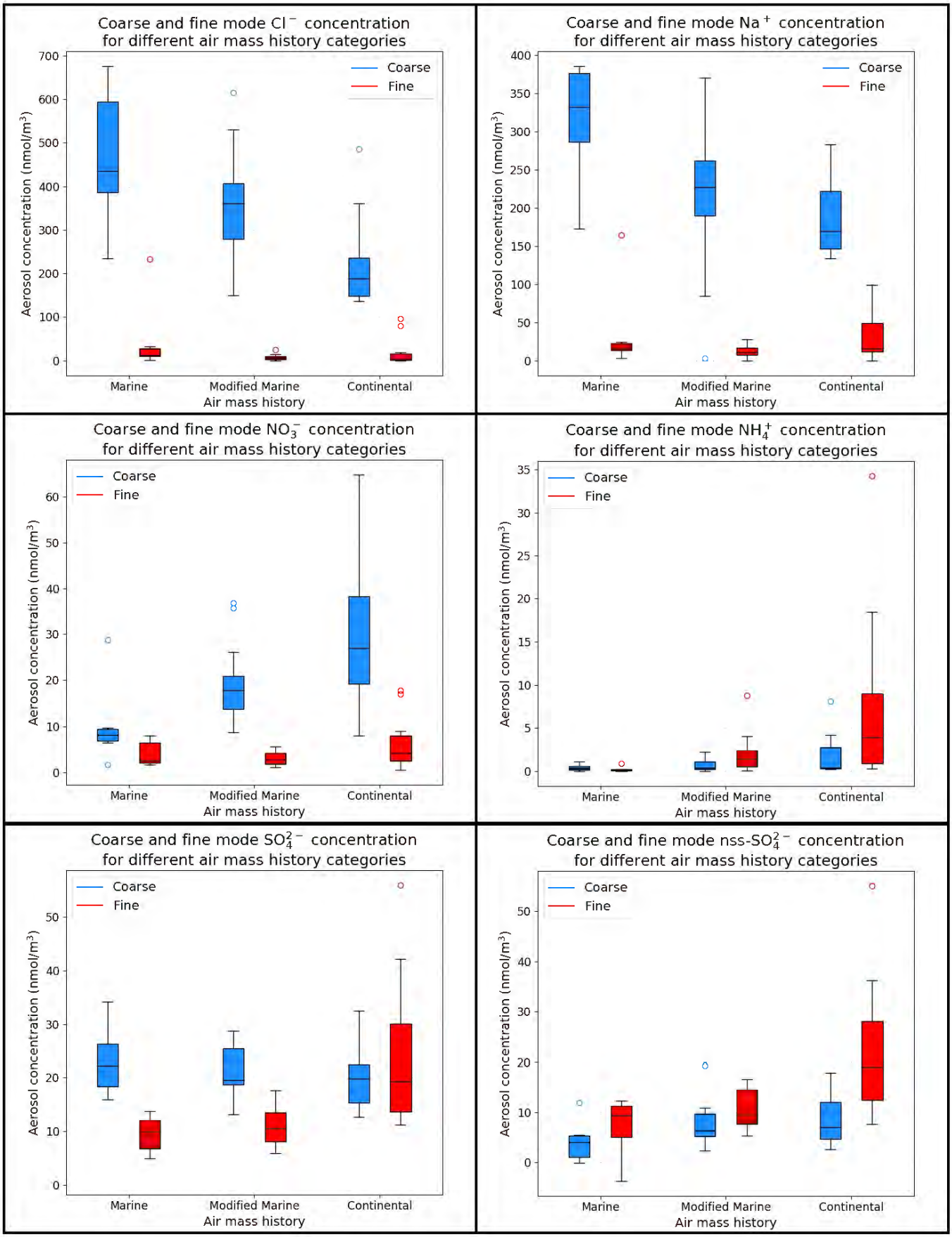

Figure 3.10: Box and whisker plots of ground-based HVAS aerosol concentrations for classified samples.

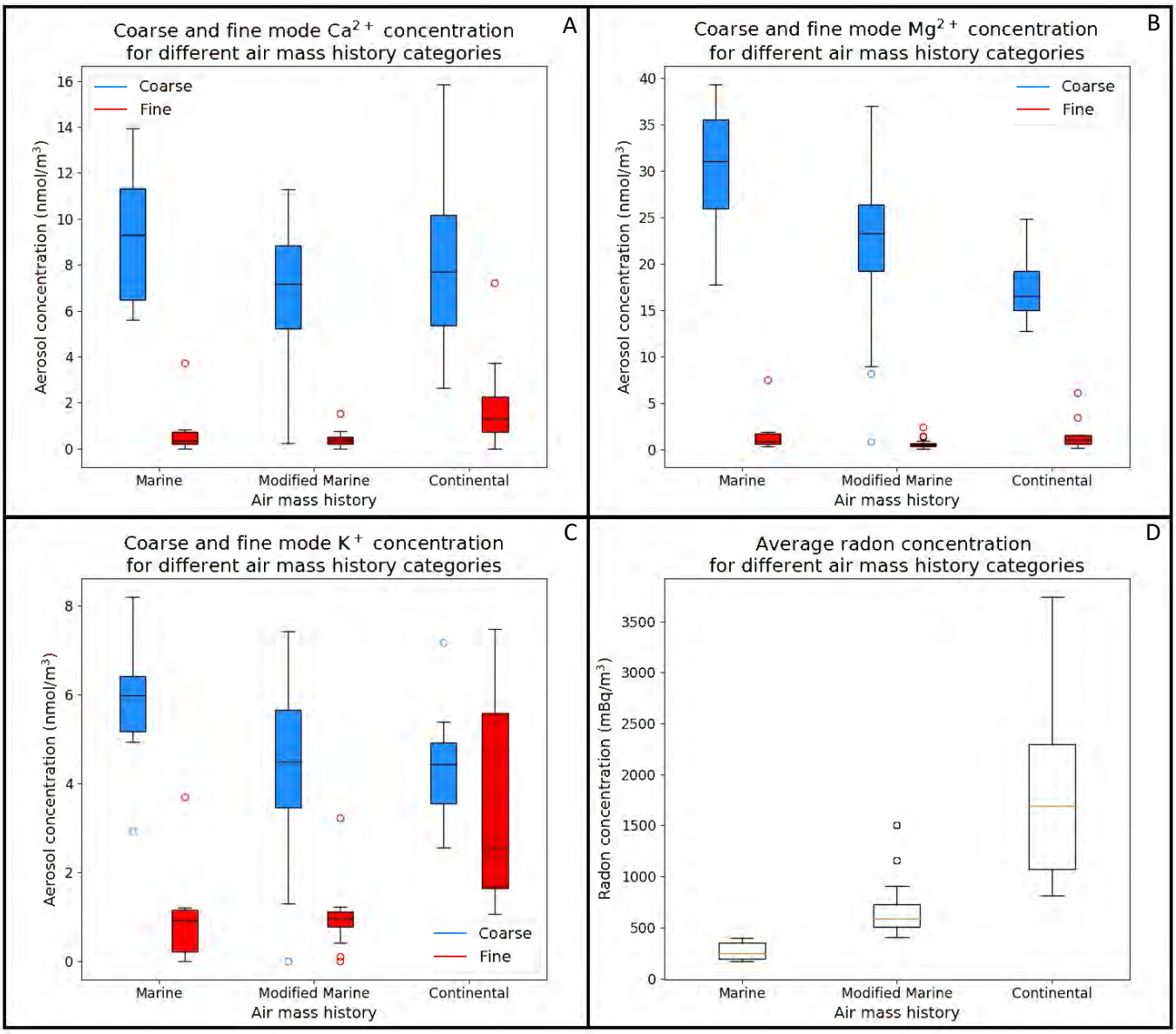

Figure 3.10 (continued): Ground-based HVAS aerosol concentration ranges for classified samples.

4. Discussion and conclusion

The primary objective of this thesis was to establish the Cape Point GAW station as a reliable field site to collect and study marine aerosols that originate in the remote atmosphere of the Southern Ocean. This thesis focuses on all major inorganic ions, but particularly nitrogen-containing aerosols due to their biogeochemical and climate relevance, as well as potential for complex mixed sources and chemistry in polluted coastal regions. In order to address this objective, the aims of the thesis were to:

1) Compare existing tall-tower and newly installed ground-level aerosol collection systems at the GAW station.
2) Install and test a sector-controller for excluding anthropogenic and continental influences from aerosol collection at the GAW station.
3) Characterize aerosol chemical composition as a function of aerosol size, atmospheric source region, and season.

4.1 Comparison of tall-tower and ground-level aerosol collection systems

During the sampling campaign there was an overlap from the PM_{10} tall-tower sampling and the HVAS ground-level sampling, from 16 April 2018 to 24 August 2018. During the overlap of sampling, 21 samples were collected with the tall-tower PM_{10} system and 19 from the ground-based HVAS. The difference in the number of samples is due to the tall-tower PM_{10} samples being changed over twice during the period of one ground-based HVAS sample, which occurred twice. The tall-tower PM_{10} samples that were changed twice in the period of one ground-based HVAS samples were averaged to be comparable to the single ground-based HVAS sample. For the HVAS data to be compared to the tall-tower PM_{10} data, each stage of the ground-based HVAS samples were summed together to give the total aerosol concentration.

The ground-based HVAS data compare reasonably well with the tall-tower PM_{10} data, with both datasets showing similar temporal trends (i.e., maxima and minima in the concentrations at the same time). However, the ground-based HVAS data have higher concentrations for all ions, except NH_4^+ which is quite similar (figure 4.1). Scatter plots (figure 4.2) show the relationship between the ground-based HVAS and tall-tower PM_{10} samples, with an average R-squared value of 0.670 (standard deviation of 0.131). The scatter plots (figure 4.2) have a 1:1 line plotted on them, which clearly shows the ground-based HVAS samples have higher concentrations than the tall-tower PM_{10} samples, except for NH_4^+.

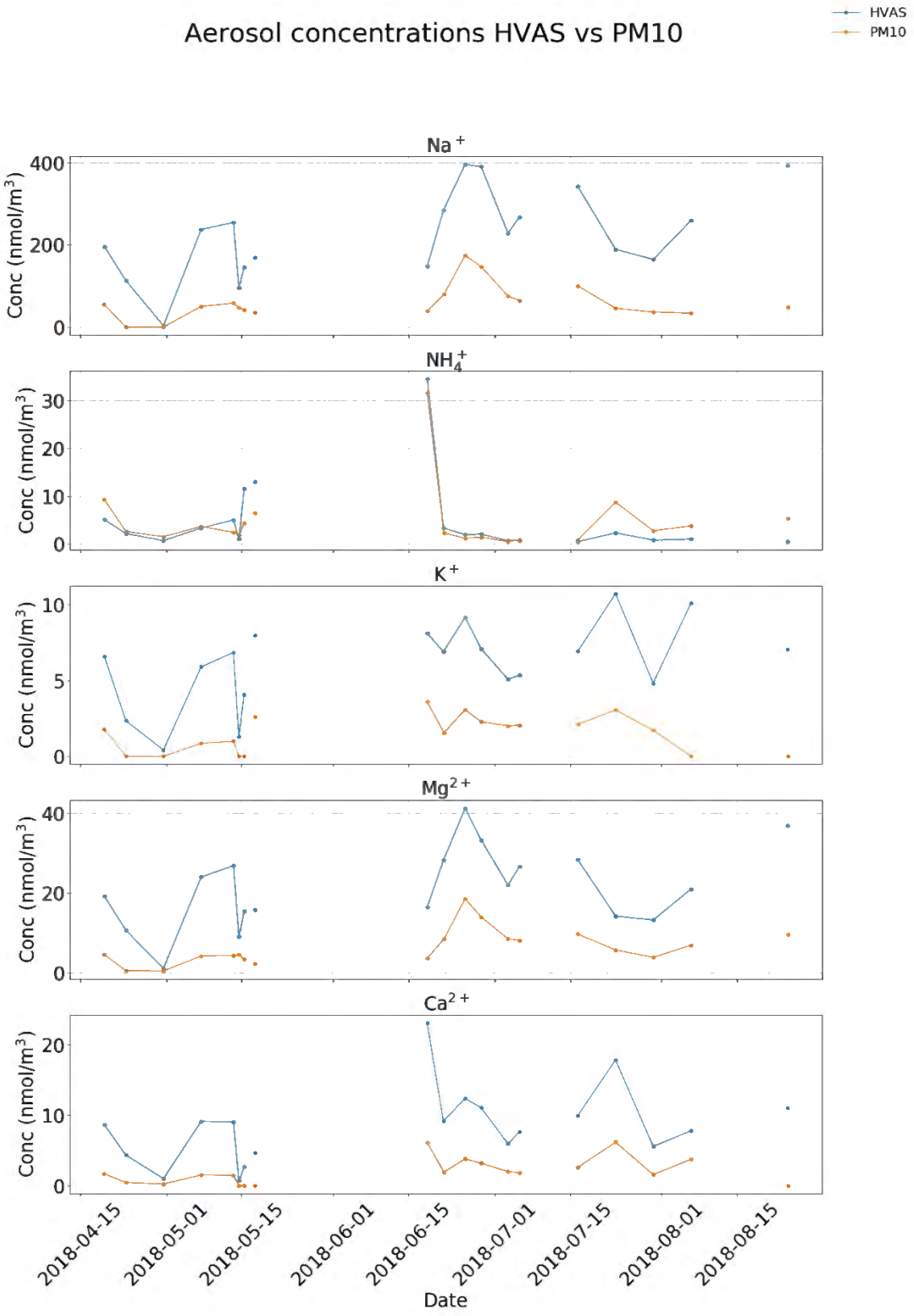

Figure 4.1: Comparison of the total ground-based HVAS and tall-tower PM_{10} aerosol concentrations during the sampling overlap.

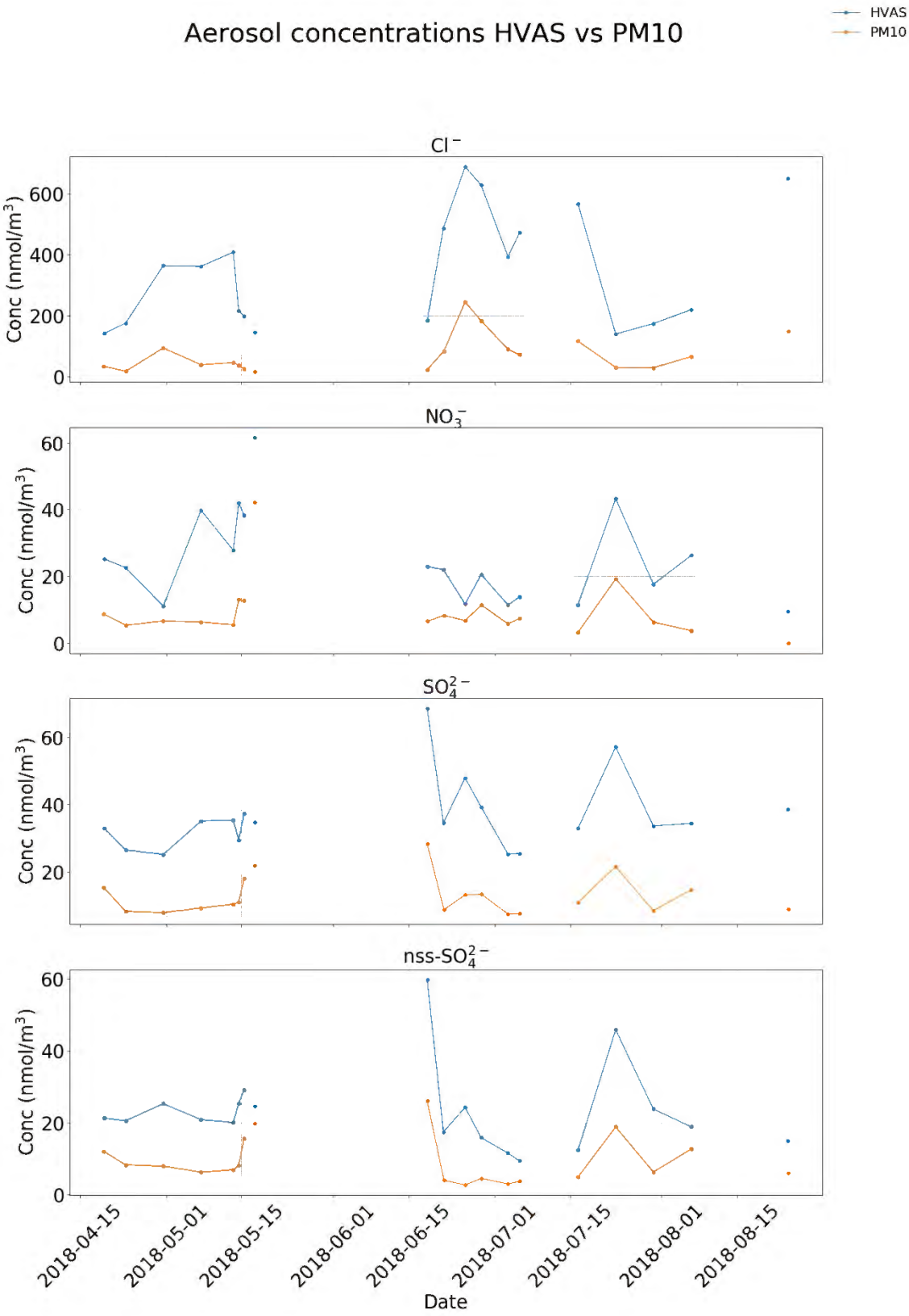

Figure 4.1 (continued): Comparison of the total ground-based HVAS and tall-tower PM_{10} aerosol concentrations during the sampling overlap.

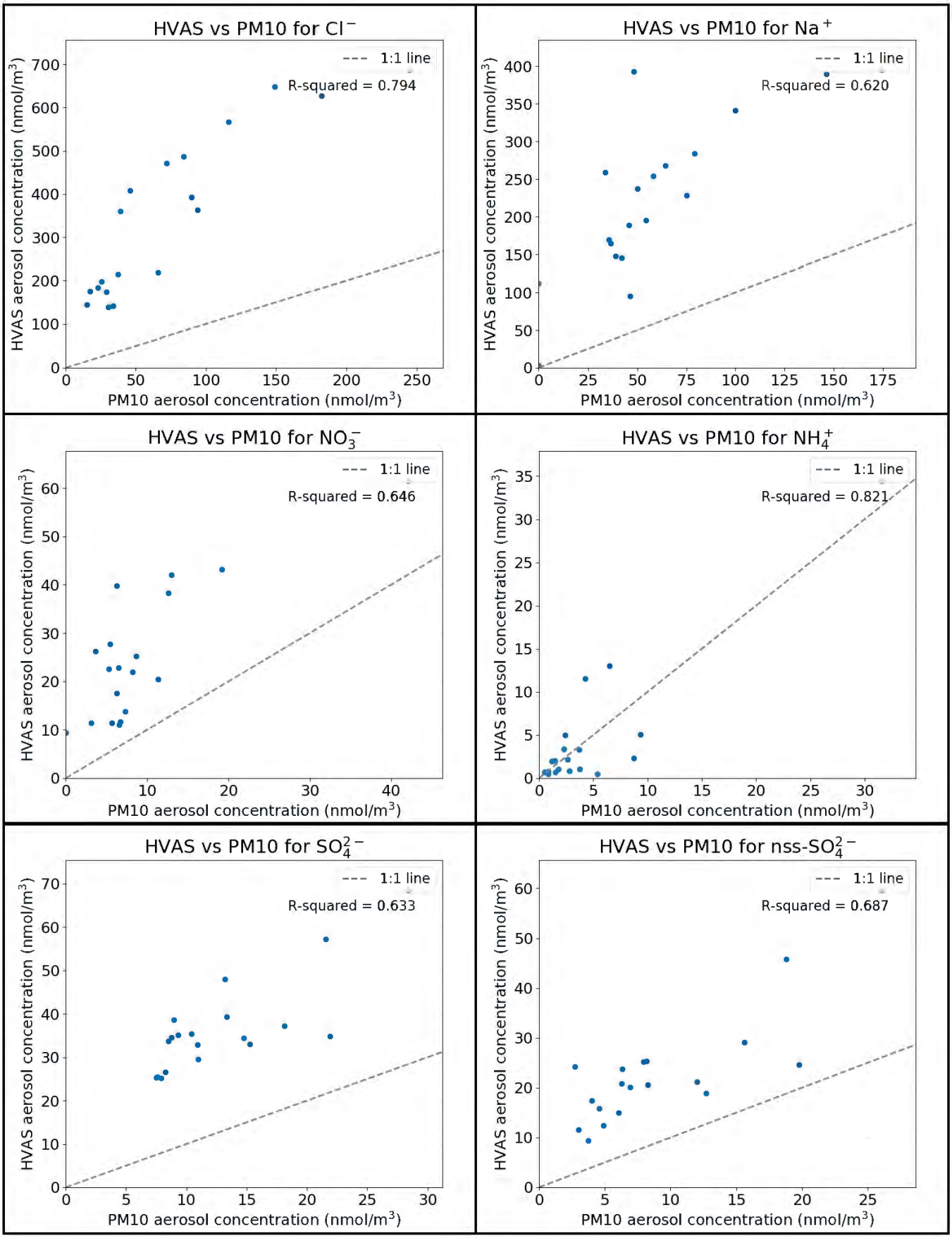

Figure 4.2: Scatter plots of the total ground-based HVAS and tall-tower PM_{10} aerosol concentrations. A 1:1 line and the R-squared value has been displayed.

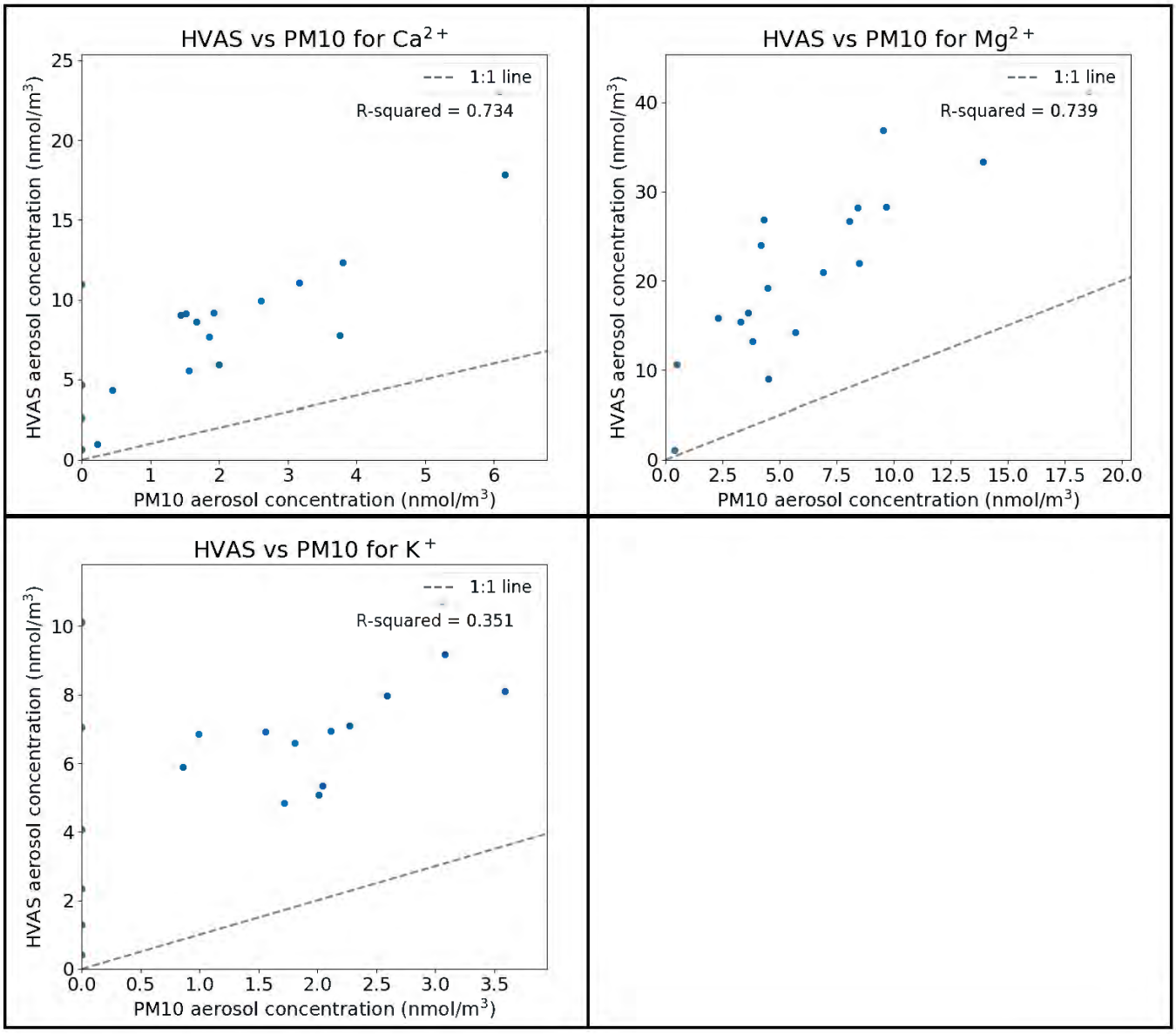

Figure 4.2 (continued): Scatter plots of the total ground-based HVAS and tall-tower PM_{10} aerosol concentrations. A 1:1 line and the R-squared value has been displayed.

The comparison of the ground-based HVAS data to the tall-tower PM_{10} data shows that the ground-based HVAS measures higher concentrations for most of the ions. A notable exception is that the NH_4^+ concentrations are very similar between the ground-based HVAS and tall-tower PM_{10} and fall around the 1:1 line. The nss-SO_4^{2-} is higher in the ground-based HVAS samples than the tall-tower PM_{10} samples but falls closer to the 1:1 line than the other ions. NH_4^+ and nss-SO_4^{2-} are typically associated with smaller aerosol sizes and are more abundant in the fine mode than coarse mode (Figure 3.4, Appendix figure A4). All the other ions are more abundant in the coarse mode than the fine mode (Figure 3.4, Appendix Figure A4), these ions also have a larger deviation from the 1:1 line and are more abundant in the ground-based HVAS samples than the tall-tower PM_{10}

samples. There is a discrepancy with the coarse mode aerosols, where the ground-based HVAS has higher concentrations than the tall-tower PM_{10}.

There are some differences between the sampling systems, the HVAS was installed at the base of the PM_{10} tower. It samples the air in the immediate vicinity, making it more susceptible to ground-level influences. The tall-tower PM_{10} system is situated in the laboratory at the base of the 30 m tower, but it samples air from the top of the tower that is pulled through tubing into the laboratory. This will avoid ground-level influences but does mean the air being sampled first travels through a long distance of tubing. The ground-based HVAS is subject to environmental changes, such as fluctuations of temperature and humidity, whereas the tall-tower PM_{10} samples are collected inside the laboratory, which is temperature and humidity controlled. The intake tube for the tall-tower PM_{10} system is heated to keep humidity below 50%, this may cause semi-volatile materials to be lost. However, if the loss of semi-volatile material occurs due to the heated intake, it is more likely to impact the fine mode fraction than the coarse mode fraction (Allen et al., 1997).

The discrepancy in the coarse mode aerosol concentrations between the two sampling systems could be due to the systems sampling air masses at different heights, as the intakes are 30 m apart. However, that is unlikely as they are both situated on top of a cliff 200 m above sea level, which is the nearest source of coarse mode aerosols. If we accept that the systems are both sampling the same air masses, then the discrepancy is most likely due to differences in the sampling systems. The first stage of the ground-based HVAS samples aerosols > 7.2 µm with no upper cut-off, whereas the tall-tower PM_{10} collects everything < 10 µm. As such, a possible explanation is that the ground-based HVAS may be including more of the coarse mode aerosols given that it samples a larger size range than the tall-tower PM_{10}. An alternative explanation is that the tall-tower PM_{10} sampling system is under sampling the coarse mode fraction. This could be due to coarse mode aerosols settling out within the tall-tower PM_{10} intake tube coming from the top of the tower before they reach the sampling filter.

If the tall-tower PM_{10} sampling system is under sampling coarse mode aerosols, or if the ground-based HVAS is sampling a larger size range, then it would lead to the ground-based HVAS values being higher than the tall-tower PM_{10} values. A two-sided T-test between the tall-tower PM_{10} and total ground-based HVAS revealed that all ions, except NH_4^+, have statistically different means (p-values < 0.05, Appendix Table A2). Comparing the tall-tower PM_{10} data to the ground-based HVAS data without the larger coarse mode sizes (i.e., HVAS S3-BU; total HVAS excluding stages 1 and 2) should result in more comparable values. Indeed, when stages 1 and 2 are excluded, Na^+, NH_4^+, Mg^{2+}, Ca^{2+}, Cl^-, and NO_3^- all have statistically identical means (two-sided T-test, p-values > 0.05,

Appendix Table A2). Scatter plots of tall-tower PM_{10} vs HVAS S3-BU fall around the 1:1 line for most of the ions (Figure 4.3). Given that NH_4^+ is not typically present in the coarse mode, it is not surprising that it compares well between the ground-based HVAS and tall-tower PM_{10} sampler even if stages 1 and 2 are included. These comparisons were also done for HVAS S2-BU (excluding only stage 1, Appendix Table A2) and HVAS S4-BU (excluding stages 1, 2 and 3, Appendix Table A2), but most of the coarse mode ions matched best with HVAS S3-BU. If the issue were simply that the ground-based HVAS included aerosols larger than 10 µm than the S2-BU data should be most comparable to the tall-tower PM_{10}, however that does not appear to be the case. Given the evidence that the tall-tower PM_{10} sampling system is under sampling the coarse mode fraction, then the tall-tower PM_{10} dataset is not giving the bulk aerosol concentration, but rather particles approximately ≤ 3 µm (assuming it is equivalent to HVAS S3-BU).

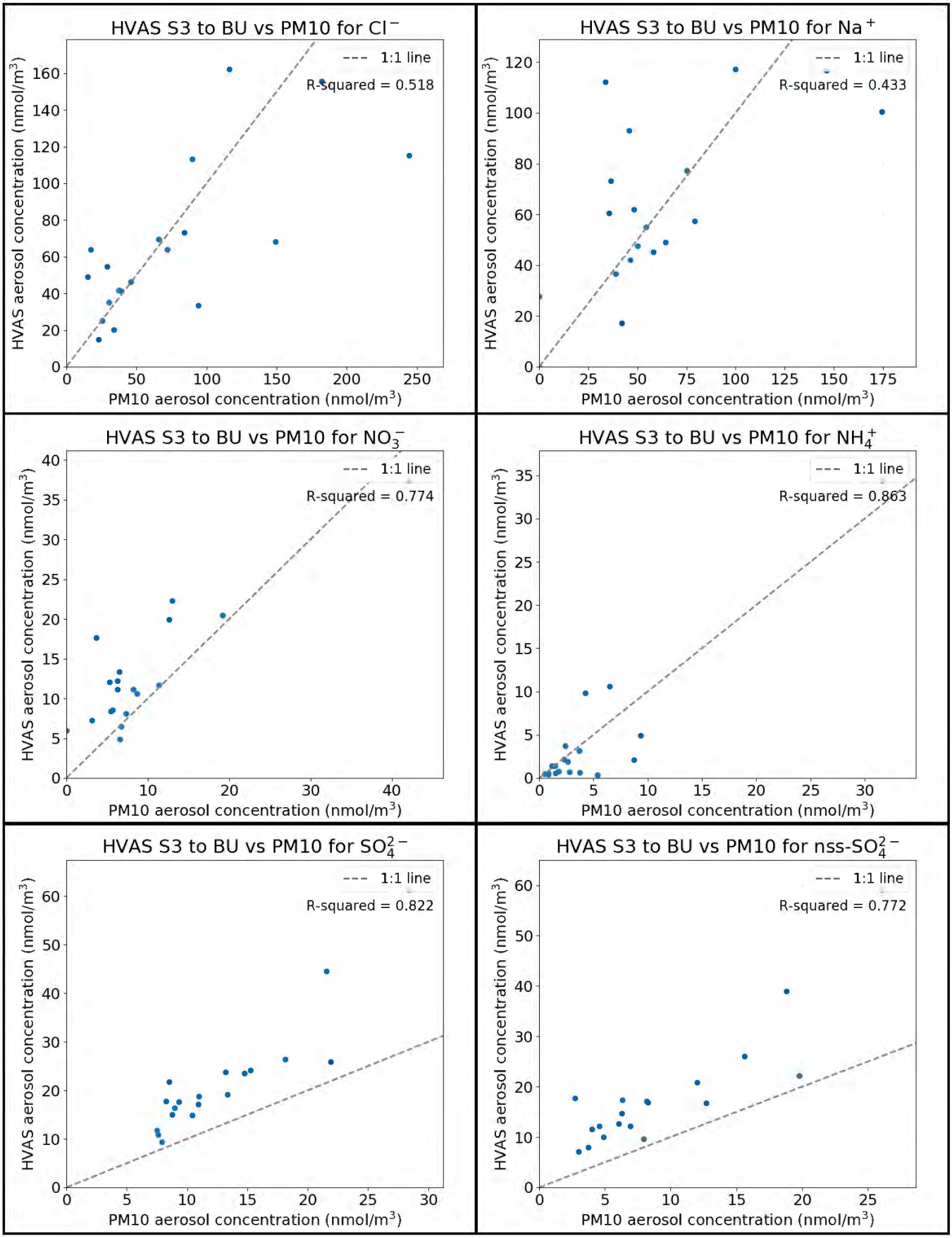

Figure 4.3: Scatter plots of ground-based HVAS stage 3 to back up and tall-tower PM_{10} aerosol concentrations. A 1:1 line and the R-squared value has been displayed.

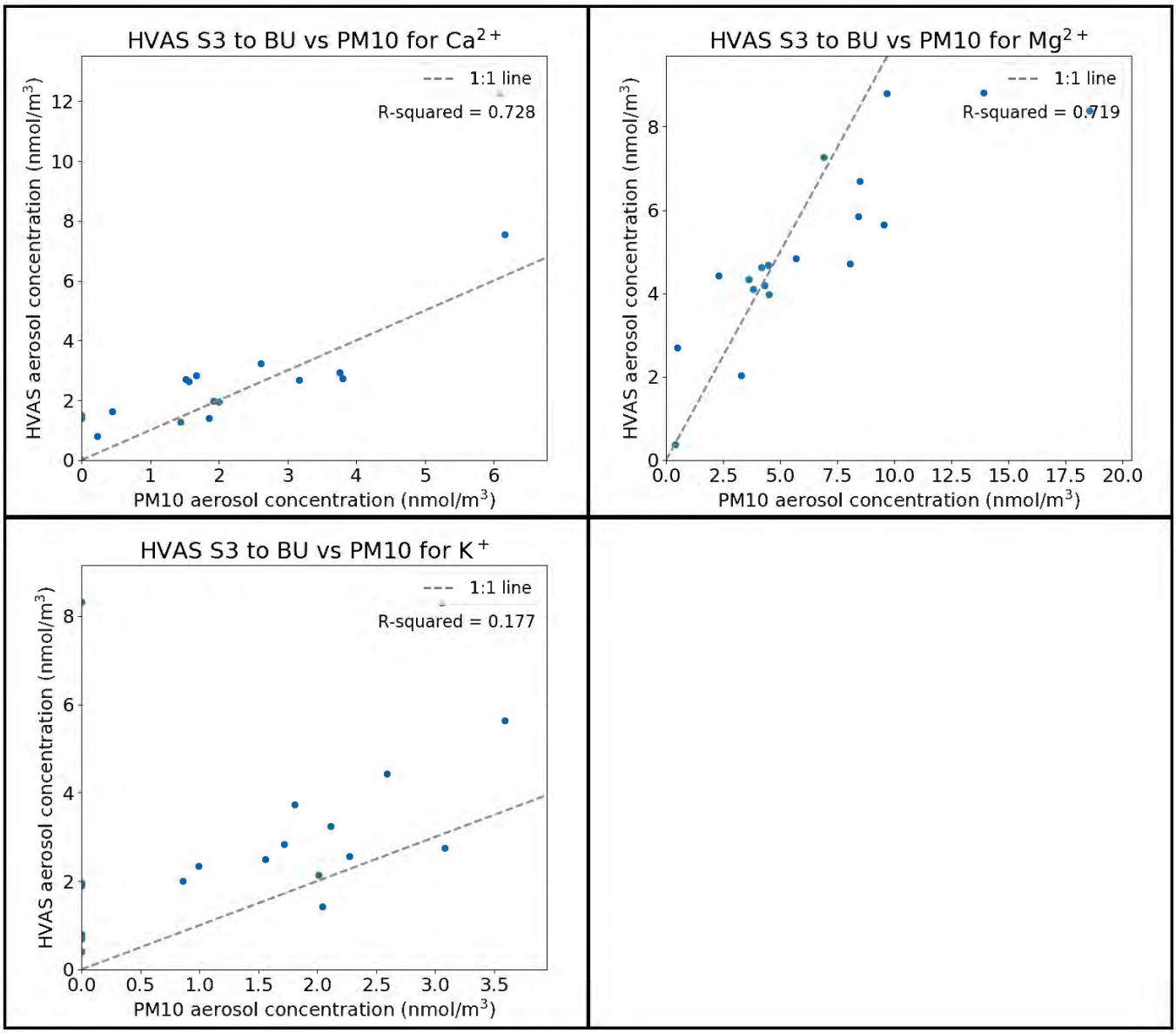

Figure 4.3 (continued): Scatter plots of ground-based HVAS stage 3 to back up and tall-tower PM_{10} aerosol concentrations. A 1:1 line and the R-squared value has been displayed.

4.2 Evaluation of the sector-controller

4.2.1 Impact on sampled air masses

The sector-controller worked as designed in that it turned off the sampling pumps when the wind came from the specified sector and turned the pumps on when the wind was coming from the correct sector for the specified period of time (Figures 4.4-4.6). The sector-controller prevented the immediate sampling of any continental pollution episodes, which resulted in samples that would have otherwise been categorised as modified marine to be categorised as marine samples (Figure 4.5). However, the sector-controller was not entirely successful at excluding all continental pollution episodes as some continental air masses circulate over the ocean prior to being sampled (Figure 4.6). This demonstrates the importance of and continued need for classifying samples

individually with air mass back trajectories and radon concentrations, even when the sector-controller is operational.

Other coastal sampling sites have installed similar measures to selectively sample marine air masses. They have improved on the criteria for sampling by not only using wind direction to control the sampling, but also other variables such as particle number and black carbon (O'Dowd et al., 2014).

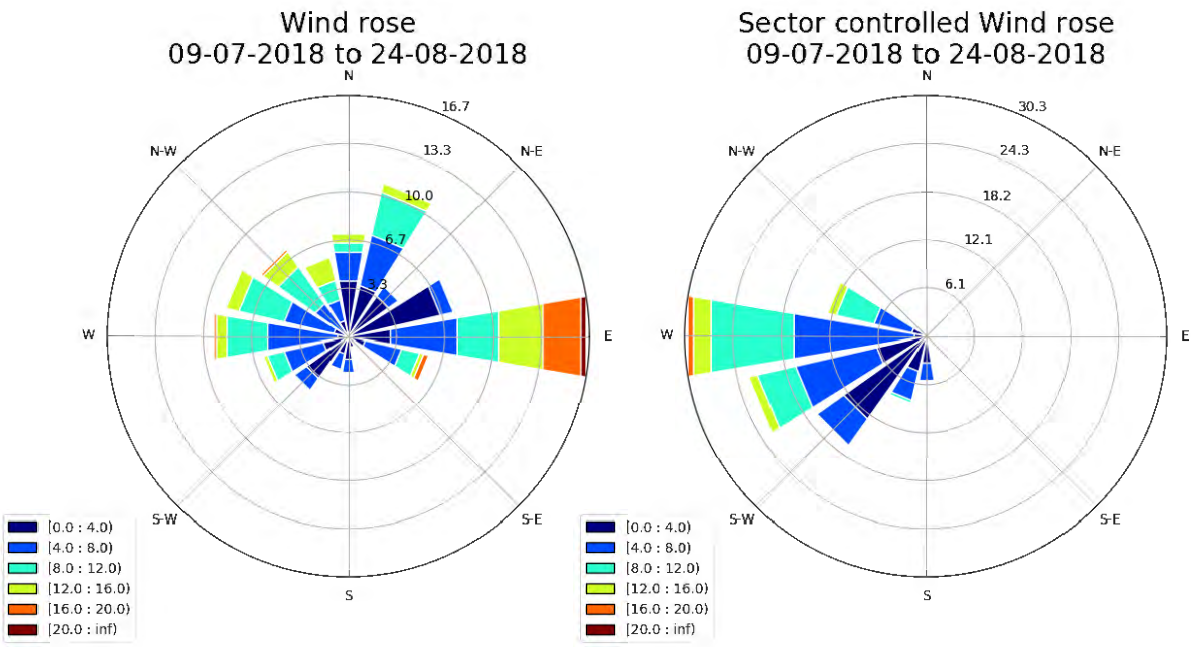

Figure 4.4: Wind roses from 09-07-2018 to 24-08-2018, a) wind rose for entire period, b) wind rose when pumps were sampling under sector-control.

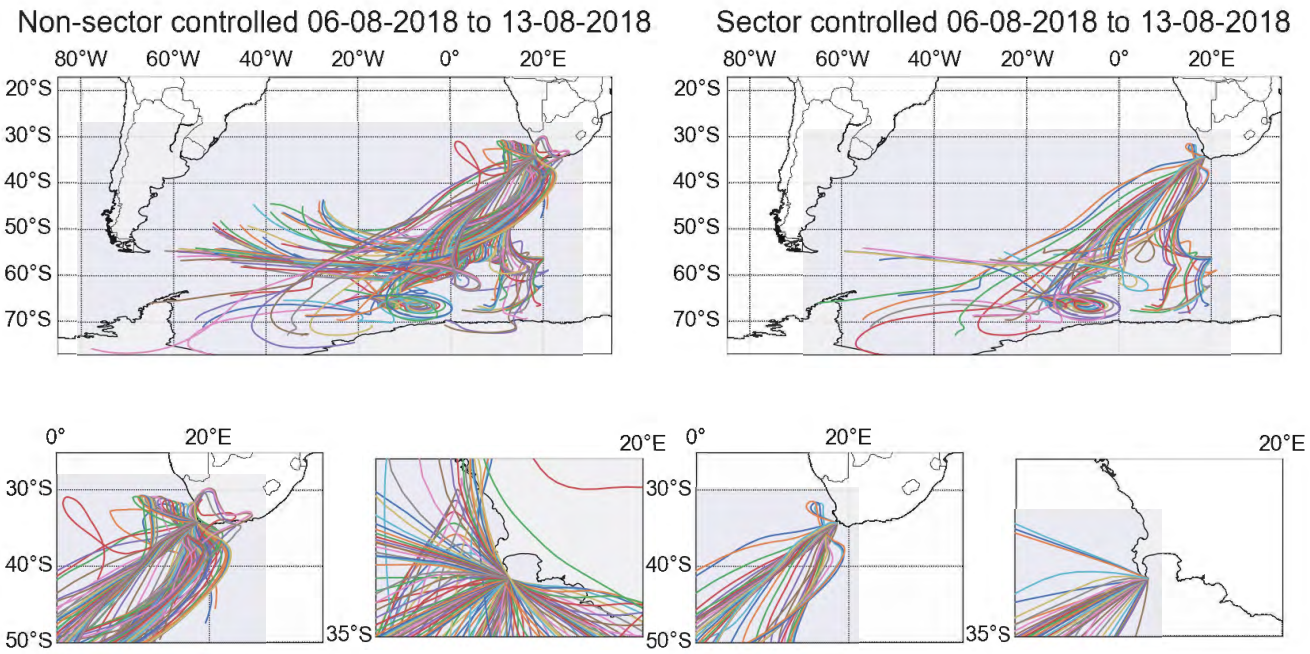

Figure 4.5: HYSPLIT air mass back trajectories from 06-08-2018 to 13-08-2018, left) every hour for the entire period, right) every hour the pumps were running at least 45 min of the hour under sector-control. Note the bottom two images in each panel are zoomed in portions of the main image.

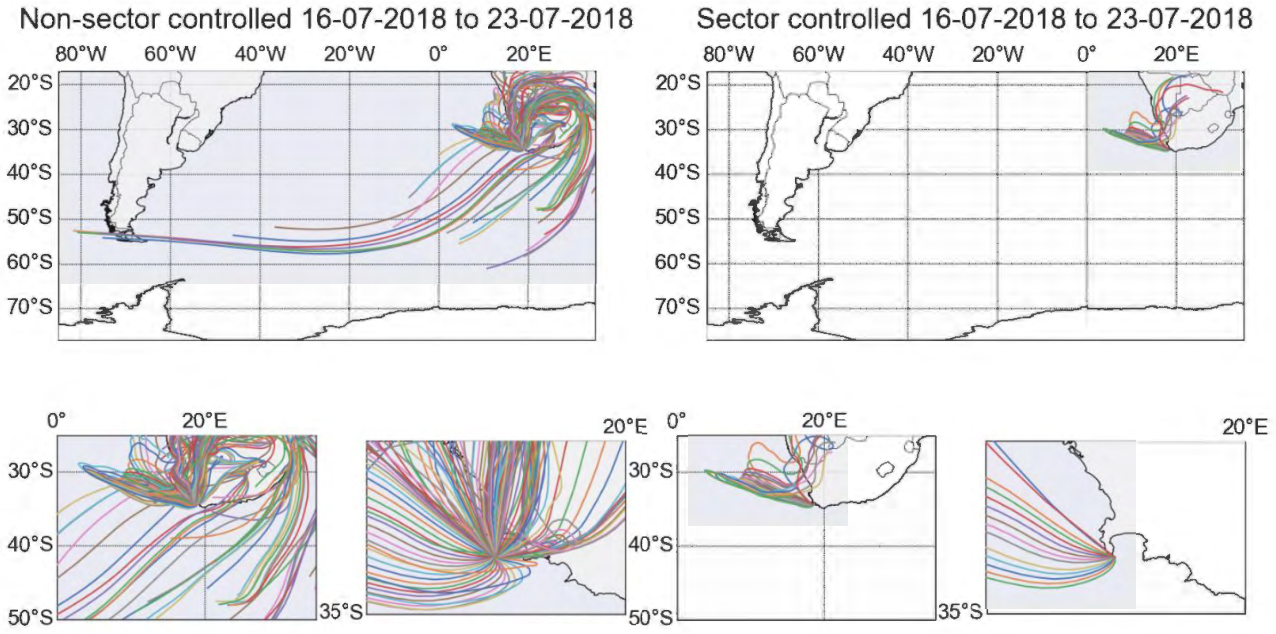

Figure 4.6: HYSPLIT air mass back trajectories from 16-07-2018 to 23-07-2018, left) every hour for the entire period, right) every hour the pumps were running at least 45 min of the hour under sector-control. Note the bottom two images in each panel are zoomed in portions of the main image.

4.2.2 Comparison of sector- and non-sector aerosol chemical composition

The sector-controller was only operational and connected to the tall-tower PM_{10} sampler during winter 2018, and as a result there are only 7 sector-controlled tall-tower PM_{10} aerosol samples for comparison with the non-sector-controlled samples. Therefore, we compare the sector-controlled tall-tower PM_{10} data (Figure 3.3) with the non-sector-controlled tall-tower PM_{10} winter data (Figure 3.3), while noting that 4 of the sector-controlled tall-tower PM_{10} samples are classified as continental samples due to recirculating air masses. Based on the typical seasonality of the Cape Point GAW station, winter should be a time when the continental/anthropogenic influence would be greatest. Under sector-controlled sampling, species with continental and/or pollutant sources such as NH_4^+, K^+, NO_3^-, and nss-SO_4^{2-} have lower concentrations than under non-sector-controlled conditions, when comparing within winter. This suggests that the sector-controller is effective at eliminating at least some portion of the continental/anthropogenic air masses that reach the sampling site. However, we note that a larger dataset is required for a true evaluation of the impact of the sector-controller on the aerosol chemical composition.

4.3 Characterizing aerosol chemical composition

Cape Point has a distinct seasonality with most seasons having a dominant east/southeast wind direction, except for winter which is more variable and predominantly west/northwest (figure 3.2). Winter also has higher radon concentrations than the other seasons, indicating a higher continental influence (figure 3.6, Appendix figure A5) (Brunke et al., 2004). Interestingly, in this dataset, winter has both the highest number and highest proportion of marine samples (Table 3.9 and 3.10). It is important to note that there were fewer samples collected in summer than in the other seasons, but regardless, winter should be the time of the least number of marine samples. Therefore, the air mass origins of a sample cannot be assumed based on seasonality and need to be determined individually.

Furthermore, looking at the seasonality of non-marine aerosols that typically have anthropogenic sources, such as NO_3^-, NH_4^+, and nss-SO_4^{2-}, there is not only no significant concentration increase during winter, as expected, but no strong seasonality more generally (figure 3.3, and 3.4; Welch test p-values > 0.05 in tall-tower PM_{10} and ground-based HVAS for these ions across all seasons (except for ground-based HVAS NO_3^- which was significantly lower in winter than autumn), Appendix Table A7 and A13). Whereas if you look at the same aerosol species plotted by their air mass history, a clear trend occurs with significantly higher concentrations in continental samples as opposed to marine samples (Figures 3.9 and 3.10; Welch test p-values < 0.05 in tall-tower PM_{10}

and ground-based HVAS (in the dominant size class for the ion) for these ions in continental compared to marine samples, Appendix Table A11 and A15).

This is also true for marine aerosols such as Cl^-, Na^+, and Mg^{2+}, which show a stronger trend with air mass history than with season (Figures 3.3, 3.9, and 3.10). The only significant seasonal difference for these ions was that autumn had significantly lower average concentrations than winter and spring (Welch test p-values < 0.05 in tall-tower PM_{10} and ground-based HVAS (in the dominant size class for the ion), Appendix Table A7 and A13). The comparison between air mass history categories shows these ions have significantly higher concentrations in marine air mass samples than continental air mass samples (Welch test p-values < 0.05 in tall-tower PM_{10} and ground-based HVAS (in the dominant size class of the ion), Appendix Table A11 and A15). Grouping samples by air mass history shows clear and expected trends based on major sources, whereas grouping samples by season does not show any clear trends. This is further supported by the radon data (figures 3.3 and 3.9).

This point is further echoed and enhanced by the size segregated ground-based HVAS data, where both the aerosol concentration trends and aerosol size class are consistent with expected trends for the air mass history (figures 3.4 and 3.10). Using K^+ as an example, the size segregated seasonality does not show any clear trends, but the size segregated sources show an interesting trend. K^+ has a coarse mode fraction that decreases with continental air mass samples and a fine mode fraction that increases with continental air mass samples (figures 3.4 and 3.10). This is consistent with expectations that coarse mode K^+ comes from a marine source, such as sea spray, whereas fine mode K^+ comes from a continental source, such as biomass burning (Andreae, 1983).

Aerosol species with a strong marine component include Na^+, Cl^-, and Mg^{2+} in both tall-tower PM_{10} and ground-based HVAS data. These all had the highest concentrations in marine samples, and lower concentrations in more continental samples (Figures 3.9 and 3.10). These species all exist predominantly in the coarse mode (Figure 3.10). The elevated concentrations of these species in marine samples are most likely due to them originating from sea spray (Saltzman, 2009).

Aerosol species with a strong continental source include NO_3^-, NH_4^+, and nss-SO_4^{2-} in both tall-tower PM_{10} and ground-based HVAS data. These species all had the highest concentrations in continental samples and lower concentrations in marine samples (Figures 3.9 and 3.10). NO_3^- is found predominantly in the coarse mode, whereas NH_4^+ and nss-SO_4^{2-} are found mostly in the fine mode (Figures 3.10). Possible continental sources include vehicle emissions, industrial emissions, and agricultural emissions (Galloway et al., 2004; Saltzman, 2009). While there is a strong continental component, there is also a marine component from sea spray and outgassing of NH_3

and DMS and their subsequent conversions to NH_4^+ and nss-SO_4^{2-} respectively. The presence of coarse mode nitrate is consistent with expectations for a polluted coastal area (Yeatman, Spokes & Jickells, 2001). NH_3 and HNO_3 concentrations decrease from polluted to coastal areas due to dilution with relatively clean marine air, causing fine-mode NH_4NO_3 aerosols to dissociate back to their gas-phase precursors. As a result, the inorganic chemical composition in marine areas is dominated by fine-mode $(NH_4)HSO_4$ (and, if enough NH_3 is present, $(NH_4)_2SO_4$) and coarse-mode $NaNO_3$ aerosols (Saltzman, 2009).

The rest of the aerosol species have a combination of continental and marine sources. SO_4^{2-} and K^+ both have a coarse mode marine component that decreases with continental samples as well as a fine mode continental component that is lower with marine samples and increases with continental samples (Figures 3.9 and 3.10). Ca^{2+} is predominantly in the coarse mode and this fraction is slightly higher in the marine samples, there is also a smaller fine mode component that increases with continental samples (Figures 3.9 and 3.10). Possible sources include sea spray, dust, biomass burning, construction of buildings, quarries, and vehicle exhaust emissions (Pio et al., 2007; Saltzman, 2009).

4.4 Comparison to other coastal and open ocean studies

Compiling data generated from a number of sources (Xu et al., 2013; Yeatman, Spokes & Jickells, 2001; Cavalli, 2004; Rinaldi et al., 2009; Baker et al., 2010; Zhang et al., 2010; Mkoma et al., 2014) combines aerosol concentration data from the coastal sites of Mace Head (Ireland), Baía de Todos os Santos (Brazil), Weybourne (England), and the Zhongshan station (East Antarctica) and aerosol concentration data from cruises through the North Atlantic Ocean, Southern Ocean, Pacific Ocean, South Atlantic Ocean, and Mediterranean Sea (Table 4.1). Most of the data from the listed papers is from the open ocean or coastal sites that restrict sampling to ensure only marine air is sampled, although there is some data from continental air masses, which is noted in the table. All of these studies used high volume samplers without an upper cut off, except for Mkoma et al., 2014 who had a 10 µm cut off.

The aerosol data generated from this work are comparable to other coastal sampling sites and cruises in the open ocean. Comparing the tall-tower PM_{10} and ground-based HVAS data in Tables 4.1 to the other studies in the table, the tall-tower PM_{10} NH_4^+ concentrations are similar to those found by other studies, with tall-tower PM_{10} marine samples slightly lower than the marine samples from the listed studies and the tall-tower PM_{10} continental slightly higher than the marine samples from the listed studies. Interestingly, the continental samples from the literature had much higher NH_4^+ concentrations than any observed in this study. The ground-based HVAS NH_4^+

data follow a similar trend, but the marine concentrations are lower than the tall-tower PM_{10} marine and the ground-based HVAS continental are higher than the tall-tower PM_{10} continental. The ground-based HVAS NH_4^+ continental data are therefore more similar to the continental samples from the South Atlantic Ocean but is still considerably lower than the continental samples from Mace Head and Weybourne. The concentration of NO_3^- from the listed studies ranges from 0.66 - 23.39 nmol/m^3 for clean samples and 9.50 - 790.00 nmol/m^3 for continental samples. The tall-tower PM_{10} NO_3^- marine samples have a slightly higher concentration than most of the clean samples in the literature, but still towards the lower end of the range, and the tall-tower PM_{10} continental samples have concentrations similar to the lower end of the continental range in the literature. The ground-based HVAS NO_3^- marine concentrations were higher than most of the clean samples from the literature, whereas the ground-based HVAS continental samples were similar to the lower end of the continental range from the literature. The tall-tower PM_{10} nss-SO_4^{2-} marine concentrations are at the lower end of the range of the clean samples in the literature, whereas the tall-tower PM_{10} continental concentrations are slightly higher than the lowest continental concentrations from the listed literature. The ground-based HVAS nss-SO_4^{2-} marine concentrations are higher than most of the clean samples, but still within the range from the literature. The ground-based HVAS nss-SO_4^{2-} continental samples are at the mid to lower end of the range of the continental samples. Most of the studies in the compiled table did not report concentrations for the other major ions (Na^+, K^+, Mg^{2+}, Ca^{2+}, Cl^-, and SO_4^{2-}). For those that did, the tall-tower PM_{10} concentrations were generally at the lower end of the literature range, if not below the range, whereas the ground-based HVAS concentrations were generally in the mid to upper end of the literature range. The tall-tower PM_{10} comparison shows the tall-tower PM_{10} data is in the mid to lower end of the ranges from the listed studies for the fine mode aerosols, but low to below the range for coarse mode aerosols. This is most likely due to the majority of the studies listed here not having a 10 µm cut off and sampling at a lower altitude, therefore having a larger contribution from coarse mode aerosols.

Table 4.1: Compiled aerosol concentrations from multiple papers and multiple regions, tall-tower PM_{10} and ground-based HVAS data are from this study (nmol/m^3; rounded to two significant figures).

Reference	Location	Coastal/open ocean	Classification	Na^+	NH_4^+	K^+	Mg^{2+}	Ca^{2+}	Cl^-	NO_3^-	SO_4^{2-}	nss-SO_4^{2-}
	Cape Point	Coastal	Marine	110	1.1	2.4	12	2.9	160	3.2	10	3.9
Tall-tower PM_{10}	Cape Point	Coastal	Continental	66	6.8	2.4	6.7	2.8	77	12	16	12
Ground-based	Cape Point	Coastal	Marine	220	0.4	4.3	20	6.4	320	9.1	21	7.2
HVAS	Cape Point	Coastal	Continental	140	6.2	4.9	12	6.5	160	23	28	20
	Mace Head	Coastal	Marine	N/A	3.4	N/A	N/A	N/A	N/A	2.9	N/A	5.0
(Rinaldi et al., 2009)	North Atlantic Ocean	Open ocean	Marine	N/A	3.5	N/A	N/A	N/A	N/A	2.1	N/A	5.3
(Mkoma et al., 2014)	Brazil	Coastal	Marine	110	2.8	15	11	7.8	14	2.8	5.8	N/A
	Eastern Antarctica	Coastal	N/A	N/A	2.3	N/A	N/A	N/A	N/A	0.66	N/A	4.4
(Xu et al., 2013)	Southern Ocean	Open ocean	N/A	N/A	5.3	N/A	N/A	N/A	N/A	0.81	N/A	5.0
(Cavalli, 2004)	Mace Head	Coastal	Marine	N/A	5.3	N/A	N/A	N/A	N/A	2.3	N/A	3.1
	Mace Head	Coastal	Marine	220	11	N/A	N/A	N/A	N/A	8.6	N/A	7.8
	Mace Head	Coastal	Continental	81	180	N/A	N/A	N/A	N/A	130	N/A	69
(Yeatman, Spokes	Weybourne	Coastal	Marine	500	45	N/A	N/A	N/A	N/A	13	N/A	3.6
& Jickells, 2001)	Weybourne	Coastal	Continental	110	1000	N/A	N/A	N/A	N/A	790	N/A	160
	North Atlantic Ocean 1	Open ocean	Marine	130	0.0	2.5	18	9.3	110	11	14	5.9
	North Atlantic Ocean 2	Open ocean	Marine	300	0.0	7.7	40	67	243	23	38	20
	Pacific Ocean	Open ocean	Marine	250	0.0	5.9	30	11	250	1.9	22	6.7
	South Atlantic Ocean	Open ocean	Marine	200	0.42	5.2	32	38	140	17	20	8.5
(Zhang et al., 2010)	Mediterranean Sea	Open ocean	Continental	180	0.76	3.3	20	42	98	15	21	10
	North Atlantic	Open ocean	Marine	N/A	6.5	N/A	N/A	N/A	N/A	7.3	N/A	N/A
	South Atlantic Ocean	Open ocean	Marine	N/A	3.3	N/A	N/A	N/A	N/A	2.7	N/A	N/A
(Baker et al., 2010)	South Atlantic Ocean	Open ocean	Continental	N/A	13	N/A	N/A	N/A	N/A	9.5	N/A	N/A

4.5 Conclusions

The primary objective and aims for this thesis have been achieved. An aerosol sampling system was installed at the Cape Point GAW station that collects clean marine samples that originate in the remote Southern Ocean.

The existing tall-tower PM_{10} sampling system and the newly installed ground-level HVAS both show similar temporal trends in the inorganic aerosol concentrations. However, the tall-tower PM_{10} sampling system appears to be under sampling the coarse mode fraction of aerosols when compared to the ground-based HVAS. It is possible that this is due to large aerosol particles settling out in the 30 m long intake tube. It is therefore recommended to use the ground-based HVAS for future work as it seems to sample the air masses more completely across the full size spectrum.

The sector-controller was successfully installed and tested. It was found to exclude air masses coming directly from the continent and did help to minimize contamination from continental air. However, it did not completely prevent sampling of continental air masses that circulated over the ocean before being sampled. Recommended improvements for the sector-controller to prevent sampling continental air masses would be to add additional cut-off limits for the sampling, such that it is not only turned off due to wind direction, but also from particle concentration, black carbon concentration and/or carbon monoxide concentration.

The aerosol samples' chemical composition was characterized as a function of size, atmospheric source region, and season. The size distribution of the major ions is as expected with Cl^-, Na^+, NO_3^-, Ca^{2+}, and Mg^{2+} predominantly in the coarse mode, NH_4^+, and nss-SO_4^{2-} predominantly in the fine mode, and SO_4^{2-} and K^+ being distributed through both the coarse and fine modes. This size distribution is expected as the coarse mode species are generally primary aerosols and emitted directly via sea spray or dust, whereas the fine mode species are generally secondary aerosols and emitted as a gas and form particles. A very strong relationship was observed between the concentration of different ions and different air mass source regions. The main source regions for each aerosol sample were classified as marine, modified marine, or continental depending on the 120 hour air mass back trajectories and ^{222}Rn concentrations. The Cl^-, Na^+, and Mg^{2+} concentrations were lower in samples with more continental influence, consistent with these species having a marine source. The NO_3^-, NH_4^+, and nss-SO_4^{2-} concentrations were higher in samples with more continental influence, consistent with an anthropogenic source for these species. The SO_4^{2-} and K^+ concentrations had an interesting distribution as the concentration in the coarse mode decreased

with more continental influence, and the fine mode concentration increased with more continental influence. This indicates both marine and continental sources for those ions.

There is a seasonality at Cape Point with a dominant east/southeast wind most of the year and a shift to west/northwest winds during winter. This causes winter to have high levels of continental influence, but also the most marine samples as there is a sharp gradient from clean marine air to polluted air in the northwest region (Figure 2.1). The seasonality in the chemical composition of the aerosols is dominated by the changing wind regimes. The changes that can be noted between different seasons can be explained by the changes in the source regions of the air masses passing over different regions in different seasons. Therefore, regardless of season or dominant wind direction, each aerosol sample collected needs to be individually classified by means of air mass back trajectory and ^{222}Rn concentrations.

The major inorganic aerosol concentrations measured here are comparable to what is observed at other coastal sampling sites. The concentration of aerosols from remote regions with little to no anthropogenic influence can give an indication of the natural concentration levels. These background concentration levels can be used as a proxy for the preindustrial atmosphere, which is required to understand the influence of anthropogenic perturbations to the natural system. These can be used in models to further predict how the system will be affected in the future under a variety of different pollution scenarios.

Acknowledgments

I would like to acknowledge bursary funding for this work from the South African National Research Foundation (NRF) through a Freestanding, Innovation and Scarce Skills Development Fund Masters Scholarship (113193). This research was supported by funding from the NRF Competitive Programme for Rated Researchers (CPRR) (111716) and Department of Science and Innovation Biogeochemistry Research Infrastructure Platform (BIOGRIP).

I would like to acknowledge the South African weather service for use of the station and data from the Cape Point station.

Thank you to my supervisor, Katye Altieri, for affording me with incredible opportunities and providing me with mentorship and support, I am very appreciative.

I am grateful to my co-supervisor, Casper Labuschagne, for providing me with assistance in the field and insights into SAWS data.

I am thankful for being part of a great research group where I can get assistance and discuss my work.

Lastly, I would like to thank my friends and family for supporting and encouraging me.

References

(30) Calibration and Operation of a High Volume Mass Flow Controlled Ambient Particulate Sampler - YouTube. n.d. Available: https://www.youtube.com/watch?v=QPuuOPdJ77s&t=16s [2019, December 17].

Allen, A.G., Harrison, R.M. & Erisman, J.-W. 1989. Field measurements of the dissociation of ammonium nitrate and ammonium chloride aerosols. *Atmospheric Environment (1967)*. 23(7):1591–1599. DOI: 10.1016/0004-6981(89)90418-6.

Allen, G., Sioutas, C., Koutrakis, P., Reiss, R., Lurmann, F.W. & Roberts, P.T. 1997. Evaluation of the TEOM ® Method for Measurement of Ambient Particulate Mass in Urban Areas. *Journal of the Air & Waste Management Association*. 47(6):682–689. DOI: 10.1080/10473289.1997.10463923.

Altieri, K.E., Hastings, M.G., Peters, A.J., Oleynik, S. & Sigman, D.M. 2014. Isotopic evidence for a marine ammonium source in rainwater at Bermuda. *Global Biogeochemical Cycles*. 28(10):1066–1080. DOI: 10.1002/2014GB004809.

Altieri, K.E., Fawcett, S.E. & Hastings, M.G. 2021. Reactive Nitrogen Cycling in the Atmosphere and Ocean. *Annual Review of Earth and Planetary Sciences*. 49(1):513–540. DOI: 10.1146/annurev-earth-083120-052147.

Andreae, M.O. 1983. Soot Carbon and Excess Fine Potassium: Long-Range Transport of Combustion-Derived Aerosols. *Science (New York, N.Y.)*. 220:10–13. Available: http://www.sciencemag.org/content/220/4602/1148.short.

Background and History | World Metereological Organization. n.d. Available: https://community.wmo.int/background-and-history [2019, June 25].

Baker, A.R., Lesworth, T., Adams, C., Jickells, T.D. & Ganzeveld, L. 2010. Estimation of atmospheric nutrient inputs to the Atlantic ocean from 50°N to 50°S based on large-scale field sampling: Fixed nitrogen and dry deposition of phosphorus. *Global Biogeochemical Cycles*. 24(7):1–16. DOI: 10.1029/2009GB003634.

Boucher, O., Randall, D., Artaxo, P., Bretherton, C., Feingold, G., Forster, P., Kerminen, V., Kondo, Y., et al. 2013. Clouds and Aerosols. In *Climate Change 2013 - The Physical Science Basis*. Intergovernmental Panel on Climate Change, Ed. Cambridge: Cambridge University Press. 571–658. DOI: 10.1017/CBO9781107415324.016.

Brévière, E. & SOLAS Scientific Steering Committee (eds.). 2016. *Solas 2015-2025: Science Plan and Organisation.* Available: http://www.solas-int.org.

Brunke, E.G., Labuschagne, C., Parker, B., Scheel, H.E. & Whittlestone, S. 2004. Baseline air mass selection at Cape Point, South Africa: Application of 222Rn and other filter criteria to CO2. *Atmospheric Environment*. 38(33):5693–5702. DOI: 10.1016/j.atmosenv.2004.04.024.

Calvo, A.I., Alves, C., Castro, A., Pont, V., Vicente, A.M. & Fraile, R. 2013. Research on aerosol sources and chemical composition: Past, current and emerging issues. *Atmospheric Research*. 120–121:1–28. DOI: 10.1016/j.atmosres.2012.09.021.

Cavalli, F. 2004. Advances in characterization of size-resolved organic matter in marine aerosol over the North Atlantic. *Journal of Geophysical Research*. 109(D24):D24215. DOI: 10.1029/2004JD005137.

Ceburnis, D., O'Dowd, C.D., Jennings, G.S., Facchini, M.C., Emblico, L., Decesari, S., Fuzzi, S. & Sakalys, J. 2008. Marine aerosol chemistry gradients: Elucidating primary and secondary processes and fluxes. *Geophysical Research Letters*. 35(7). DOI: 10.1029/2008GL033462.

Charlson, R.J., Lovelock, J.E., Andreae, M.O. & Warren, S.G. 1987. Oceanic phytoplankton, atmospheric sulphur, cloud albedo and climate. *Nature*. 326(6114):655–661. DOI: 10.1038/326655a0.

Cross, M. 2015. PySPLIT: a Package for the Generation, Analysis, and Visualization of HYSPLIT Air Parcel Trajectories. In *Proceedings of the 14th Python in Science Conference*. SciPy. 133–137. DOI: 10.25080/majora-7b98e3ed-014.

Davidson, E.A. & Kingerlee, W. 1997. A global inventory of nitric oxide emissions from soils. *Nutrient Cycling in Agroecosystems 1997 48:1*. 48(1):37–50. DOI: 10.1023/A:1009738715891.

Díaz, J.P., Expósito, F.J., Torres, C.J., Herrera, F., Prospero, J.M. & Romero, M.C. 2001. Radiative properties of aerosols in Saharan dust outbreaks using ground-based and satellite data: Applications to radiative forcing. *Journal of Geophysical Research Atmospheres*. 106(D16):18403–18416. DOI: 10.1029/2001JD900020.

Duce, R.A., LaRoche, J., Altieri, K., Arrigo, K.R., Baker, A.R., Capone, D.G., Cornell, S., Dentener, F., et al. 2008. Impacts of Atmospheric Anthropogenic Nitrogen on the Open Ocean. *Science*. 320(5878):893–897. DOI: 10.1126/science.1150369.

Erisman, J.W., Sutton, M.A., Galloway, J., Klimont, Z. & Winiwarter, W. 2008. How a century of ammonia synthesis changed the world. *Nature Geoscience*. 1(10):636–639. DOI: 10.1038/ngeo325.

Erisman, J.W., Galloway, J.N., Seitzinger, S., Bleeker, A., Dise, N.B., Petrescu, A.M.R., Leach, A.M., Vries, W. De, et al. 2013. Consequences of human modification of the global nitrogen cycle.

Finlayson-Pitts, B.J. & Pitts, J.N. 2000. Chemistry of the Upper and Lower Atmosphere: Theory, Experiments, and Applications. 969. Available: http://www.sciencedirect.com/science/book/9780122570605 [2021, July 08].

Follett, R.F. & Hatfield, J.L. 2001. Nitrogen in the Environment: Sources, Problems, and Management. *TheScientificWorldJOURNAL*. 1:920–926. DOI: 10.1100/TSW.2001.269.

Forster, C., Wandinger, U., Wotawa, G., James, P., Mattis, I., Althausen, D., Simmonds, P., O'Doherty, S., et al. 2001. Transport of boreal forest fire emissions from Canada to Europe. *Journal of Geophysical Research Atmospheres*. 106(D19):22887–22906. DOI: 10.1029/2001JD900115.

Fowler, D., Coyle, M., Skiba, U., Sutton, M.A., Cape, J.N., Reis, S., Sheppard, L.J., Jenkins, A., et al. 2013. The global nitrogen cycle in the Twentyfirst century. *Philosophical Transactions of the Royal Society B: Biological Sciences*. 368(1621). DOI: 10.1098/rstb.2013.0164.

Freeman, B., Gharabaghi, B., Thé, J., Munshed, M., Faisal, S., Abdullah, M. & Al Aseed, A. 2017. Mapping air quality zones for coastal urban centers. *Journal of the Air and Waste Management Association*. 67(5):565–581. DOI: 10.1080/10962247.2016.1265025.

Galloway, J.N. 1998. The global nitrogen cycle: changes and consequences. *Environmental Pollution*. 102(1):15–24. DOI: 10.1016/S0269-7491(98)80010-9.

Galloway, J.N., Schlesinger, W.H., Levy, H., Michaels, A. & Schnoor, J.L. 1995. Nitrogen fixation: Anthropogenic enhancement-environmental response. *Global Biogeochemical Cycles*. 9(2):235–252. DOI: 10.1029/95GB00158.

Galloway, J.N., Aber, J.D., Erisman, J.W., Seitzinger, S.P., Howarth, R.W., Cowling, E.B. & Cosby, B.J. 2003. The Nitrogen Cascade. *BioScience*. 53(4):341. DOI: 10.1641/0006-3568(2003)053[0341:tnc]2.0.co;2.

Galloway, J.N., Dentener, F.J., Capone, D.G., Boyer, E.W., Howarth, R.W., Seitzinger, S.P., Asner, G.P., Cleveland, C.C., et al. 2004. *Nitrogen Cycles: Past, Present, and Future.* Available: papers://aa15ed4a-8b41-4036-84a6-41087bba0cd6/Paper/p3387.

Galloway, J.N., Townsend, A.R., Erisman, J.W., Bekunda, M., Cai, Z., Freney, J.R., Martinelli, L.A.,

Seitzinger, S.P., et al. 2008. Transformation of the Nitrogen Cycle: Recent Trends, Questions, and Potential Solutions. *Science*. 320(5878):889–892. DOI: 10.1126/science.1136674.

Galloway, J.N., Winiwarter, W., Leip, A., Leach, A.M., Bleeker, A. & Erisman, J.W. 2014. Nitrogen footprints: Past, present and future. *Environmental Research Letters*. 9(11). DOI: 10.1088/1748-9326/9/11/115003.

GAW stations network and other measurements | World Metereological Organization. n.d. Available: https://community.wmo.int/gaw-stations-network-and-other-measurements [2019, June 25].

Ginoux, P., Chin, M., Tegen, I., Prospero, J.M., Holben, B., Dubovik, O. & Lin, S.J. 2001. Sources and distributions of dust aerosols simulated with the GOCART model. *Journal of Geophysical Research Atmospheres*. 106(D17):20255–20273. DOI: 10.1029/2000JD000053.

Global Atmosphere Watch Station Information System (GAWSIS). n.d. Available: https://gawsis.meteoswiss.ch/GAWSIS/#/search/station/stationReportDetails/465 [2019, June 25].

Gruber, N. & Galloway, J.N. 2008. An Earth-system perspective of the global nitrogen cycle. *Nature*. 451(7176):293–296. DOI: 10.1038/nature06592.

Hamilton, D.S., Lee, L.A., Pringle, K.J., Reddington, C.L., Spracklen, D. V. & Carslaw, K.S. 2014. Occurrence of pristine aerosol environments on a polluted planet. *Proceedings of the National Academy of Sciences of the United States of America*. 111(52):18466–18471. DOI: 10.1073/pnas.1415440111.

Henning, S., Weingartner, E., Schwikowski, M., Gaggeler, H.W., Gehrig, R., Hinz, K.-P., Trimbom, A., Spengler, B., et al. 2003. *Seasonal variation of water-soluble ions of the aerosol at the high-alpine site Jungfraujoch (3580 m asl)*.

History of Mace Head. n.d. Available: http://www.macehead.org/index.php?option=com_content&view=article&id=45&Itemid=58 [2021, May 27].

HiVol Cascade Impactors - Tisch Environmental. n.d. Available: https://tisch-env.com/impactors/hivol-cascade-impactors/ [2019, December 11].

Jickells, T.D., Dorling, S., Deuser, W.G., Church, T.M., Arimoto, R. & Prospero, J.M. 1998. Air-borne dust fluxes to a deep water sediment trap in the Sargasso Sea. *Global Biogeochemical Cycles*. 12(2):311–320. DOI: 10.1029/97GB03368.

Jickells, T.D., Kelly, S.D., Baker, A.R., Biswas, K., Dennis, P.F., Spokes, L.J., Witt, M. & Yeatman, S.G.

2003. Isotopic evidence for a marine ammonia source. *Geophysical Research Letters*. 30(7):30–33. DOI: 10.1029/2002GL016728.

Jickells, T.D., Buitenhuis, E., Altieri, K., Baker, A.R., Capone, D., Duce, R.A., Dentener, F., Fennel, K., et al. 2017. A reevaluation of the magnitude and impacts of anthropogenic atmospheric nitrogen inputs on the ocean. *Global Biogeochemical Cycles*. 31(2):289–305. DOI: 10.1002/2016GB005586.

Johnson, M.T. & Bell, T.G. 2008. Coupling between dimethylsulfide emissions and the ocean-atmosphere exchange of ammonia. *Environmental Chemistry*. 5(4):259–267. DOI: 10.1071/EN08030.

Kamezaki, K., Hattori, S., Iwamoto, Y., Ishino, S., Furutani, H., Miki, Y., Uematsu, M., Miura, K., et al. 2019. Tracing the Sources and Formation Pathways of Atmospheric Particulate Nitrate over the Pacific Ocean Using Stable Isotopes. *Atmospheric Environment*. DOI: 10.1016/j.atmosenv.2019.04.026.

Karl, D.M. & Michaels, A.F. 2001. Nitrogen Cycle. In *Encyclopedia of Ocean Sciences*. Elsevier. 1876–1884. DOI: 10.1006/rwos.2001.0275.

Klouda, K., Brdka, S. & Othal, P. 2012. Experiences with Anthropogenic Aerosol Spread in the Environment. In *Atmospheric Aerosols - Regional Characteristics - Chemistry and Physics*. InTech. DOI: 10.5772/48439.

Levy, H. 1988. The Aeroce Project. In *Tropospheric Ozone*. Dordrecht: Springer Netherlands. 365–370. DOI: 10.1007/978-94-009-2913-5_22.

Li, J., Pósfai, M., Hobbs, P. V & Buseck, P.R. 2003. Individual aerosol particles from biomass burning in southern Africa: 2, Compositions and aging of inorganic particles. *J. Geophys. Res*. 108(D13):8484. DOI: 10.1029/2002JD002310.

Li, L., Tutone, A.F., Drummond, R.S.M., Gardner, R.C. & Luan, S. 2001. A Novel Family of Magnesium Transport Genes in Arabidopsis. *The Plant Cell*. 13(12):2761–2775. DOI: 10.1105/tpc.010352.

Luo, L., Zhang, Y.Y., Xiao, H.Y., Xiao, H.W., Zheng, N.J., Zhang, Z.Y., Xie, Y.J. & Liu, C. 2019. Spatial distributions and sources of inorganic chlorine in PM2.5 across China in winter. *Atmosphere*. 10(9):505. DOI: 10.3390/atmos10090505.

Maring, H., Savoie, D.L., Izaguirre, M.A., McCormick, C., Arimoto, R., Prospero, J.M. & Pilinis, C. 2000. Aerosol physical and optical properties and their relationship to aerosol composition in the free troposphere at Izaña, Tenerife, Canary Islands, during July 1995. *Journal of Geophysical Research Atmospheres*. 105(D11):14677–14700. DOI: 10.1029/2000JD900106.

Millero, F.J. 2013. *Chemical oceanography fourth edition*. DOI: 10.1016/S0422-9894(08)70141-7.

Mkoma, S.L., Da Rocha, G.O., Domingos, J.S.S., Santos, J.V.S., Cardoso, M.P., Da Silva, R.L. & De Andrade, J.B. 2014. Atmospheric particle dry deposition of major ions to the South Atlantic coastal area observed at Baía de Todos os Santos, Brazil. *An Acad Bras Cienc*. 86(1). DOI: 10.1590/0001-3765201420130234.

Mlonka-Mędrala, A., Magdziarz, A., Gajek, M., Nowińska, K. & Nowak, W. 2020. Alkali metals association in biomass and their impact on ash melting behaviour. *Fuel*. 261:116421. DOI: 10.1016/j.fuel.2019.116421.

Monks, P.S., Granier, C., Fuzzi, S., Stohl, A., Williams, M.L., Akimoto, H., Amann, M., Baklanov, A., et al. 2009. Atmospheric composition change – global and regional air quality. *Atmospheric Environment*. 43(33):5268–5350. DOI: 10.1016/J.ATMOSENV.2009.08.021.

Moody, J.L., Oltmans, S.J., Levy, H. & Merrill, J.T. 1995. Transport climatology of tropospheric ozone: Bermuda, 1988-1991. *Journal of Geophysical Research*. 100(D4):7179–7194. DOI: 10.1029/94JD02830.

Mulcahy, J.P., O'Dowd, C.D., Jennings, S.G. & Ceburnis, D. 2008. Significant enhancement of aerosol optical depth in marine air under high wind conditions. *Geophysical Research Letters*. 35(16):16810. DOI: 10.1029/2008GL034303.

Nixon, S.W. 1988. Physical energy inputs and the comparative ecology of lake and marine ecosystems. *Limnology and Oceanography*. 33(4part2):1005–1025. DOI: 10.4319/lo.1988.33.4part2.1005.

O'Connor, T.C., Jennings, S.G. & O'Dowd, C.D. 2008. Highlights of fifty years of atmospheric aerosol research at Mace Head. *Atmospheric Research*. 90(2–4):338–355. DOI: 10.1016/j.atmosres.2008.08.014.

O'dowd, C.D., Jimenez, J.L., Bahreini, R., Flagan, R.C., Seinfeld, J.H., Hämerl, K., Pirjola, L., Kulmala, M., et al. 2002. Marine aerosol formation from biogenic iodine emissions. *Nature*. 417(6889):632–636. DOI: 10.1038/nature00775.

O'Dowd, C., Ceburnis, D., Ovadnevaite, J., Vaishya, A., Rinaldi, M. & Facchini, M.C. 2014. Do anthropogenic, continental or coastal aerosol sources impact on a marine aerosol signature at Mace Head? *Atmospheric Chemistry and Physics*. 14(19):10687–10704. DOI: 10.5194/acp-14-10687-2014.

Oltmans, S.J., Levy, H., Harris, J.M., Merrill, J.T., Moody, J.L., Lathrop, J.A., Cuevas, E., Trainer, M., et al. 1996. Summer and spring ozone profiles over the North Atlantic from ozonesonde measurements. *Journal of Geophysical Research Atmospheres*. 101(22):29179–29200. DOI: 10.1029/96jd01713.

Pachon, J.E., Weber, R.J., Zhang, X., Mulholland, J.A. & Russell, A.G. 2013. Revising the use of

potassium (K) in the source apportionment of PM2.5. *Atmospheric Pollution Research*. 4(1):14–21. DOI: 10.5094/APR.2013.002.

Pakkanen, T.A. 1996. Study of formation of coarse particle nitrate aerosol. *Atmospheric Environment*. 30(14):2475–2482. DOI: 10.1016/1352-2310(95)00492-0.

Park, S.S. & Kim, Y.J. 2005. Source contributions to fine particulate matter in an urban atmosphere. *Chemosphere*. 59(2):217–226. DOI: 10.1016/j.chemosphere.2004.11.001.

Paton-walsh, C., Guérette, É., Kubistin, D., Humphries, R., Wilson, S.R., Dominick, D., Galbally, I., Buchholz, R., et al. 2017. The MUMBA campaign : measurements of urban , marine and biogenic air. 349–362.

Paton-Walsh, C., Guérette, É.A., Emmerson, K., Cope, M., Kubistin, D., Humphries, R., Wilson, S., Buchholz, R., et al. 2018. Urban air quality in a coastal city: Wollongong during the MUMBA campaign. *Atmosphere*. 9(12). DOI: 10.3390/atmos9120500.

Paulot, F., Jacob, D.J., Johnson, M.T., Bell, T.G., Baker, A.R., Keene, W.C., Lima, I.D., Doney, S.C., et al. 2015. Global oceanic emission of ammonia: Constraints from seawater and atmospheric observations. *Global Biogeochemical Cycles*. 29(8):1165–1178. DOI: 10.1002/2015GB005106.

Penner, J.E., Andreae, M.O., Annegarn, H., Barrie, L.A., Feichter, J., Hegg, D., Jayaraman, A., Leaitch, R., et al. 2001. Aerosols, their Direct and Indirect Effects. In *CLIMATE CHANGE 2001: THE SCIENTIFIC BASIS. Contribution of Working Group I to the Third Assessment Report of the Intergovernmental Panel on Climate Change*. and C.A.J. Houghton, J.T., Y. Ding, D.J. Griggs, M. Noguer, P.J. van der Linden, X. Dai, K. Maskell, Ed. Cambridge University Press, Cambridge, United Kingdom and New York, NY, USA.

Pio, C.A., Legrand, M., Oliveira, T., Afonso, J., Santos, C., Caseiro, A., Fialho, P., Barata, F., et al. 2007. Climatology of aerosol composition (organic versus inorganic) at nonurban sites on a west-east transect across Europe. *Journal of Geophysical Research Atmospheres*. 112(23). DOI: 10.1029/2006JD008038.

Pio, C.A., Legrand, M., Alves, C.A., Oliveira, T., Afonso, J., Caseiro, A., Puxbaum, H., Sanchez-Ochoa, A., et al. 2008. Chemical composition of atmospheric aerosols during the 2003 summer intense forest fire period. *Atmospheric Environment*. 42(32):7530–7543. DOI: 10.1016/j.atmosenv.2008.05.032.

Pope, C.A., Thun, M.J., Namboodiri, M.M., Dockery, D.W., Evans, J.S., Speizer, F.E. & Heath, C.W. 1995. Particulate air pollution as a predictor of mortality in a prospective study of U.S. Adults. *American Journal of Respiratory and Critical Care Medicine*. 151(3 I):669–674. DOI: 10.1164/ajrccm.151.3.7881654.

Popescu, F. & Ionel, I. 2010. Anthropogenic Air Pollution Sources. In *Air Quality*. Sciyo. DOI: 10.5772/9751.

Popovicheva, O., Kozlov, V., Kireeva, E., Persianseva, N., Engling, G., Eleftheriadis, K., Diapouli, E. & Saraga, D. 2014. Aerosol in emissions of Siberian biomass burning : small-scale fire study. (July). DOI: 10.14644/dust.2014.066.

Prados, A.I., Dickerson, R.R., Doddridge, B.G., Milne, P.A., Moody, J.L. & Merrill, J.T. 1999. Transport of ozone and pollutants from North America to the North Atlantic Ocean during the 1996 Atmosphere/Ocean Chemistry Experiment (AEROCE) intensive. *Journal of Geophysical Research Atmospheres*. 104(D21):26219–26233. DOI: 10.1029/1999JD900444.

Prospero, J.M. 1999. Assessing the impact of advected african dust on air quality and health in the eastern United States. *Human and Ecological Risk Assessment (HERA)*. 5(3):471–479. DOI: 10.1080/10807039.1999.10518872.

Prospero, J.M. 2001. The Atmosphere-Ocean Chemistry Experiment (AEROCE): Background and major accomplishments. *IGACtivities News*. (24):3–5. Available: https://igacproject.org/sites/default/files/2016-07/Issue_24_Aug_2001.pdf [2021, June 15].

Richardson, K. & Jørgensen, B.B. 1996. Eutrophication: Definition, history and effects. In *Eutrophication in Coastal Marine Ecosystems*. V. 52. 1–19. DOI: 10.1029/CE052p0001.

Rinaldi, M., Facchini, M.C., Decesari, S., Carbone, C., Finessi, E., Mircea, M., Fuzzi, S., Ceburnis, D., et al. 2009. On the representativeness of coastal aerosol studies to open ocean studies: Mace Head-a case study. *Atmospheric Chemistry and Physics*. 9(24):9635–9646. DOI: 10.5194/acp-9-9635-2009.

Safai, P.D., Budhavant, K.B., Rao, P.S.P., Ali, K. & Sinha, A. 2010. Source characterization for aerosol constituents and changing roles of calcium and ammonium aerosols in the neutralization of aerosol acidity at a semi-urban site in SW India. *Atmospheric Research*. 98(1):78–88. DOI: 10.1016/j.atmosres.2010.05.011.

Saltzman, E.S. 2009. Marine aerosols. In *Surface Ocean-Lower Atmosphere Processes*. 17–35. DOI: 10.1029/2008GM000769.

Savoie, D.L. 2001. AEROCE - 10 Years of Atmospheric Chemistry at Bermuda. *AGUFM*. OS52C-05. Available: https://ui.adsabs.harvard.edu/abs/2001AGUFMOS52C..05S/abstract [2021, May 26].

Savoie, D.L. 2002. Marine biogenic and anthropogenic contributions to non-sea-salt sulfate in the marine boundary layer over the North Atlantic Ocean. *Journal of Geophysical Research*. 107(D18):4356. DOI: 10.1029/2001JD000970.

Scarchilli, C., Frezzotti, M. & Ruti, P.M. 2011. Snow precipitation at four ice core sites in East Antarctica: Provenance, seasonality and blocking factors. *Climate Dynamics*. 37(9–10):2107–2125. DOI: 10.1007/s00382-010-0946-4.

Schumann, U. & Huntrieser, H. 2007. The global lightning-induced nitrogen oxides source. *Atmospheric Chemistry and Physics*. 7(14):3823–3907. DOI: 10.5194/acp-7-3823-2007.

Seinfeld, J.H., Bretherton, C., Carslaw, K.S., Coe, H., DeMott, P.J., Dunlea, E.J., Feingold, G., Ghan, S., et al. 2016. Improving our fundamental understanding of the role of aerosol-cloud interactions in the climate system. *Proceedings of the National Academy of Sciences of the United States of America*. 113(21):5781–5790. DOI: 10.1073/pnas.1514043113.

Seitzinger, S.P. & Kroeze, C. 1998. Global distribution of nitrous oxide production and N inputs in freshwater and coastal marine ecosystems. *Global Biogeochemical Cycles*. 12(1):93–113. DOI: 10.1029/97GB03657.

Sigman, D.M. & Hain, M.P. 2012. The Biological Productivity of the Ocean. *Nature Education Knowledge*. 3(6):1–16. Available: https://www.nature.com/scitable/knowledge/library/the-biological-productivity-of-the-ocean-70631104/.

Steinberg, D.K. & Saba, G.K. 2008. Nitrogen Consumption and Metabolism in Marine Zooplankton. In *Nitrogen in the Marine Environment*. Elsevier Inc. 1135–1196. DOI: 10.1016/B978-0-12-372522-6.00026-8.

Thor, K. 2019. Calcium—Nutrient and Messenger. *Frontiers in Plant Science*. 10:440. DOI: 10.3389/fpls.2019.00440.

Vaattovaara, P., Huttunen, P.E., Yoon, Y.J., Joutsensaari, J., Lehtinen, K.E.J., O'Dowd, C.D. & Laaksonen, A. 2006. The composition of nucleation and Aitken modes particles during coastal nucleation events: Evidence for marine secondary organic contribution. *Atmospheric Chemistry and Physics*. 6(12):4601–4616. DOI: 10.5194/acp-6-4601-2006.

Vignati, E., de Leeuw, G., Schulz, M. & Plate, E. 1999. Characterization of aerosols at a coastal site near Vindeby (Denmark). *Journal of Geophysical Research: Oceans*. 104(C2):3277–3287. DOI: 10.1029/1998JC900019.

Voss, M. & Hietanen, S. 2013. Biogeochemistry: The depths of nitrogen cycling. *Nature*. 493(7434):616–618. DOI: 10.1038/493616a.

Wentworth, G.R., Murphy, J.G., Croft, B., Martin, R. V., Pierce, J.R., Côté, J.S., Courchesne, I., Tremblay, J.É., et al. 2016. Ammonia in the summertime Arctic marine boundary layer: Sources, sinks, and

implications. *Atmospheric Chemistry and Physics*. 16(4):1937–1953. DOI: 10.5194/acp-16-1937-2016.

Wolfe, A.H. & Patz, J.A. 2002. Reactive nitrogen and human health: Acute and long-term implications. *Ambio*. 31(2):120–125. DOI: 10.1579/0044-7447-31.2.120.

Xu, G., Gao, Y., Lin, Q., Li, W. & Chen, L. (in press). Characteristics of water-soluble inorganic and organic ions in aerosols over the Southern Ocean and coastal East Antarctica during austral summer. *Journal of Geophysical Research: Atmospheres*. 118(23):13,303-13,318. DOI: 10.1002/2013JD019496.

Yeatman, S.G., Spokes, L.J. & Jickells, T.D. 2001. Comparisons of coarse-mode aerosol nitrate and ammonium at two polluted coastal sites. *Atmospheric Environment*. 35(7):1321–1335. DOI: 10.1016/S1352-2310(00)00452-0.

Yoon, Y.J., Ceburnis, D., Cavalli, F., Jourdan, O., Putaud, J.P., Facchini, M.C., Decesari, S., Fuzzi, S., et al. 2007. Seasonal characteristics of the physicochemical properties of North Atlantic marine atmospheric aerosols. *Journal of Geophysical Research*. 112(D4):D04206. DOI: 10.1029/2005JD007044.

Zhang, M., Chen, J.M., Wang, T., Cheng, T.T., Lin, L., Bhatia, R.S. & Hanvey, M. 2010. Chemical characterization of aerosols over the Atlantic Ocean and the Pacific Ocean during two cruises in 2007 and 2008. *Journal of Geophysical Research Atmospheres*. 115(22):22302. DOI: 10.1029/2010JD014246.

Appendix

Table A1: Average concentration of major ions (nmol/filter) in ground-based HVAS field blanks for each stage (standard deviation in parenthesis).

	Na^+	NH_4^+	K^+	Mg^{2+}	Ca^{2+}	Cl^-	NO_3^-	SO_4^{2-}
Stage 1	10136.1 (2436.8)	137.8 (29.6)	598.4 (118.9)	44.5 (11.8)	241.2 (54.6)	3256.6 (1868.8)	361.6 (146.6)	53.7 (38.0)
Stage 2	11849.4 (3089.1)	148.8 (41.5)	918.0 (389.7)	34.4 (5.2)	177.9 (90.8)	3856.4 (2059.7)	407.3 (135.0)	116.0 (26.7)
Stage 3	11512.4 (3203.4)	162.4 (47.8)	692.4 (171.5)	56.3 (29.1)	287.5 (121.4)	3653.4 (1963.3)	339.7 (258.3)	40.6 (57.4)
Stage 4	10865.5 (2970.2)	150.0 (41.8)	573.8 (79.3)	46.0 (21.4)	243.8 (68.0)	4068.1 (2059.7)	159.7 (225.8)	36.4 (51.5)
Stage 5	12000.2 (3240.1)	158.1 (30.7)	915.9 (310.1)	68.2 (25.6)	401.6 (182.6)	3382.2 (1803.4)	466.8 (160.4)	40.8 (57.7)
Back up	38888.4 (5001.8)	332.3 (57.4)	1891.0 (142.1)	104.1 (5.4)	400.4 (61.3)	16854.6 (3884.6)	571.2 (504.0)	97.4 (137.7)

Table A2: P-values for t-test comparing PM_{10} to total HVAS, HVAS S2-BU, HVAS S3-BU, and HVAS S4-BU (>0.05 is significant)

	Na^+	NH_4^+	K^+	Mg^{2+}	Ca^{2+}	Cl^-	NO_3^-	SO_4^{2-}	nss-SO_4^{2-}
PM_{10}-HVAS	0.000	0.999	0.000	0.000	0.000	0.000	0.000	0.000	0.000
PM_{10}-HVAS S2-BU	0.000	0.957	0.000	0.000	0.000	0.000	0.000	0.000	0.001
PM_{10}-HVAS S3-BU	0.901	0.804	0.001	0.241	0.215	0.671	0.169	0.008	0.010
PM_{10}-HVAS S4-BU	0.004	0.747	0.041	0.000	0.554	0.001	0.442	0.096	0.030

TE-5170 Calibration

Site Information

Location:	Cape poi nt , Cape Town	**Site ID:**		**Date:**	11/ 06/ 2018 - 12: 20
Sampler:	TE- 5170	**Serial No:**		**Tech:**	Kur t Spence / Br andon Cpi e

Site Conditions

Barometric Pressure (mBar):	997, 40	**Corrected Pressure (mm Hg):**	748
Temperature (deg C):	18	**Temperature (deg K):**	291
Average Press. (mBar):	995, 00	**Corrected Average (mm Hg):**	746
Average Temp. (deg C):	20	**Average Temp. (deg K):**	293

Calibration Orifice

Make:	Ti sch	**Qstd Slope:**	1, 55683
Model:	TE- 5028A	**Qstd Intercept:**	- 0, 00238
Serial#:	1179	**Date Certified:**	22/ 08/ 2016

Calibration Information

Plate or Test #	H2O (cm)	Qstd (m3/min)	I (chart)	IC (corrected)	Linear Regression	
1	6, 04	0, 996	59, 6	59, 83	**Slope:**	54,5966
2	4, 30	0, 840	51, 8	52, 00	**Intercept:**	6,0495
3	2, 86	0, 686	42, 7	42, 86	**Corr. Coeff:**	0,9992
4	2, 22	0, 604	39, 0	39, 15		
5	3, 41	0, 749	46, 5	46, 68	**# of Observations:**	12
6	5, 24	0, 928	56, 0	56, 21		
7	6, 38	1, 023	61, 8	62, 04		
8	4, 91	0, 898	54, 6	54, 81		
9	3, 75	0, 785	48, 6	48, 79		
10	2, 47	0, 637	40, 2	40, 35		
11	4, 37	0, 847	52, 3	52, 50		
12	5, 84	0, 979	59, 1	59, 33		

Calculations

Qstd = 1/m[Sqrt(H2O(Pa/Pstd)(Tstd/Ta))-b]

IC = I[Sqrt(Pa/Pstd)(Tstd/Ta)]

Qstd = standard flow rate

IC = corrected chart response

I = actual chart response

m = calibrator Qstd slope

b = calibrator Qstd intercept

Ta = actual temperature during calibration (deg K)

Pa = actual pressure during calibration (mm Hg)

Tstd = 298 deg K

Pstd = 760 mm Hg

For subsequent calculation of sampler flow:

1/m((I)[Sqrt(298/Tav)(Pav/760)]-b)

m = sampler slope

b = sampler intercept

I = chart response

Tav = daily average temperature

Pav = daily average pressure

Average I (chart):	44, 0
Average Flow Calculation m3/min	
0,694601759	
Average Flow Calculation in CFM	
24,5263881	
Sample Time (Hrs):	24, 0
Total Volume in m3	
1000,226532	
Total Flow in CF	
35317,99886	

NOTE: Ensure calibration orifice has been certified within 12 months of use

Tisch Environmental 145 South Miami Ave, Cleves OH 45002 ● 877.263.7610 ● sales@tisch-env.com ● www.tisch-env.com

Figure A1: High volume air sampler calibration sheet from 11/06/2018

TE-5170 Calibration Worksheet

Site Information

Location:	Cape poi nt , Cape Town	**Site ID:**		**Date:**	09/ 09/ 2018
Sampler:	TE- 5170	**Serial No:**		**Tech:**	Kur t Spence

Site Conditions

Barometric Pressure (mBar):	1000, 90	**Corrected Pressure (mm Hg):**	751
Temperature (deg C):	16	**Temperature (deg K):**	289
Average Press. (mBar):	995, 00	**Corrected Average (mm Hg):**	746
Average Temp. (deg C):	20	**Average Temp. (deg K):**	293

Calibration Orifice

Make:	Ti sch	**Qstd Slope:**	1, 55683
Model:	TE- 5028A	**Qstd Intercept:**	- 0, 00238
Serial#:	3202	**Date Certified:**	22/ 08/ 2016

Calibration Information

Plate or Test #	H2O (cm)	Qstd (m3/min)	I (chart)	IC (corrected)	Linear Regression	
1	6, 50	1, 039	62, 1	62, 68	**Slope:**	54,5154
2	5, 89	0, 989	59, 8	60, 36	**Intercept:**	6,1477
3	5, 23	0, 932	56, 3	56, 83	**Corr. Coeff:**	0,9996
4	3, 90	0, 805	49, 3	49, 76		
5	2, 86	0, 690	43, 5	43, 91	**# of Observations:**	6
6	2, 30	0, 619	40, 1	40, 48		

Calculations

Qstd = 1/m[Sqrt(H2O(Pa/Pstd)(Tstd/Ta))-b]

IC = I[Sqrt(Pa/Pstd)(Tstd/Ta)]

Qstd = standard flow rate

IC = corrected chart response

I = actual chart response

m = calibrator Qstd slope

b = calibrator Qstd intercept

Ta = actual temperature during calibration (deg K)

Pa = actual pressure during calibration (mm Hg)

Tstd = 298 deg K

Pstd = 760 mm Hg

For subsequent calculation of sampler flow:

1/m((I)[Sqrt(298/Tav)(Pav/760)]-b)

m = sampler slope

b = sampler intercept

I = chart response

Tav = daily average temperature

Pav = daily average pressure

Average I (chart):	44, 0
Average Flow Calculation m3/min	
0,693835033	
Average Flow Calculation in CFM	
24,49931503	
Sample Time (Hrs):	24, 0
Total Volume in m3	
999,122448	
Total Flow in CF	
35279,01364	

NOTE: Ensure calibration orifice has been certified within 12 months of use

Tisch Environmental 145 South Miami Ave, Cleves OH 45002 ● 877.263.7610 ● sales@tisch-env.com ● www.tisch-env.com

Figure A2: High volume air sampler calibration sheet from 09/09/2018

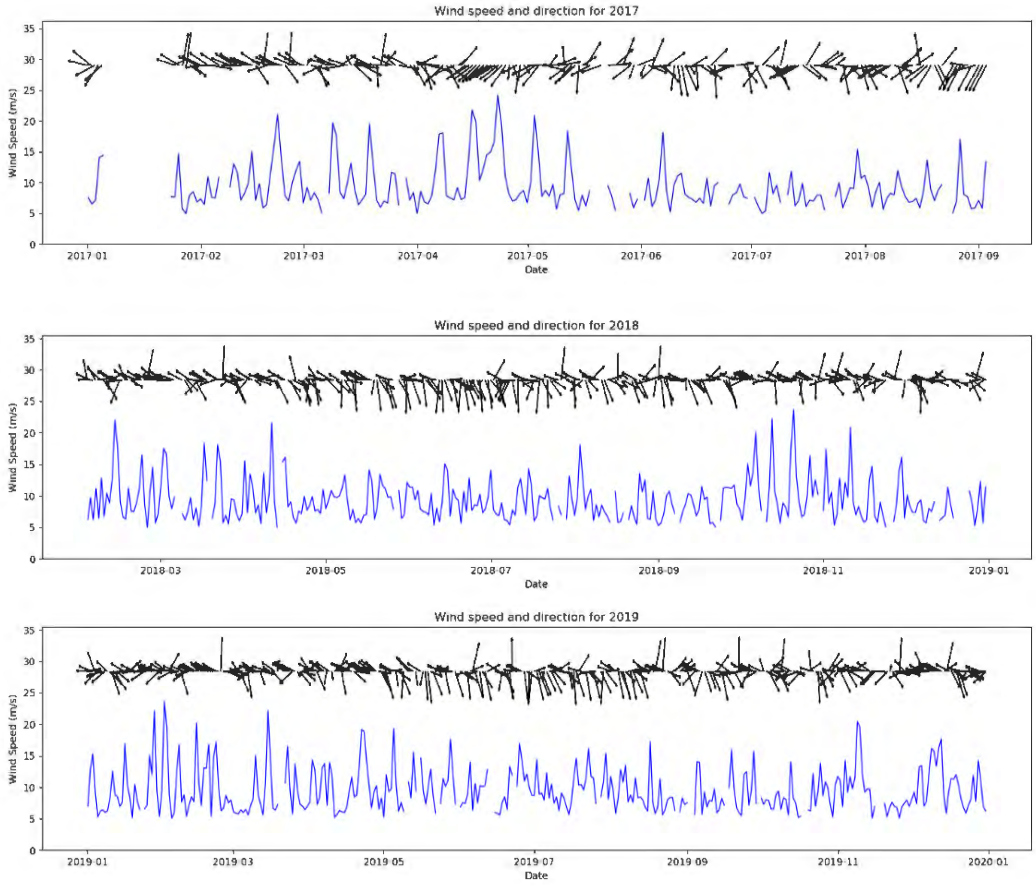

Figure A3: Wind speed and direction (vector arrows) for Cape Point 2017-2019

Table A3: Tall-tower PM_{10} aerosol concentrations (nmol/m^3) for non-sector-controlled tower samples (19 June 2017 to 05 July 2018; n= 73)

NSC	Na^+	NH_4^+	K^+	Mg^{2+}	Ca^{2+}	Cl^-	NO_3^-	SO_4^{2-}	nss-SO_4^{2-}
Average	76.6	5.4	2.2	8.2	2.6	102.1	8.7	12.1	7.5
Standard deviation	39.8	5.1	1.3	4.2	1.4	61.0	7.5	7.1	7.4
Minimum	0.0	0.5	0.0	0.4	0.0	11.9	0.3	5.0	-3.1
Maximum	183.9	31.6	7.7	20.9	7.0	263.1	45.0	59.5	56.4

Table A4: Seasonal average tall-tower PM_{10} aerosol concentrations (nmol/m^3) for non-sector-controlled tower samples (standard deviation in parentheses)

NSC	Na^+	NH_4^+	K^+	Mg^{2+}	Ca^{2+}	Cl^-	NO_3^-	SO_4^{2-}	nss-SO_4^{2-}
Summer (n=3)	67.9 (20.9)	5.0 (1.4)	3.6 (3.0)	8.4 (1.1)	3.3 (1.7)	114.7 (19.9)	6.5 (1.5)	12.5 (2.9)	8.4 (1.8)
Autumn (n=24)	44.5 (22.8)	5.2 (5.0)	1.3 (0.8)	4.8 (2.3)	1.4 (0.9)	55.2 (30.3)	10.3 (10.8)	12.7 (10.6)	10.0 (10.6)
Winter (n=27)	90.7 (38.2)	5.2 (6.3)	2.3 (0.8)	9.5 (4.2)	3.0 (1.3)	113.4 (62.9)	7.2 (3.2)	10.9 (4.6)	5.4 (5.2)
Spring (n=19)	98.4 (36.5)	5.9 (3.9)	3.0 (1.5)	10.8 (3.6)	3.3 (1.3)	143.2 (54.8)	9.0 (7.3)	13.0 (4.6)	7.1 (4.5)

Table A5: Tall-tower PM_{10} aerosol concentrations (nmol/m^3) for sector-controlled tower samples (09 July 2018 to 24 August 2018; n= 7)

SC	Na^+	NH_4^+	K^+	Mg^{2+}	Ca^{2+}	Cl^-	NO_3^-	SO_4^{2-}	nss-SO_4^{2-}
Average	65.2	3.7	1.2	8.3	2.7	90.5	4.8	11.7	7.8
Standard deviation	32.2	2.7	1.2	3.5	1.9	50.3	6.8	5.0	5.9
Minimum	33.6	0.8	0.0	3.8	0.0	29.1	0.0	7.0	2.3
Maximum	113.5	8.7	3.1	14.7	6.2	148.9	19.2	21.6	18.8

Table A6: Seasonal average ground-based HVAS aerosol concentrations (nmol/m^3, standard deviation in parentheses)

	Na^+	NH_4^+	K^+	Mg^{2+}	Ca^{2+}	Cl^-	NO_3^-	SO_4^{2-}	nss-SO_4^{2-}
Autumn (n=8)									
Total	151.6 (81.9)	5.2 (4.7)	4.4 (2.8)	15.2 (8.4)	5.0 (3.5)	250.9 (108.6)	33.5 (15.3)	32.1 (4.5)	23.4 (3.2)
Coarse mode	142.6 (79.9)	1.4 (1.7)	3.2 (2.1)	14.6 (8.4)	4.4 (3.4)	245.4 (112.3)	28.3 (11.6)	17.8 (4.5)	9.4 (4.9)
Fine mode	9.0 (9.5)	3.8 (3.2)	1.3 (0.9)	0.7 (0.8)	0.6 (0.6)	5.5 (8.5)	5.3 (5.5)	14.3 (5.1)	14.0 (5.1)
Winter (n=16)									
Total	280.7 (97.9)	3.9 (8.5)	7.0 (2.2)	25.4 (8.6)	10.1 (4.9)	403.4 (193.9)	18.9 (10.7)	36.7 (12.6)	19.8 (14.8)
Coarse mode	250.1 (84.5)	0.6 (0.5)	4.9 (1.5)	23.9 (8.1)	8.8 (3.5)	377.7 (177.6)	15.5 (10.1)	21.8 (5.9)	6.7 (3.9)
Fine mode	30.6 (39.1)	3.3 (8.5)	2.1 (2.2)	1.5 (1.8)	1.3 (1.9)	25.7 (58.5)	3.4 (1.7)	14.9 (12.9)	13.1 (13.4)
Spring (n=9)									
Total	287.8 (72.0)	4.8 (8.4)	6.8 (3.1)	26.3 (6.5)	9.1 (3.4)	359.9 (96.7)	28.6 (21.7)	37.6 (15.1)	20.2 (13.8)
Coarse mode	264.4 (67.5)	1.3 (2.7)	5.2 (1.5)	25.1 (6.8)	8.4 (2.8)	340.7 (96.5)	23.6 (16.6)	22.3 (5.3)	6.3 (5.2)
Fine mode	23.4 (28.5)	3.5 (5.8)	1.6 (1.9)	1.2 (1.9)	0.6 (1.2)	19.2 (30.3)	5.0 (5.2)	15.3 (10.7)	13.9 (9.1)

Table A7: P-values for Welch test on seasonal average ground-based HVAS aerosol concentrations (>0.05 is significant; vales correspond to Table A6)

	Na^+	NH_4^+	K^+	Mg^{2+}	Ca^{2+}	Cl^-	NO_3^-	SO_4^{2-}	nss-SO_4^{2-}
Total									
Autumn-Winter	0.003	0.612	0.045	0.014	0.009	0.022	0.035	0.206	0.370
Autumn-Spring	0.003	0.892	0.117	0.010	0.029	0.047	0.592	0.327	0.520
Winter-Spring	0.837	0.794	0.880	0.776	0.555	0.463	0.237	0.892	0.949
Coarse mode									
Autumn-Winter	0.008	0.192	0.064	0.021	0.010	0.038	0.021	0.082	0.211
Autumn-Spring	0.005	0.912	0.040	0.014	0.019	0.083	0.509	0.080	0.237
Winter-Spring	0.649	0.436	0.615	0.713	0.810	0.507	0.211	0.843	0.845
Fine mode									
Autumn-Winter	0.051	0.828	0.202	0.129	0.179	0.194	0.372	0.862	0.809
Autumn-Spring	0.183	0.885	0.645	0.416	0.942	0.224	0.916	0.804	0.968
Winter-Spring	0.606	0.945	0.560	0.747	0.272	0.718	0.391	0.941	0.863

Table A8: Ground-based HVAS Non-sector-controlled major ion concentrations (16 April 2018 to 05 July 2018, 24 August 2018 to 30 August 2018, and 05 November 2018 to 10 November 2018, standard deviation in parentheses, nmol/m^3, n =20)

NSC	Na^+	NH_4^+	K^+	Mg^{2+}	Ca^{2+}	Cl^-	NO_3^-	SO_4^{2-}	nss-SO_4^{2-}
Total	231.2 (111.6)	5.1 (7.9)	5.7 (2.5)	22.1 (9.7)	7.9 (5.0)	354.3 (169.1)	24.0 (14.0)	34.1 (10.6)	20.4 (11.9)
Coarse mode	211.9 (95.9)	1.0 (1.1)	4.3 (2.0)	21.0 (9.2)	7.0 (3.9)	337.0 (155.2)	20.0 (11.9)	20.2 (6.0)	7.5 (4.2)
Fine mode	19.3 (35.1)	4.1 (7.7)	1.3 (1.2)	1.1 (1.6)	1.0 (1.7)	17.3 (51.2)	4.1 (3.8)	13.9 (11.0)	12.9 (11.5)

Table A9: Ground-based HVAS Sector-controlled major ion concentrations (09 July 2018 to 24 August 2018, and 30 August 2018 to 05 November 2018, standard deviation in parentheses, nmol/m^3, n=13)

SC	Na^+	NH_4^+	K^+	Mg^{2+}	Ca^{2+}	Cl^-	NO_3^-	SO_4^{2-}	nss-SO_4^{2-}
Total	282.3 (81.9)	3.4 (7.2)	7.3 (2.9)	24.9 (8.0)	9.5 (3.9)	355.0 (158.9)	26.7 (19.6)	38.5 (13.6)	21.5 (13.7)
Coarse mode	252.6 (80.9)	1.0 (2.2)	4.9 (1.5)	23.5 (8.0)	8.7 (3.3)	333.2 (150.5)	22.1 (15.6)	22.2 (4.7)	7.0 (5.3)
Fine mode	29.7 (26.3)	2.4 (5.0)	2.4 (2.5)	1.4 (1.6)	0.9 (1.1)	21.7 (30.8)	4.6 (4.3)	16.3 (10.2)	14.5 (9.1)

Table A10: Tall-tower PM_{10} aerosol ion concentrations (nmol/m^3) and radon concentrations (mBq/m^3) for different air mass history categories.

	Na^+	NH_4^+	K^+	Mg^{2+}	Ca^{2+}	Cl^-	NO_3^-	SO_4^{2-}	nss-SO_4^{2-}	Radon
Marine (n=8)										
Average	109.1	1.1	2.4	11.8	2.9	164.0	3.2	10.4	3.9	294.2
Standard deviation	44.5	1.0	1.5	4.4	1.5	58.1	3.1	3.1	1.7	62.8
Minimum	48.3	0.1	0.0	6.5	0.0	97.5	0.0	7.0	1.9	183.6
Maximum	174.3	2.9	4.7	18.5	4.5	244.3	7.3	15.0	6.4	390.5
Modified marine (n=45)										
Average	75.4	2.7	1.9	8.5	2.4	104.7	7.0	10.2	5.7	771.9
Standard deviation	39.3	2.7	1.0	4.0	1.3	54.8	3.9	2.6	3.2	376.5
Minimum	0.0	0.0	0.0	0.4	0.0	15.9	1.0	5.0	-3.1	385.9
Maximum	183.9	12.2	4.7	20.9	7.0	263.1	22.3	20.8	16.5	2049.8
Continental (n=27)										
Average	66.0	6.8	2.4	6.7	2.8	76.5	12.0	15.6	11.6	1814.4
Standard deviation	32.8	6.8	1.7	3.5	1.8	55.3	10.8	10.5	10.6	1050.7
Minimum	19.5	0.4	0.0	2.1	0.0	11.9	2.6	5.1	2.4	590.3
Maximum	140.6	36.1	7.7	14.7	6.2	209.3	45.0	59.5	56.4	4644.6

Table A11: P-values for Welch test on tall-tower PM_{10} aerosol concentrations for different air mass history categories (values correspond to Table A10)

	Na^+	NH_4^+	K^+	Mg^{2+}	Ca^{2+}	Cl^-	NO_3^-	SO_4^{2-}	nss-SO_4^{2-}
Marine - Modified Marine	0.075	0.077	0.359	0.088	0.439	0.024	0.010	0.847	0.028
Marine - Continental	0.030	0.001	0.954	0.015	0.865	0.003	0.001	0.031	0.001
Modified Marine - Continental	0.277	0.006	0.195	0.049	0.397	0.040	0.027	0.014	0.008

Table A12: Average tall-tower PM_{10} aerosol concentrations (nmol/m^3) by season and air mass history (with standard deviation in parentheses).

	Na^+	NH_4^+	K^+	Mg^{2+}	Ca^{2+}	Cl^-	NO_3^-	SO_4^{2-}	nss-SO_4^{2-}
Summer (n=3)									
All	67.9 (20.9)	3.4 (1.1)	3.6 (3.0)	8.4 (1.1)	3.3 (1.7)	114.7 (19.9)	6.5 (1.5)	12.5 (2.9)	8.4 (1.8)
Marine (n=0)	--	--	--	--	--	--	--	--	--
Modified marine (n=2)	57.0 (12.5)	3.7 (1.3)	1.9 (0.8)	8.2 (1.4)	2.5 (1.6)	105.3 (16.4)	6.4 (2.1)	11.3 (2.9)	7.9 (2.2)
Continental (n=1)	89.9	2.7	7.0	8.9	4.8	133.3	6.5	14.8	9.4
Autumn (n=24)									
All	44.5 (22.8)	3.7 (3.1)	1.4 (0.8)	4.9 (2.3)	1.4 (0.9)	55.2 (30.3)	10.3 (10.8)	12.7 (10.6)	10.0 (10.6)
Marine (n=1)	95.1	0.1	1.5	6.5	2.5	101.5	0.3	7.6	1.9
Modified marine (n=15)	39.7 (22.2)	2.6 (2.3)	1.3 (0.9)	5.0 (2.5)	1.5 (0.9)	60.6 (30.9)	7.1 (2.7)	9.5 (1.3)	7.1 (1.9)
Continental (n=8)	47.2 (17.4)	6.2 (3.0)	1.4 (0.8)	4.3 (2.2)	1.1 (0.9)	39.1 (21.1)	17.6 (16.4)	19.4 (16.9)	16.6 (16.8)
Winter (n=34)									
All	85.5 (38.0)	4.1 (6.7)	2.0 (0.9)	9.2 (4.0)	2.9 (1.4)	108.7 (60.6)	6.7 (4.2)	11.0 (4.6)	5.9 (5.4)
Marine (n=5)	114.3 (50.7)	1.0 (0.8)	1.9 (1.2)	13.1 (4.4)	2.9 (1.8)	178.3 (58.2)	3.3 (3.1)	10.7 (2.6)	3.8 (1.5)
Modified marine (n=19)	95.1 (29.1)	2.5 (3.1)	2.1 (0.9)	10.0 (3.3)	2.7 (1.2)	116.6 (48.8)	7.0 (3.9)	9.6 (2.5)	3.9 (2.9)
Continental (n=10)	52.7 (24.9)	8.6 (10.5)	2.1 (1.0)	5.9 (2.6)	3.3 (1.7)	59.0 (40.0)	7.9 (4.6)	13.9 (7.1)	10.7 (7.3)
Spring (n=19)									
All	98.5 (36.5)	4.0 (3.3)	3.0 (1.5)	10.8 (3.6)	3.3 (1.3)	143.2 (54.8)	9.0 (7.3)	13.0 (4.6)	7.01 (4.5)
Marine (n=2)	103.2 (56.2)	1.9 (1.5)	4.2 (0.8)	11.0 (4.6)	3.0 (1.3)	159.3 (71.5)	4.5 (4.0)	11.2 (5.3)	5.0 (1.9)
Modified marine (n=9)	97.5 (41.8)	3.0 (3.1)	2.6 (1.1)	11.5 (4.0)	3.2 (1.2)	152.7 (53.8)	7.1 (5.9)	12.4 (3.5)	6.5 (4.4)
Continental (n=8)	98.4 (31.1)	5.7 (3.3)	3.3 (2.0)	10.0 (3.3)	3.5 (1.5)	128.5 (57.0)	12.4 (8.5)	14.1 (5.9)	8.2 (5.1)

Table A13: P-values for Welch test on average tall-tower PM_{10} aerosol concentrations by season and air mass history (values correspond to Table A12).

	Na^+	NH_4^+	K^+	Mg^{2+}	Ca^{2+}	Cl^-	NO_3^-	SO_4^{2-}	nss-SO_4^{2-}
All									
Summer - Autumn	0.181	0.895	0.326	0.006	0.199	0.016	0.113	0.926	0.492
Summer - Winter	0.284	0.932	0.467	0.413	0.738	0.714	0.848	0.498	0.120
Summer - Spring	0.102	0.496	0.777	0.041	0.977	0.131	0.188	0.805	0.394
Autumn - Winter	0.000	0.839	0.005	0.000	0.000	0.000	0.125	0.470	0.087
Autumn - Spring	0.000	0.615	0.000	0.000	0.000	0.000	0.643	0.914	0.220
Winter - Spring	0.229	0.466	0.017	0.152	0.275	0.041	0.207	0.151	0.404
Marine									
Winter - Spring	0.834	0.679	0.053	0.636	0.890	0.777	0.754	0.914	0.539
Modified Marine									
Summer - Autumn	0.244	0.429	0.505	0.114	0.537	0.080	0.729	0.542	0.706
Summer - Winter	0.057	0.365	0.807	0.267	0.891	0.528	0.795	0.569	0.195
Summer - Spring	0.045	0.752	0.443	0.097	0.648	0.064	0.793	0.696	0.569
Autumn - Winter	0.000	0.759	0.021	0.000	0.002	0.000	0.883	0.815	0.000
Autumn - Spring	0.003	0.526	0.010	0.001	0.003	0.001	0.995	0.039	0.717
Winter - Spring	0.884	0.414	0.252	0.338	0.318	0.109	0.944	0.056	0.131
Continental									
Autumn - Winter	0.589	0.938	0.134	0.172	0.003	0.198	0.142	0.406	0.379
Autumn - Spring	0.002	0.865	0.031	0.001	0.002	0.003	0.440	0.423	0.212
Winter - Spring	0.005	0.800	0.144	0.012	0.748	0.013	0.207	0.939	0.402

Table A14: Size segregated ground-based HVAS aerosol concentrations categorized by air mass history (nmol/m^3, standard deviation in parentheses)

	Na^+	NH_4^+	K^+	Mg^{2+}	Ca^{2+}	Cl^-	NO_3^-	SO_4^{2-}	nss-SO_4^{2-}
Marine (n=6)									
Total HVAS	353.7 (100.4)	0.7 (0.7)	6.9 (2.2)	32.1 (8.4)	10.2 (3.31)	516.5 (177.3)	14.5 (10.9)	32.7 (9.8)	11.5 (8.6)
Coarse mode HVAS	314.1 (82.1)	0.4 (0.4)	5.8 (1.8)	30.1 (8.0)	9.3 (3.3)	466.2 (166.5)	10.5 (9.4)	23.2 (6.8)	4.3 (4.4)
Fine mode HVAS	39.5 (61.5)	0.2 (0.3)	1.1 (1.4)	2.0 (2.7)	0.9 (1.4)	50.3 (90.3)	4.1 (3.0)	9.5 (3.5)	7.2 (6.1)
Modified marine (n=17)									
Total HVAS	234.2 (99.8)	2.6 (2.6)	5.2 (2.5)	22.5 (9.3)	7.0 (3.3)	360.7 (123.8)	21.9 (9.2)	32.0 (6.4)	18.1 (5.6)
Coarse mode HVAS	221.5 (96.1)	0.7 (0.8)	4.3 (2.0)	21.7 (9.2)	6.6 (3.2)	353.9 (124.2)	18.8 (8.2)	20.8 (4.9)	7.5 (4.0)
Fine mode HVAS	12.7 (8.0)	1.9 (2.1)	1.0 (0.7)	0.7 (0.6)	0.4 (0.4)	6.8 (6.3)	3.1 (1.4)	11.2 (4.0)	10.5 (3.9)
Continental (n=10)									
Total HVAS	219.0 (74.0)	9.9 (11.9)	7.8 (2.8)	19.1 (5.0)	10.4 (6.3)	247.0 (137.4)	36.9 (21.6)	44.2 (16.2)	31.1 (16.2)
Coarse mode HVAS	187.3 (50.6)	1.8 (2.7)	4.4 (1.4)	17.5 (4.1)	8.4 (4.4)	225.9 (113.4)	30.4 (16.6)	19.9 (6.0)	8.6 (5.2)
Fine mode HVAS	31.8 (30.6)	8.1 (10.8)	3.5 (2.3)	1.6 (1.8)	1.9 (2.2)	21.2 (35.9)	6.5 (6.2)	24.3 (14.9)	22.5 (14.5)

Table A15: P-values for Welch test on ground-based HVAS aerosol concentrations categorized by air mass history (values correspond to Table A14)

	Na^+	NH_4^+	K^+	Mg^{2+}	Ca^{2+}	Cl^-	NO_3^-	SO_4^{2-}	nss-SO_4^{2-}
Total HVAS									
Marine - Modified marine	0.034	0.010	0.156	0.043	0.070	0.088	0.181	0.873	0.124
Marine - Continental	0.021	0.036	0.458	0.011	0.937	0.012	0.016	0.100	0.007
Modified marine - Continental	0.656	0.087	0.026	0.236	0.138	0.046	0.061	0.045	0.034
Coarse mode									
Marine - Modified marine	0.046	0.244	0.109	0.062	0.118	0.174	0.090	0.450	0.150
Marine - Continental	0.010	0.141	0.131	0.010	0.676	0.014	0.008	0.342	0.100
Modified marine - Continental	0.238	0.238	0.862	0.111	0.254	0.013	0.062	0.680	0.582
Fine mode									
Marine - Modified marine	0.335	0.006	0.809	0.304	0.418	0.291	0.473	0.352	0.246
Marine - Continental	0.782	0.047	0.023	0.781	0.270	0.478	0.311	0.012	0.012
Modified marine - Continental	0.083	0.105	0.008	0.150	0.053	0.240	0.120	0.022	0.030

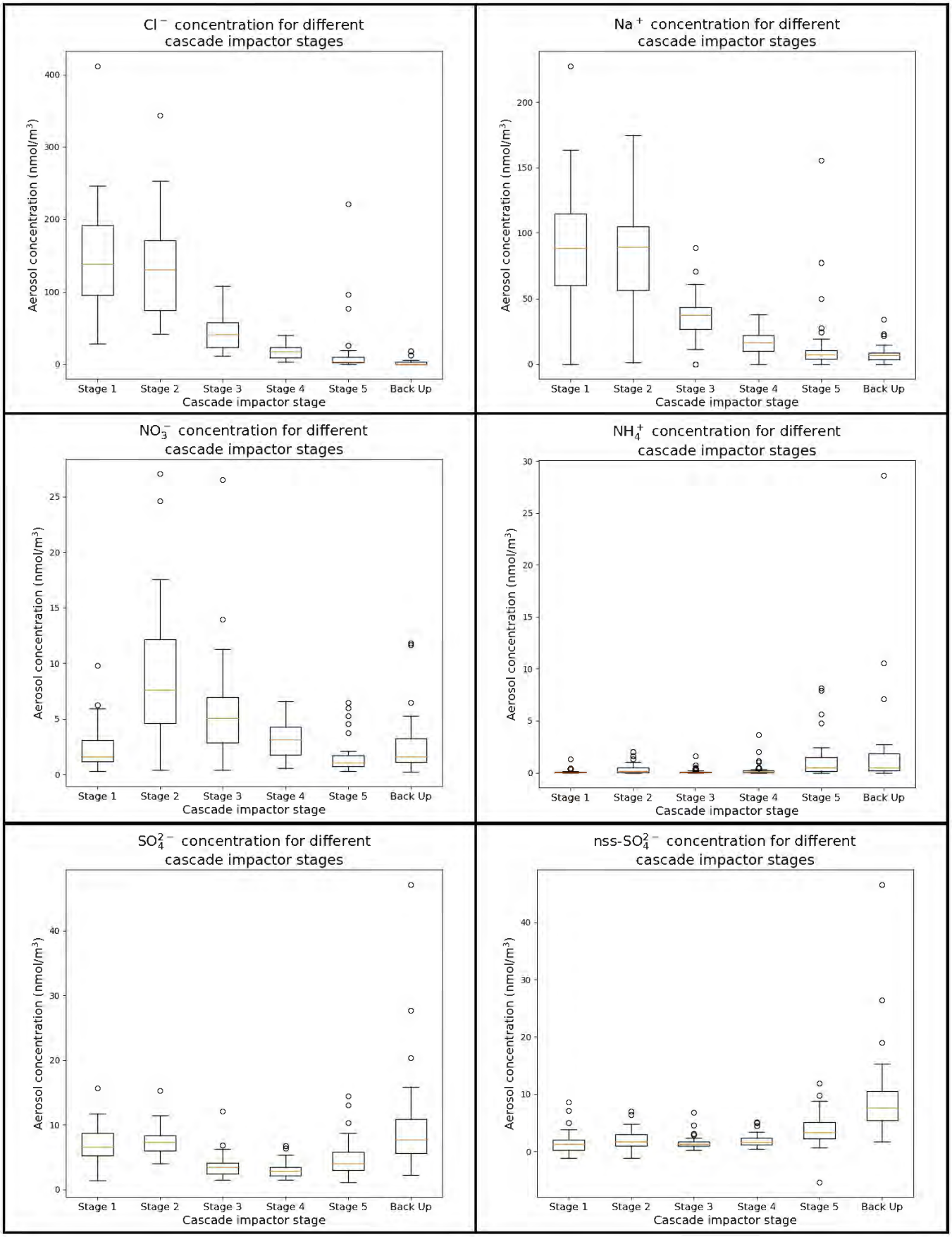

Figure A4: Box and whisker plots of average ground-based HVAS aerosol concentrations for each cascade impactor stage.

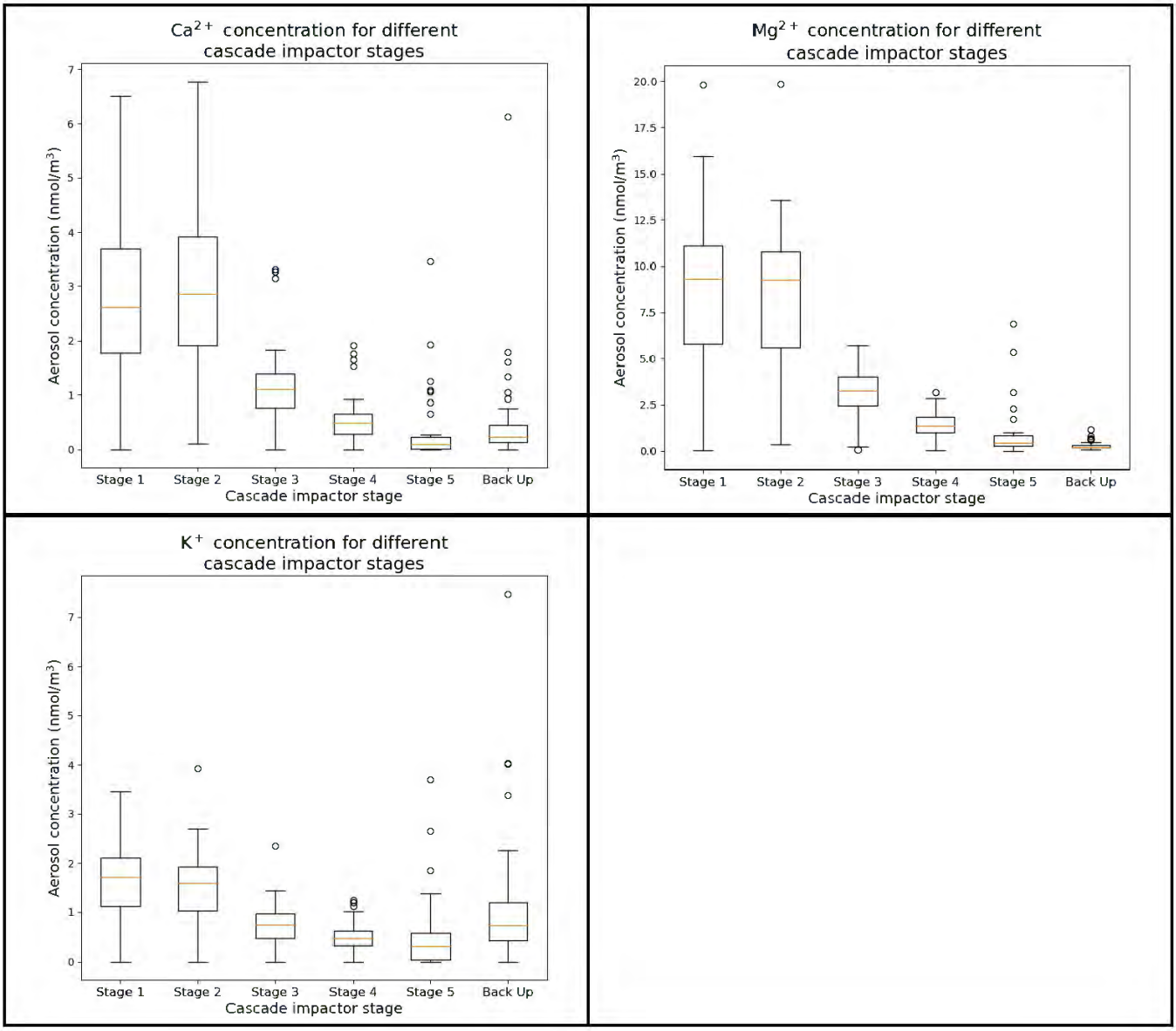

Figure A4 (continued): Box and whisker plots of average ground-based HVAS aerosol concentrations for each cascade impactor stage.

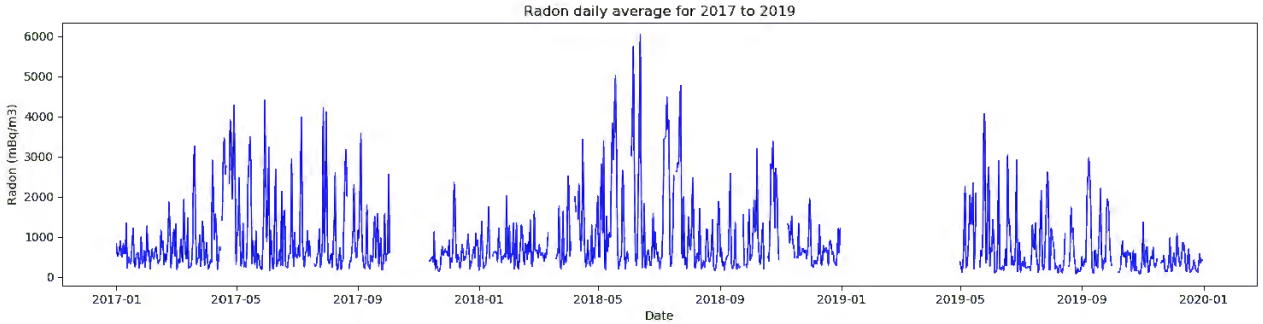

Figure A5: Daily average radon concentration for 2017 – 2019